ADAPTATIONS ENABLING PBP1A-DRIVEN POLAR GROWTH IN *AGROBACTERIUM TUMEFACIENS*

A Dissertation

Presented to

The Faculty of the Graduate School

At the University of Missouri

In Partial Fulfillment

of the Requirements for the Degree

Doctor of Philosophy

By

JACOB M. BOUCHIER

Dr. Pamela J.B. Brown, Dissertation Supervisor

MAY 2023

The undersigned, appointed by the dean of the Graduate School,

have examined the dissertation entitled

ADAPTATIONS TO CELL WALL STRESS DURING POLAR GROWTH IN *AGROBACTERIUM TUMEFACIENS*

Presented by JACOB M. BOUCHIER

A candidate for the degree of

Doctor of Philosophy

And hereby certify that, in their opinion, it is worthy of acceptance.

_____

Dr. Pamela J.B. Brown

_____

Dr. Ruthie Angelovici

_____

Dr. Elizabeth King

_____

Dr. Antje Heese

ACKNOWLEDGEMENTS

First, I would like to express my deepest gratitude to my PhD advisor, Dr. Pamela Brown, for her unwavering support and guidance throughout my academic journey. Dr. Brown's invaluable insights and expertise have been instrumental in shaping my research and professional development. Her encouragement and exceptional mentorship have been critical in helping me achieve my academic goals. I am truly grateful for her dedication, patience, and commitment to my success.

I would also like to extend my sincere gratitude to my mentors at Truman State University, Dr. Janick Bucker and Dr. Brent Buckner, for their exceptional guidance and support. During a time when I felt lost, they were there to guide me and help me realize my potential. They saw something in me that I didn't know existed and encouraged me to pursue graduate school. I will always cherish the four years I spent learning from and getting to know both.

I also want to express my appreciation to my current lab mates, Brody Aubry, Dr. Robert Kazmierczak, Dr. Emily Knebel, Jen Amstutz, Gustavo Santiago, and Laurie Agosto, and my students, Rhett Wakefield, Amara Mason, Carli McCurry, Cooper Barnes, Kaihre Brightwater, and Meredith Farmer, as well as my past lab mates, Amelia Randich, Michelle Williams, Matt Howell, Wanda Figueroa-Cuilan, Hedieh Attai, and Jeremy Daniels. Working alongside such intelligent and supportive individuals has been an honor. Your teamwork and friendship were crucial to my success, and I am so grateful for all that you have done for me.

To my committee, Dr. Ruhie Angelovici, Dr. Libby King, and Dr. Antje Heese, I thank you for the time and effort you put into helping me grow as a researcher and for your guidance on my project over the years.

To the ACES team, thank you for helping me feel included for the four years I served in the group. The team is made up of some of some of the most incredible and welcoming people. I am lucky to have gotten to know and work with each of you.

I extend my sincere gratitude to the Life Sciences Fellowship, and in particular, Dr. Mark Hannink and Debbie Allen, for selecting me to receive funding for four years. The support and resources provided by the fellowship have been essential to my academic and research accomplishments. I would also like to express my appreciation for Debbie's encouragement, organization, and weekly reminders for due dates, which were instrumental in keeping me on track throughout my time at Mizzou. Your efforts did not go unnoticed, and I am deeply grateful for everything you have done for me. Debbie, you will be truly missed at Mizzou, but I wish you all the happiness in your well-deserved retirement.

I would also like to express my heartfelt appreciation to my friends and family, particularly my parents Jane and DJ, and my sister Katy. Your support and encouragement have been vital to my success, and I am deeply grateful for the love and understanding you have shown me throughout my PhD journey. Your belief in me and constant motivation have helped me to overcome challenges and reach my goals. The memories and bonds we have formed will always hold a special place in my heart.

And finally, I would like to extend a special thanks to my fiancé Allison. Your unwavering support, patience, love, and understanding have helped me through the most difficult times of my graduate school journey. Your love and encouragement have been a constant source of motivation for me, and I am forever grateful to have you by my side. Your sacrifices and understanding of my commitment to my studies have been invaluable, and I look forward to the next chapter of our lives together.

TABLE OF CONTENTS

LIST OF FIGURES

LIST OF TABLES

ADAPTATIONS ENABLING PBP1A-DRIVEN POLAR GROWTH IN *AGROBACTERIUM TUMEFACIENS*

Jacob Bouchier

Pamela Brown, Dissertation Supervisor

ABSTRACT

For bacteria with complex life cycles involving several environmental niches, adaptability is key. The plant pathogen *Agrobacterium tumefaciens* is a master of adaptability as it lives two distinct lifestyles that each pose a unique set of challenges. In one, *A. tumefaciens* freely lives in the soil where it encounters many environmental stressors such as salinity, antibiotics, nutrient availability, changes in pH, and temperature that hinder its ability to grow. Upon encountering a potential host plant, *A. tumefaciens* transitions into a virulent, host-invading lifestyle state where it must adapt to survive a barrage of host defenses. This transformation and adaptability are driven by activation of the two-component signaling pathway ChvG-ChvI. However, ChvG and ChvI are conserved in many bacteria that are not host-associated, suggesting that adaptation for host invasion is not the primary function of the pathway. Here, we demonstrate activation of the pathway upon depletion of PBP1a, the primary driver of polar growth in *A. tumefaciens*, suggesting that ChvG-ChvI may be a more generalized stress pathway in response to defective polar growth. Additionally, we expand on the role of ChvG-ChvI during host invasion and demonstrate its importance for growth during treatment with cell-wall targeting antibiotics and for growth in

complex media. To better understand PBP1a's contributions to polar growth, we sought to characterize the structure and function of PBP1a domains. We found that the enzymatic domains are necessary for PBP1a to function in elongation. In addition, we found that an OB-fold extension likely interacts with a negative regulator of PBP1a activity. To identify candidate regulators of PBP1a activity, we used PBP1a as a bait protein in an immunoprecipitation experiment and identified proteins that complex with PBP1a. These efforts have revealed several proteins involved in the synthesis and regulation of peptidoglycan metabolism and elongation. Overall, this work has improved our understanding of how polar growth is regulated in *A. tumefaciens.*

CHAPTER 1

Functional and structural diversification of bacterial class A penicillin-binding proteins

Author Contributions

Jacob Bouchier wrote the original draft and completed the visualization and Jacob Bouchier and Pamela Brown reviewed and edited this dissertation chapter

ABSTRACT

Peptidoglycan synthesis is a fundamental process for the growth and division of most bacteria. Historically, the glycosyltransferase and transpeptidases activities of bifunctional class A penicillin-binding proteins (aPBPs) were believed to be the primary drivers of this process. However, in *E. coli* and *B. subtilis*, the combined glycosyltransferase activity of SEDS (shape determination, elongation, division, and sporulation) proteins and the transpeptidase activity of monofunctional class B penicillin-binding proteins (bPBPs) function in complex known as the elongasome to drive peptidoglycan synthesis. As a result, aPBPs are now thought to have ancillary and redundant functions in most bacteria. Despite this, there are examples of aPBPs serving specific, essential functions in growth and division. This introduction aims to highlight these specific roles.

INTRODUCTION

Penicillin-binding proteins (PBPs) are a group of enzymes crucial to the synthesis of peptidoglycan (PG), the primary structural component of the bacterial cell wall. PBPs can be classified into three classes based on their specific functions. Class A PBPs (aPBPs) are bifunctional enzymes. The glycosyltransferase activity enables expansion of PG by extension of preexisting glycan chains, and the transpeptidase activity crosslinks the peptide stems between adjacent glycan chains (Figure 1). Most bacteria have multiple aPBPs, but only a subset of these enzymes are essential for growth[1–4], raising the question of why bacterial cell wall synthesis requires such redundancy. Despite the well-established

importance of the cell wall, the significance of the apparent redundancy of aPBPs remains unresolved. Monofunctional class B PBPs (bPBPs) have only transpeptidase activity. The structural integrity of the bacterial cell wall relies heavily on crosslinking, mediated either by aPBPs and bPBPs. Thus, beta-lactam antibiotics that mimic the terminal D-alanine, D-alanine substrates of PBP transpeptidase domains are some of the most effective broad-spectrum treatments for targeting bacteria. Indeed, the inactivation of peptidoglycan crosslinking enzymes is causes cell lysis due simply to the osmotic pressure of the bacterial cytoplasm[5]. Finally, class C PBPs consist mainly of hydrolases, involved in modifying peptide stems to generate substrates for aPBP and bPBP crosslinking.

Class A PBPs exhibit structural diversity

While all bacteria with cell walls have PBPs, the aPBPs can vary in structure and function across different bacterial phyla (Figure 2). For instance, Proteobacteria (see green in Figure 2), one of the largest bacterial phyla, has three conserved groups of aPBPs, designated as PBP1a, PBP1b, and PBP1c, named after the three aPBPs in *Escherichia coli* [6]. The aPBPs in Proteobacteria have been extensively studied, yet key questions regarding their coordination, regulation, and significance of their enzymatic activities remain.

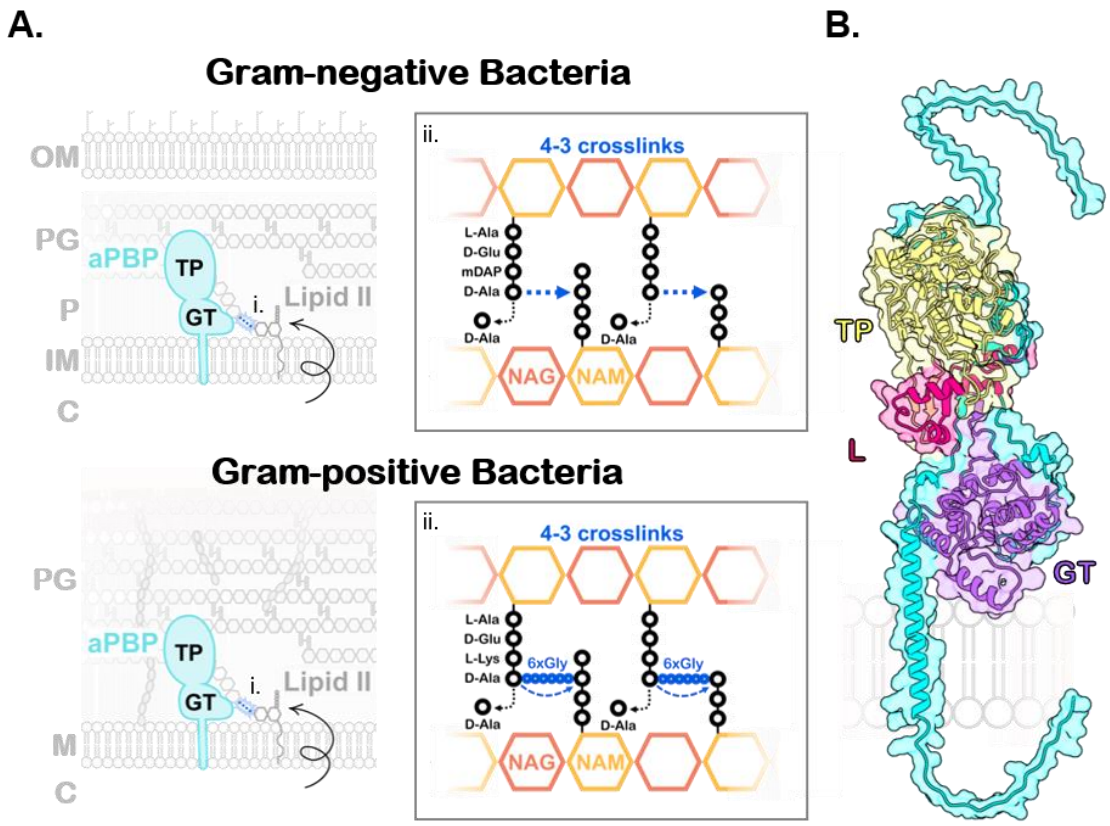

Figure 1.1. aPBP-mediated cell wall synthesis in Gram-negative and Gram-positive bacteria. The cell surface of Gram-negative bacteria is comprised of an inner membrane (IM), periplasmic space (P) which contains the thin layer of peptidoglycan (PG), and an outer membrane (OM). The cell surface of Gram-positive bacteria contains the membrane (M) and a thick PG layer. The M and PG are linked by teichoic acid chains. **A.** PG precursors called Lipid II are manufactured in the bacterial cytoplasm (C) and then flipped across the membrane by the activity of a flippase to be incorporated into the PG macromolecule. i) Incorporation of nascent PG is catalyzed by the glycosyltransferase domain of an aPBP (GT) and is then ii) sequentially crosslinked by the transpeptidase domain (TP). Crosslinking is a two-step

reaction first involving the removal of the terminal D-alanine from a pentapeptide stem, freeing the second terminal D-alanine for crosslinking with a meso-diaminopimelic acid (M-DAP) in Gram-negative bacteria or L-lysine in Gram-positive bacteria. Crosslinking between D-alanine and M-DAP is direct, while crosslinking between D-alanine and L-lysine is facilitated by a 6x glycine crossbridge. **B.** AlphaFold predicted structure of PBP2 from Staphylococcus aureus (A0A385MK73). TP, Transpeptidase domain; L, Linker; GT, Glycosyltransferase domain.

The transpeptidase domains of PBP1a proteins in Alpha-, Beta-, and Gammaproteobacteria contain a distinctive OB-fold extension. Representative structures of proteobacterial PBP1a proteins from *E. coli, A. tumefaciens*, and *D. vulgaris* are shown in Figure 2 with the OB-fold in royal blue. Although this extension has been identified as a binding site for lipoproteins like LpoA in *E. coli* [7,8], its ancestral function remains unclear and no interaction partners for the OB-fold have been described in either the Alpha- or Betaproteobacterial PBP1a homologs. The PBP1a proteins in the Alpha and Gammaproteobacteria also possess an extended structural loop that links their transpeptidase domains and linker domains (Figure 2B). Despite its prevalence, the function of these extended structural loops remains undescribed.

PBP1b proteins of Gammaproteobacteria have a discrete extension called a UB2H domain (see orange highlight in the representative structure from *Serratia inhibens*, Figure 2) that is the site of regulation through interaction of LpoB and LpoP in Gammaproteobacteria [9,10]. In addition, CpoB binds this domain and the transpeptidase domain. This binding enhances LpoB activation of transpeptidation in PBP1b [11]. While the OB-fold is conserved across a broad range of organisms, the UB2H domain is more limited in its conservation and is primarily found within the Gammaproteobacteria.

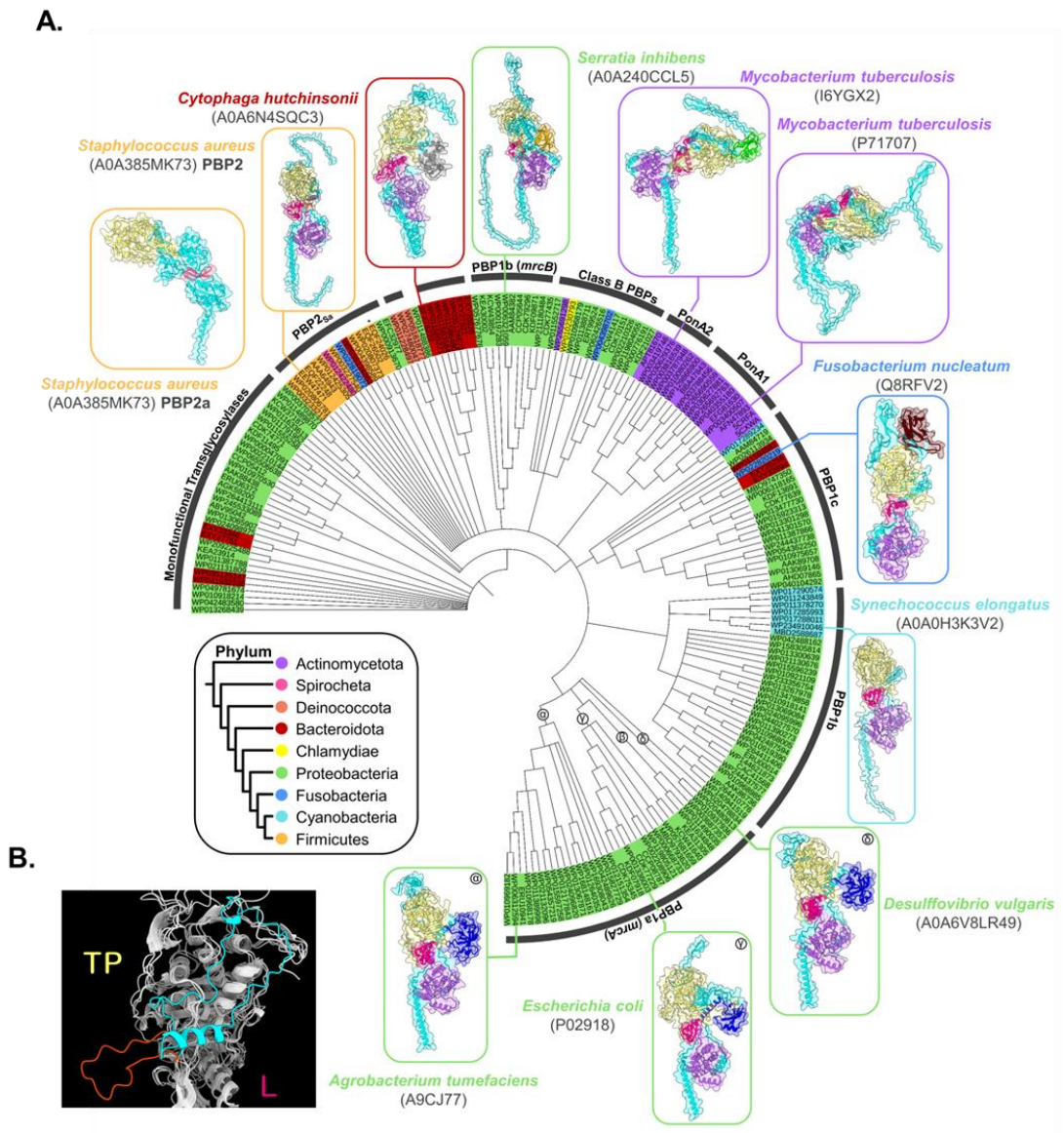

Figure 1.2. Phylogenetic and structural diversity of bacterial PBPs. **A.** The evolutionary history was inferred using the Minimum Evolution method. The Neighbor-joining algorithm was used to generate the initial tree. This analysis involved 196 amino acid sequences. All ambiguous positions were removed for each sequence pair (pairwise deletion option). There were a total of 1821 positions in the final dataset. Evolutionary analyses were conducted in MEGA X. Color code of bacterial phyla is boxed. AlphaFold predicted structures of representative PBPs are shown. Domains are color coded as follow:

transpeptidase domain, yellow; linker, pink; glycosyltransferase domain, purple; OB-fold, royal blue; UB2H domain, orange; BIPBP_C domain, brown; PASTA domain, green. **B.** Structural alignments of PBP1a from Agrobacterium tumefaciens (A9CJ77), Escherichia coli (P02918), and Desulfovibrio vulgaris (A0A6V8L49), representing Alpha-, Gamma-, and Deltaproteobacteria, respectively. Extended loop structure colored by organism, except for D. vulgaris which lacks the loop. A. tumefaciens, Red; *E. coli*, Cyan; Rest of PBP1a structures, White; TP, Transpeptidase; L, Linker.

PBP1c proteins are characterized by a large, uncharacterized terminal domain annotated as BIPBP_C (see brown highlight in representative structure from *Fusobacterium nucleatum*, Figure 2). Despite its structural similarity to other penicillin-binding proteins, PBP1c cannot complement the growth of an *E. coli* double mutant lacking PBP1a and PBP1b [6]. Moreover, loss of PBP1c does not affect the bacterial doubling time [12]. The PBP1c transpeptidase domain is unable to bind most beta-lactam antibiotics, suggesting that it may no longer have a functional role in PG synthesis. Instead, it is hypothesized that PBP1c may play a non-essential role in coordinating PG synthesis [6].

Other bacterial phyla, such as Actinobacteria (formerly Actinomycetota) and Bacteroidetes (formerly Bacteroidota), also have distinct class aPBP clades that are separate from those found in Proteobacteria (Figure 2). Many aPBPs of the Actinobacteria have PASTA (PBP and Serine/Threonine kinase associated) domains (see green highlight in representative structure I6YGX2 from *Mycobacterium tuberculosis*, Figure 2). While some of these domains have been characterized in the binding of muropeptides and beta lactams [13,14], others have functions that remain unresolved [15].

A subset of aPBPs in the Bacteroidetes phylum features a distinctive extension to their transpeptidase domains (shown in grey in the undescribed aPBP from *Cytophaga hutchinsonii,* Figure 2). Although this domain remains uncharacterized, one possibility is that it is involved in regulating aPBP activity

similarly to the functions of the OB-fold and UB2H domain of the Proteobacteria. Further investigation is necessary to shed light on the ancestral function of these extensions and loops and their roles in regulating cell wall synthesis across diverse bacterial species.

Activity of Class A PBPs are tightly regulated by accessory proteins

To reconstitute growth and division faithfully and consistently, bacteria tightly regulate the synthesis of nascent PG. Examples of direct regulation through spaciotemporal interactions with accessory proteins can be found across the bacterial domain. The regulation of PBP1a and PBP1b by outer membrane associated lipoproteins and peptidoglycan bound periplasmic proteins in *E. coli* are the most well understood mechanisms.

Activation of $PBP1a_{Ec}$ is dependent on the interaction with LpoA, a flexible outer membrane bound lipoprotein[8,9,16]. LpoA is distributed randomly across the lateral surface of the cell[9]. During of growth and cell wall damage, gaps form in PG that exposes $PBP1a_{Ec}$ to binding by LpoA[7,17] (Figure 3A). This interaction between $PBP1a_{Ec}$ and LpoA occurs through binding of the OB-fold domain of $PBP1a_{Ec}$ and stimulates both transpeptidase and glycosyltransferase activities, allowing insertion of nascent PG into exisiting gaps in the PG[8]. In a similar way,

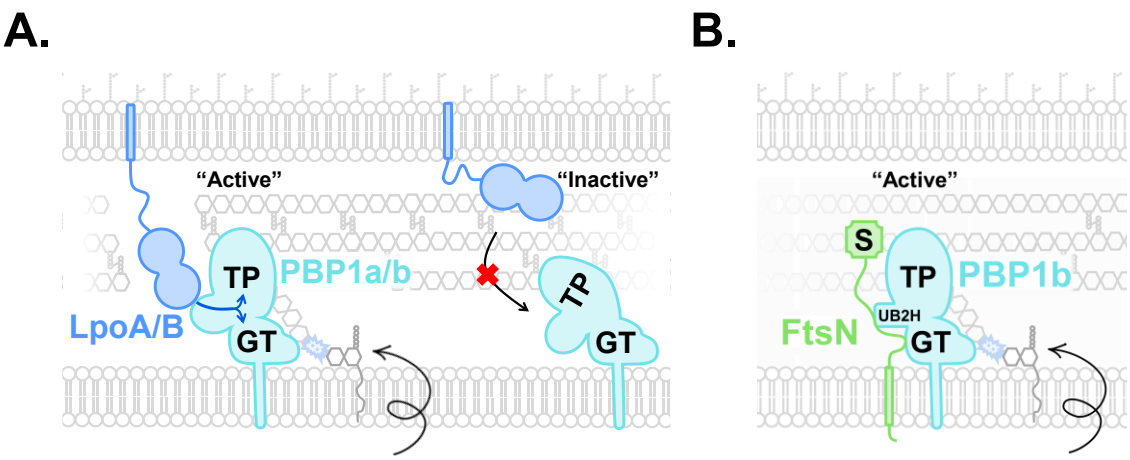

Figure 1.3. Regulation of aPBP activity in *E. coli*. **A.** Activation of PBP1a occurs when LpoA makes contact with the OB-fold (OB) and activation of PBP1b occurs when LpoB comes in contact with the UB2H. When PG is locally intact, LpoA does not have access to bind the OB-fold and PBP1a remains inactive. **B**. The FtsN SPOR domain (S) binds to regions of denuded PG at mid-cell and interacts with the glycosyltransferase (GT) domain to stimulate PBP1b activity independent of LpoB.

LpoB interacts with the UB2H domain of $PBP1b_{Ec}$ also stimulating activity enzymatic activity of PBP1b[18] (Figure 3A). $PBP1b_{Ec}$ localizes to midcell and interacts with ZipA, FtsA, and FtsN. Interaction with these proteins stimulates PBP1b activity and permits cell division to occur[19]. Notably, FtsN stimulates PBP1b by directly binding its glycosyltransferase and UB2H domains in an LpoB-independent manner (Figure 3B)[20]. Midcell localization of FtsN is maintained by amidase activity that denudes PG as a localization signal for its SPOR domain[21]. Therefore, FtsN plays a critical role as a spaciotemporal regulator of cell division.

Some Class A PBPs have essential roles in growth and division

Most bacteria have multiple aPBPs, and two essential SEDS proteins, raising the question of why bacterial cell wall synthesis requires such apparent redundancy. Although the SEDS proteins RodA and FtsW are broadly conserved, some bacteria, such as *Staphylococcus aureus* and *Mycobacterium tuberculosis* have dispensable RodA proteins. Other bacteria including the Rhizobiales clade of Alphaproteobacteria as exemplified here by *Agrobacterium tumefaciens* lack a RodA ortholog entirely. Instead, these bacteria have essential or conditionally essential aPBPs that are primary drivers of PG synthesis in the absence of RodA[1–4].

Staphylococcus aureus

In *S. aureus,* RodA contributes to PG synthesis but the absence of RodA and its cognate bPBP partner, $PBP3_{Sa}$, has minimal effects on morphology or

growth[22]. $PBP2_{Sa}$ localizes to midcell during cell division where it builds PG in tandem with the synthesis of septal PG by FtsW and $PBP1_{Sa}$[4]. Interestingly methicillin-resistant strains of *S. aureus* (MRSA) have acquired an additional beta-lactam-resistant bPBP, $PBP2a_{Sa}$, which can bypass the essentiality of $PBP2_{Sa}$ (See PBP2 and PBP2a structures, Figure 2)[23]. However, despite the emergence of beta-lactam-resistant PBPs in MRSA strains, the glycosyltransferase activity of $PBP2_{Sa}$ remains crucial for the synthesis of PG under beta-lactam challenge[23]. Together, these observations suggest that the bifunctional $PBP2a_{Sa}$ has conditionally essential function in *S. aureus*.

Mycobacterium tuberculosis

Mycobacterium tuberculosis is a bipolar-growing bacterium, where new PG is synthesized at both poles. Mycobacterial genomes contain genes encoding an ortholog of RodA and two aPBPs. Under typical lab conditions, deletion of *rodA* in *Mycobacterium tuberculosis* results in conditionally viable cells in which the activity of PonA1, an aPBP, becomes essential for growth. RodA also becomes essential during treatment with lytic PG hydrolases, suggesting that its activity may be important in fortifying the cell wall against extracellular stressors[3].

The two mycobacterial aPBPs have similar structures (outlined in purple, Figure 2), but distinct roles in growth[24]. One major difference in the structures is the presence of a PASTA domain on PonA2, but not on PonA1. The role of this domain is often associated with binding of muropeptides or beta-lactam

antibiotics[13,14], however the PASTA domain of PonA2 does not bind either[15]. Mutants of *ponA2* in *Mycobacterium smegmatis* exhibit a striking loss in rod shape during stationary phase, suggesting PonA2 likely functions under nonreplicating conditions[25]. Thus, it has evolved a specialized function in Mycobacteria that awaits further characterization. In contrast, PonA1 localizes across the lateral surface of the bacterium, but its activity is strictly localized to the pole where it is a primary driver of polar growth[3].

In *M. tuberculosis* loss of either PonA1 or PonA2 does not affect growth rate, however deletion of either results in attenuation of virulence[24]. Interestingly, both PonA1 and PonA2 inactivate penicillin and carbapenem class beta-lactam antibiotics, a function primarily attributed to beta-lactamases[26]. Recent studies on the interactions between PBPs and beta-lactam antibiotics are revealing new insights into the complex mechanisms that underlie antibiotic resistance and are informing the development of new strategies to combat antibiotic resistance.

Agrobacterium tumefaciens

Agrobacterium tumefaciens has four aPBPs, including one that is essential for growth. Depletion of the essential PBP1a results in shorter and rounder cells, suggesting that it is the major PG synthase. Additionally, depletion results in loss of incorporation of fluorescent D-amino acid dipeptides (FDAADs) at the growth pole, implicating its role in polar growth[1]. *A. tumefaciens* lacks an ortholog of RodA, and the three other aPBPs can be readily deleted with no observable

effects in morphology or viability under standard laboratory conditions. Together, these observations make *A. tumefaciens* a compelling model to study the evolutionary pressures that lead to dispensability of RodA and the adoption of aPBPs for growth.

Despite recent advances in our understanding of the key players in *A. tumefaciens* polar growth, little is known about how it is regulated. The presence of the OB-fold extension in PBP1a, suggests that a protein partner may directly regulation PBP1a activity. The absence of known PBP1a binding partners such as LpoA and FtsN in *A. tumefaciens* indicates that the Rhizobiales may use distinct mechanisms to regulate the activity of PBP1a.

CONCLUSION

In my dissertation, I investigate the regulation of peptidoglycan synthesis in *A. tumefaciens*. In Chapter 2, I provide evidence supporting the role of the ChvG-ChvI two-component system as a sensor for cell wall damage. Chapter 3 builds on this idea, proposing that ChvG tracks with the growth pole of *A. tumefaciens* and upregulates the production of succinoglycan, an exopolysaccharide that protects bacterial cells from beta-lactam antibiotics. In Chapter 4, I delve into the functions of the domains of PBP1a and identify proteins which form a complex with PBP1a to propose a model for the elongasome of *A. tumefaciens*, which includes RgsS and two novel proteins of unknown function as candidate regulators of PBP1a. Chapter 5 demonstrates that loss of RgsS results in

irregular growth and a block in cell division. Overall, my research deepens our understanding of the regulation of polar growth in *A. tumefaciens*, which is crucial to expand on our perception of how bacteria grow, divide, and maintain cell shape.

REFERENCES

1. Williams MA, Aliashkevich A, Krol E, Kuru E, Bouchier JM, Rittichier J, et al. Unipolar Peptidoglycan Synthesis in the Rhizobiales Requires an Essential Class A Penicillin-Binding Protein . MBio. 2021 [cited 9 Oct 2021]. doi:10.1128/MBIO.02346-21
2. Sher JW, Lim HC, Bernhardt TG. Polar Growth in Corynebacterium glutamicum Has a Flexible Cell Wall Synthase Requirement. Sloan Siegrist M, editor. MBio. 2021 [cited 27 Jun 2021]. doi:10.1128/mBio.00682-21
3. Melzer ES, Kado T, García-Heredia A, Gupta KR, Meniche X, Morita YS, et al. Cell Wall Damage Reveals Spatial Flexibility in Peptidoglycan Synthesis and a Nonredundant Role for RodA in Mycobacteria. J Bacteriol. 2022;204. doi:10.1128/JB.00540-21
4. Pinho MG, Errington J. Recruitment of penicillin-binding protein PBP2 to the division site of Staphylococcus aureus is dependent on its transpeptidation substrates. Mol Microbiol. 2005;55: 799–807. doi:10.1111/J.1365-2958.2004.04420.X
5. Auer GK, Weibel DB. Bacterial Cell Mechanics. Biochemistry. 2017;56: 3710–3724.

doi:10.1021/ACS.BIOCHEM.7B00346/ASSET/IMAGES/LARGE/BI-2017-00346G_0006.JPEG

6. Schiffer G, Höltje JV. Cloning and characterization of PBP 1C, a third member of the multimodular class A penicillin-binding proteins of Escherichia coli. J Biol Chem. 1999;274: 32031–32039. doi:10.1074/jbc.274.45.32031

7. Jean NL, Bougault CM, Lodge A, Derouaux A, Callens G, Egan AJF, et al. Elongated Structure of the Outer-Membrane Activator of Peptidoglycan Synthesis LpoA: Implications for PBP1A Stimulation. Structure. 2014;22: 1047–1054. doi:10.1016/J.STR.2014.04.017

8. Sardis MF, Bohrhunter JL, Greene NG, Bernhardt TG. The LpoA activator is required to stimulate the peptidoglycan polymerase activity of its cognate cell wall synthase PBP1a. Proc Natl Acad Sci U S A. 2021;118. doi:10.1073/PNAS.2108894118/-/DCSUPPLEMENTAL

9. Typas A, Banzhaf M, Van Den Berg Van Saparoea B, Verheul J, Biboy J, Nichols RJ, et al. Regulation of peptidoglycan synthesis by outer-membrane proteins. Cell. 2010;143: 1097–1109. doi:10.1016/j.cell.2010.11.038

10. Greene NG, Fumeaux C, Bernhardt TG. Conserved mechanism of cell-wall synthase regulation revealed by the identification of a new PBP activator in Pseudomonas aeruginosa. Proc Natl Acad Sci U S A. 2018;115: 3150–3155. doi:10.1073/PNAS.1717925115/-/DCSUPPLEMENTAL

11. Egan AJF, Maya-Martinez R, Ayala I, Bougault CM, Banzhaf M, Breukink

E, et al. Induced conformational changes activate the peptidoglycan synthase PBP1B. Mol Microbiol. 2018;110: 335–356. doi:10.1111/MMI.14082

12. Mueller EA, Jf Egan A, Breukink E, Vollmer W, Levin PA. Plasticity of Escherichia coli cell wall metabolism promotes fitness and antibiotic resistance across environmental conditions. [cited 7 Mar 2023]. doi:10.7554/eLife.40754.001
13. Yeats C, Finn RD, Bateman A. The PASTA domain: a β-lactam-binding domain. Trends Biochem Sci. 2002;27: 438–440. doi:10.1016/S0968-0004(02)02164-3
14. Mir M, Asong J, Li X, Cardot J, Boons GJ, Husson RN. The Extracytoplasmic Domain of the Mycobacterium tuberculosis Ser/Thr Kinase PknB Binds Specific Muropeptides and Is Required for PknB Localization. PLoS Pathog. 2011;7: 1002182. doi:10.1371/JOURNAL.PPAT.1002182
15. Calvanese L, Falcigno L, Maglione C, Marasco D, Ruggiero A, Squeglia F, et al. Structural and binding properties of the PASTA domain of PonA2, a key penicillin binding protein from Mycobacterium tuberculosis. Biopolymers. 2014;101: 712–719. doi:10.1002/BIP.22447
16. Sathiyamoorthy K, Vijayalakshmi J, Tirupati B, Fan L, Saper MA. Structural analyses of the Haemophilus influenzae peptidoglycan synthase activator LpoA suggest multiple conformations in solution. J Biol Chem. 2017;292: 17626–17642. doi:10.1074/jbc.M117.804997

17. Turner RD, Hurd AF, Cadby A, Hobbs JK, Foster SJ. Cell wall elongation mode in Gram-negative bacteria is determined by peptidoglycan architecture. Nat Commun 2013 41. 2013;4: 1–8. doi:10.1038/ncomms2503

18. Egan AJF, Jean NL, Koumoutsi A, Bougault CM, Biboy J, Sassine J, et al. Outer-membrane lipoprotein LpoB spans the periplasm to stimulate the peptidoglycan synthase PBP1B. Proc Natl Acad Sci U S A. 2014;111: 8197–8202. doi:10.1073/PNAS.1400376111/-/DCSUPPLEMENTAL/PNAS.1400376111.SAPP.PDF

19. Pazos M, Peters K, Casanova M, Palacios P, VanNieuwenhze M, Breukink E, et al. Z-ring membrane anchors associate with cell wall synthases to initiate bacterial cell division. Nat Commun 2018 91. 2018;9: 1–12. doi:10.1038/s41467-018-07559-2

20. Boes A, Kerff F, Herman R, Touze T, Breukink E, Terrak M. The bacterial cell division protein fragment EFtsN binds to and activates the major peptidoglycan synthase PBP1b. J Biol Chem. 2020;295: 18256. doi:10.1074/JBC.RA120.015951

21. Yahashiri A, Jorgenson MA, Weiss DS. The SPOR domain, a widely conserved peptidoglycan binding domain that targets proteins to the site of cell division. J Bacteriol. 2017;199. doi:10.1128/JB.00118-17/ASSET/9C9595FD-2D4C-445A-8D99-8D7C76066B8E/ASSETS/GRAPHIC/ZJB9990944290002.JPEG

22. Lee W, Do T, Zhang G, Kahne D, Meredith TC, Walker S. Antibiotic

combinations that enable one-step, targeted mutagenesis of chromosomal genes. ACS Infect Dis. 2018;4: 1007. doi:10.1021/ACSINFECDIS.8B00017

23. Pinho MG, De Lencastre H, Tomasz A. An acquired and a native penicillin-binding protein cooperate in building the cell wall of drug-resistant staphylococci. Proc Natl Acad Sci U S A. 2001;98: 10886. doi:10.1073/PNAS.191260798

24. Kieser KJ, Baranowski C, Chao MC, Long JE, Sassetti CM, Waldor MK, et al. Peptidoglycan synthesis in Mycobacterium tuberculosis is organized into networks with varying drug susceptibility. Proc Natl Acad Sci U S A. 2015;112: 13087–13092. doi:10.1073/PNAS.1514135112/SUPPL_FILE/PNAS.1514135112.SD02.XLS

25. Patru MM, Pavelka MS. A role for the class a penicillin-binding protein PonA2 in the survival of Mycobacterium smegmatis under conditions of nonreplication. J Bacteriol. 2010;192: 3043–3054. doi:10.1128/JB.00025-10/ASSET/A970A19C-A4CC-4B91-A02C-1AA4E68AEA79/ASSETS/GRAPHIC/ZJB9990996030008.JPEG

26. Kumar G, Galanis C, Batchelder HR, Townsend CA, Lamichhane G. Penicillin Binding Proteins and β-Lactamases of Mycobacterium tuberculosis: Reexamination of the Historical Paradigm. mSphere. 2022;7. doi:10.1128/MSPHERE.00039-22

CHAPTER 2

Activation of ChvG-ChvI regulon by cell wall stress confers resistance to β-lactam antibiotics and initiates surface spreading in *Agrobacterium tumefaciens*

Author Contributions

Bouchier J, Williams M, and Mason A conducted the experiments. Bouchier J, Williams M, and Brown PB designed the experiments. Bouchier J, Williams M, and Brown PB analyzed data and Bouchier J, Williams M and Brown PB wrote and edited the paper.

Citation: Williams MA, Bouchier JM, Mason AK, Brown PJB (2022) Activation of ChvG-ChvI regulon by cell wall stress confers resistance to β-lactam antibiotics and initiates surface spreading in Agrobacterium tumefaciens. PLoS Genet 18(12): e1010274. https://doi.org/10.1371/journal.pgen.1010274

ABSTRACT

A core component of nearly all bacteria, the cell wall is an ideal target for broad spectrum antibiotics. Many bacteria have evolved strategies to sense and respond to antibiotics targeting cell wall synthesis, especially in the soil where antibiotic-producing bacteria compete with one another. Here we show that cell wall stress caused by both chemical and genetic inhibition of the essential, bifunctional penicillin-binding protein PBP1a prevents microcolony formation and activates the canonical host-invasion two-component system ChvG-ChvI in *Agrobacterium tumefaciens*. Using RNA-seq, we show that depletion of PBP1a for 6 hours results in a downregulation in transcription of flagellum-dependent motility genes and an upregulation in transcription of type VI secretion and succinoglycan biosynthesis genes, a hallmark of the ChvG-ChvI regulon. Depletion of PBP1a for 16 hours, results in differential expression of many additional genes and may promote a stress response, resembling those of sigma factors in other bacteria. Remarkably, the overproduction of succinoglycan causes cell spreading and deletion of the succinoglycan biosynthesis gene *exoA* restores microcolony formation. Treatment with cefsulodin phenocopies depletion of PBP1a and we correspondingly find that *chvG* and *chvI* mutants are hypersensitive to cefsulodin. This hypersensitivity only occurs in response to treatment with β-lactam antibiotics, suggesting that the ChvG-ChvI pathway may play a key role in resistance to antibiotics targeting cell wall synthesis. Finally, we provide evidence that ChvG-ChvI likely has a conserved role in conferring

resistance to cell wall stress within the Alphaproteobacteria that is independent of the ChvG-ChvI repressor ExoR.

AUTHOR SUMMARY

Soil dwelling bacteria reside in changing environments requiring them to frequently adapt to stressful conditions to ensure survival. The bacterial envelope provides structural integrity and protection against osmotic stress and turgor pressure imposed by the environment. While the mechanisms of cell membrane and cell wall biogenesis have been extensively studied, our understanding of how diverse microbes respond to cell envelope and cell wall stress to increase their fitness remains limited. In this work, we identify ChvG-ChvI regulon as an envelope stress response system that confers protection under cell wall stress conditions in the bacterial plant pathogen *Agrobacterium tumefaciens*. This is a new function for the well-characterized ChvG-ChvI pathway which is also acid induced and promotes plant host invasion. Our results suggest that the ChvG-ChvI pathway has a broadly conserved role in protecting Alphaproteobacterial cells from extracellular stress and a more specific role in response to acid stress and promoting plant-microbe interactions.

INTRODUCTION

The soil environment is constantly in flux and can undergo rapid changes in hydration, nutrient availability, temperature, acidity levels and many other abiotic and biotic factors [1]. To survive in these conditions, soil-dwelling bacteria must

be able to monitor and respond to the changes around them. One of the main mechanisms bacteria employ to monitor changes in their environment is coupling environmental stimuli to transcriptional regulation using two-component systems (TCS) [2]. In turn transcriptional changes can modify bacterial behavior. In the plant-pathogen *Agrobacterium tumefaciens*, two TCS sense the presence of a potential host and initiate transcription programs that transition the bacterium into a virulent state [3].

The VirA-VirG histidine kinase/response-regulator pair is a characteristic of Agrobacteria and responds to plant phenolic compounds such as acetosyringone. Activation induces expression of the *vir* regulon, which encodes genes that are required for pathogenicity and plant transformation [4]. The ChvG-ChvI TCS is more broadly conserved across many Alphaproteobacteria but has been best characterized among the plant symbionts of Rhizobiales such as *Sinorhizobium meliloti* [5,6]. Activation of ChvG-ChvI is required for the transition from a free-living bacterium to a host-associated lifestyle [7].

In *S. meliloti* and *A. tumefaciens* ChvG-ChvI is regulated by the periplasmic protein ExoR. Under neutral conditions, ExoR binds to and represses ChvG; however, when cells are exposed to acidic conditions, ExoR is proteolyzed, which allows for activation of the ChvG-ChvI TCS [8,9]. ChvI induces transcriptional changes in many genes across several major pathways. For example, ChvI upregulates transcription of *mirA,* encoding a repressor of the

motility response regulator Rem and ultimately resulting in suppression of genes for motility and chemotaxis [10]. ChvI also upregulates genes for exopolysaccharide production and, in *A. tumefaciens,* induction of the Type VI Secretion System (T6SS) [11]

Conservation of the ChvG-ChvI TCS is taxonomically constrained to several orders of Alphaproteobacteria, many of whom have free-living lifestyles that are never host-associated [6]. This begs the question: why is the ChvG-ChvI pathway conserved in so many non-host-associated bacteria? Recent interest in the ChvG-ChvI pathway of *Caulobacter crescentus* (ChvGI) provides a glimpse at the function of the pathway in the context of a bacterium with a drastically different ecological niche to that of *A. tumefaciens* or *S. meliloti*. ChvGI of *C. crescentus* senses and responds to osmotic stress and mutants of ChvGI are sensitive to several cell-wall targeting antibiotics [12,13]. It remains unclear if this function is solely a characteristic of *C. crescentus* ChvGI or if it is conserved across ChvG-ChvI orthologs.

Although the cell wall is an essential feature of bacteria that protects them from environmental stressors, relatively little is known about how bacteria sense and respond to changes in the composition of their cell wall. Peptidoglycan (PG) is a heteroglycan decorated with cross-linked peptide stems and is the primary component of bacterial cell walls. During elongation in *A. tumefaciens*, nascent PG insertion is constrained to the pole. Polar growth is a characteristic of

Rhizobiales and does not require the canonical MreB-RodA-PBP2 elongation complex. Indeed, all members of Rhizobiales have lost this complex entirely [14,15]

We showed that PBP1a is essential in *A. tumefaciens* and is the primary driver of polar growth. Depletion of PBP1a eliminates nascent PG insertion at the growth pole, leading to shorter cells that have compositional changes in PG [16]. In addition to its role in polar PG insertion, here we observe that during PBP1a depletion cells spread apart rather than form microcolonies. To better understand this phenotype, we used RNA-seq to obtain transcriptional profiles of cells depleted of PBP1a after 6 hours, corresponding to the onset of the spreading phenotype, and after 16 hours. Transcriptomic changes closely mimic the transcriptome changes seen when ChvG-ChvI is activated in *A. tumefaciens*, including downregulation of genes for motility and chemotaxis and upregulation of genes for exopolysaccharide biosynthesis and T6SS. Here we experimentally validate the RNA-seq results, confirming the impacts of PBP1a depletion on the physiology and behavior of *A. tumefaciens*.

RESULTS

PBP1a depletion prevents proper microcolony formation

Here, we grew PBP1a depleted cells on agarose pads and saw that these cells exhibit surface spreading rather than forming closely packed microcolonies (Fig 1A). Additionally, when centrifuging cultures of PBP1a-depleted cells, we

observed that the cells did not pellet (S1 Fig). Considering the possibility that depletion of PBP1a somehow signals for these phenomena, we decided to look at RgsM, another enzyme required for polar elongation. Previous work points to RgsM activity being required for incorporation of nascent PG by PBP1a [17]. However, depletion of RgsM did not cause surface spreading (Fig 1A) indicating that an imbalance of PG hydrolysis and synthesis triggers spreading and the inability pellet in *A. tumefaciens*. Deletions of genes encoding other high molecular weight PBPs and *mtgA*, a PG transglycosylase, did not induce spreading (Fig 1B).

Timelapse microscopy revealed that after ~6 hours of PBP1a depletion cells spread apart, though the movement of cell appears to be confined within a relatively small region of the agarose pad (Fig 1C, S1 Movie). Since spreading is confined and occurs over the course of many hours, we suspected that this phenomenon was not simply caused by the activation of swimming motility.

PBP1a depletion induces global transcriptome changes

To understand the spreading phenotype caused by PBP1a depletion, we compared the transcriptomes of cells at the onset or late stage of the surface spreading phenotype. Cells were grown with or without the inducer Isopropyl β-D-1-thiogalactopyranoside (IPTG) for *mrcA,* encoding PBP1a, expression for 6 or 16 hours (Fig 2A). As a baseline, we compared transcriptional profiles of WT in the presence and absence of IPTG to the PBP1a depletion strain in the presence

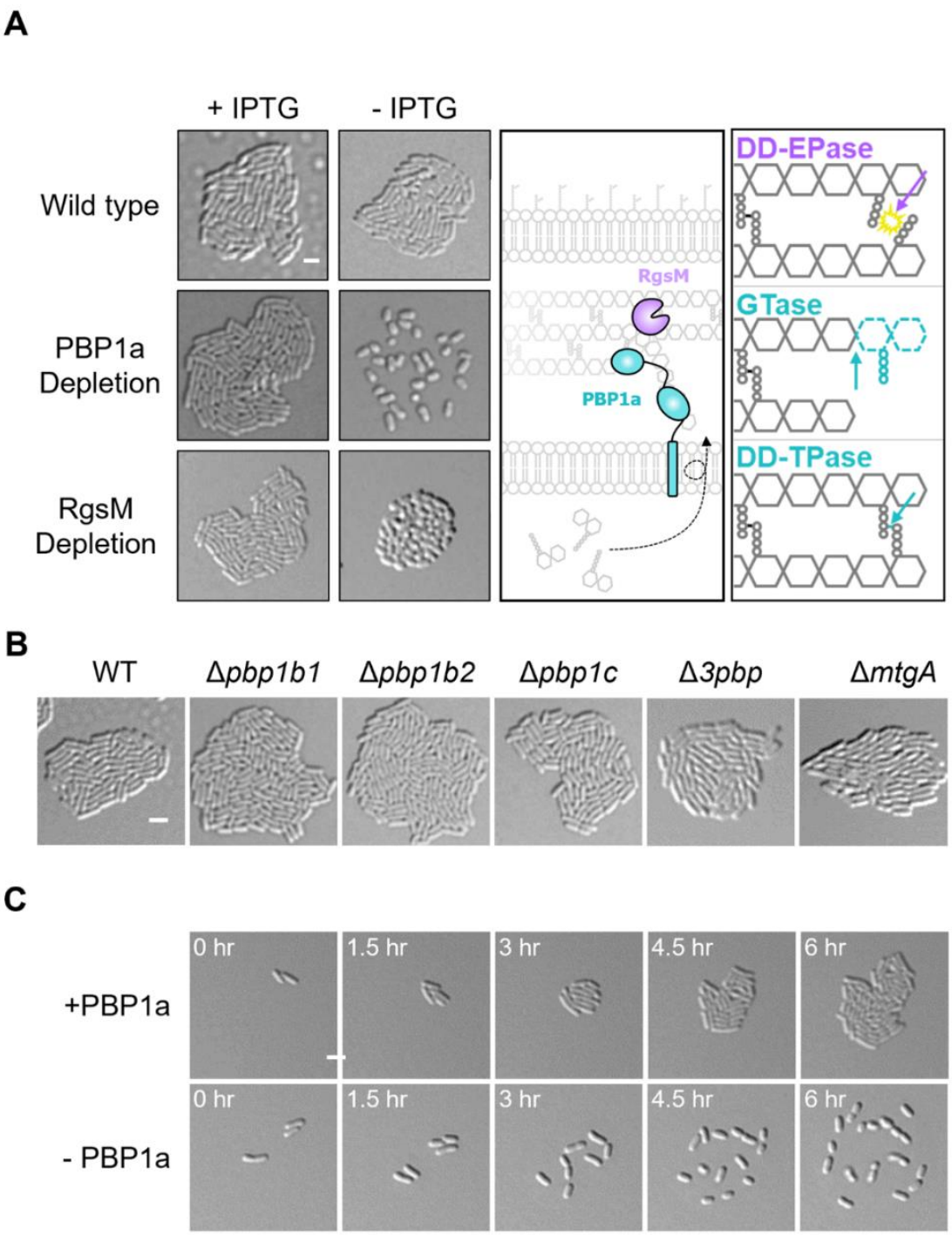

Figure 2.1. The PBP1a depletion fails to form microcolonies independent of flagellar motility. **A.** Micrographs of wildtype, PBP1a depletion, and RgsM depletion with or without 1mM IPTG inducer. Each strain was grown to exponential phase, spotted on an ATGN agar pad, allowed to grow for 16 hours,

and imaged by DIC microscopy. Scale bar depicts 2μm. The graphic depicts the working model that RgsM DD-endopeptidase activity is required for incorporation of nascent glycan strands into the preexisting peptidoglycan (PG) macromolecule by PBP1a. RgsM cleaves DD-crosslinks, PBP1a glycosyltransferase activity incorporates lipid II into the PG glycan strand, PBP1a DD-transpeptidase activity crosslinks the peptide stem of the nascent PG, fully incorporating it into the macromolecule. EPase, endopeptidase; GTase, glycosyltransferase; TPase, transpeptidase. **B.** Micrographs of wild type, Δpbp1b1, Δpbp1b2, Δpbp1c, and ΔmtgA. Each strain was grown to exponential phase, spotted on an ATGN agar pad, allowed to grow for 16 hours, and imaged by DIC microscopy. Scale bar depicts 2μm. **C.** Time-lapse microscopy of the PBP1a depletion grown on an agar pad with or without 1mM IPTG inducer. DIC images were acquired every 10 minutes. Time is shown in hours. For the -PBP1a strain, cells were washed 3X with ATGN media and grown at 28 C with shaking for 4 hours before cells were spotted on an agar pad for imaging.

of IPTG. The addition of IPTG did not alter gene expression profiles of WT cells, and only minor differences were apparent between the PBP1a depletion strain background and WT when both strains are grown in the presence of IPTG (S2 Fig). We next compared differences in the PBP1a replete strain to the PBP1a depleted strain at either 6- or 16-hours post depletion (Fig 2A). Using a false discovery rate of < 0.05 and log2 fold change (L2FC) > 2.0, we identified 91 and 306 genes that were differentially expressed in the + PBP1a strain compared to the 6- or 16-hour depletion, corresponding to 2% and 6% of the total genes, respectively.

Overall, we observed large-scale changes in a diverse and widespread range of genes that are regulated in response to PBP1a depletion. Initially, the response to PBP1a depletion is primarily mediated by chromosomally encoded rather than plasmid encoded genes. *A. tumefaciens* has a circular chromosome, which houses roughly half (51.7%) of the protein-coding genes, a linear chromosome (34.7%) and two mega plasmids, the At plasmid (10%) and Ti plasmid (3.6%). Most of the genes differentially expressed at both time points during PBP1a depletion were encoded on the linear and circular chromosomes (Fig 2A). Most of the differentially abundant genes from the 6-hour timepoint were also present in the 16-hour timepoint. For several of these genes, the magnitude of differential transcript abundance remained relatively constant. For example, the response regulator ChvI, had an increased relative abundance early in response to PBP1a

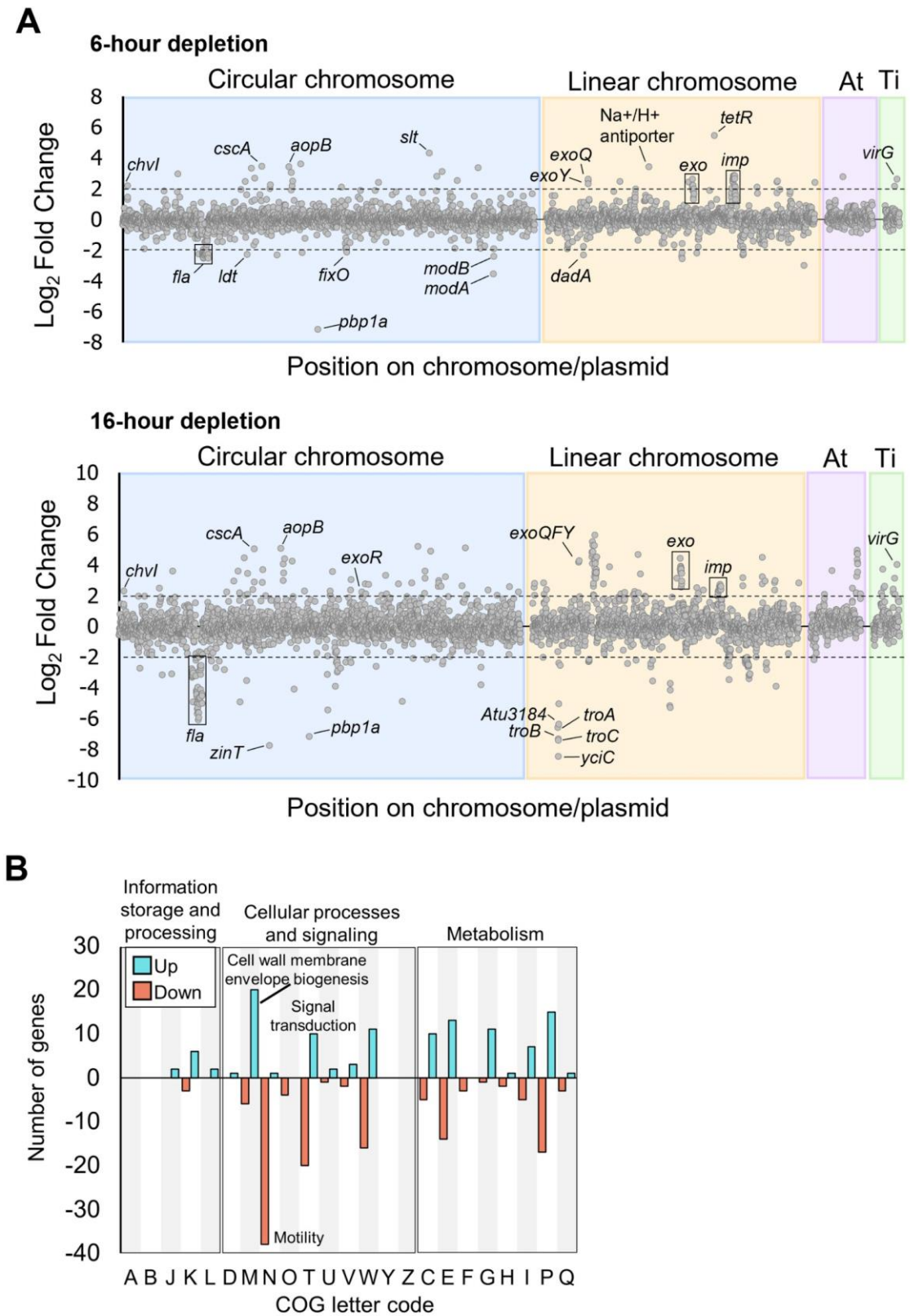

Figure 2.2. Analysis of the PBP1a depletion transcriptomes by RNA-seq. **A.**

Plots comparing Log2Fold Change of the + PBP1a transcriptome to that of the - PBP1a 6-hour transcriptome and to that of the 16-hour depletion. Gray dots represent a single transcript, and the dotted lines represent +/- 2.0 Log2Fold Change threshold. Plots are delimited by chromosome and mega plasmid. **B.** COG categorical analysis of the 16-hour depletion of PBP1a. Pink, downregulated; Cyan, upregulated.

depletion that remained constant in the 16-hour timepoint. In contrast, several genes displayed a continuous increase or decrease in transcript abundance between the 6- and 16-hour timepoints, including genes that encode proteins necessary for assembly of flagella and type 6 secretion system machinery. Finally, several genes were only differentially abundant at the 16-hour timepoint, including many genes encoding proteins important for cell envelope homeostasis such as the Tol-Pal system [18], and >30 ABC transporters.

To further categorize the diverse set of differentially abundant genes we identified Clusters of Orthologous Groups (COGs) in the 16-hour timepoint and classified them based on functional categories represented by a single letter code (Fig 2B)[19,20]. The most affected COG category was motility (N). Decreased abundance of mRNAs containing genes which encode structural flagella proteins further supports the hypothesis that the spreading phenotype is independent of flagella-based motility. The COG category with the largest proportion of increased differentially abundant genes was cell wall, membrane, and envelope biogenesis (M). Notably, no significant changes in the transcripts of other penicillin-binding proteins or glycosyltransferases were observed in response to loss of PBP1a (S1 Table). However, significant changes in transcripts encoding cell wall remodeling enzymes such as LD-transpeptidases, endopeptidases, and soluble lytic transglycosylases were detected (S1 Table). Atu0844, an LD-transpeptidase, was strongly downregulated suggesting it may play an important role in polar growth alongside PBP1a. Additionally, one

putative β-lactamase gene, Atu0933, was strongly upregulated, which may provide a strategy to protect against cell wall damage. In addition, many of the genes found in this COG category encode cell envelope homeostasis and osmotic stress response proteins, including the Tol-Pal system, several outer membrane proteins (i.e. AopB), and periplasmic sensors (i.e. CreD).

At the 16-hour timepoint, the largest changes to cellular metabolism occurred in the inorganic ion transport and metabolism (P) and amino acid metabolism and transport (E) COG categories, suggesting a shift in nutrient uptake and metabolism. These changes resemble genes under control of RpoH1 in *Sinorhizobium meliloti,* which regulates expression of genes encoding ABC transporters, cell wall biosynthetic machinery, and membrane biogenesis proteins [21]. Furthermore, the 16-hour depletion of PBP1a shows a notable upregulation in transcription of Atu2445, encoding an RpoH ortholog (L2FC = 0.66), a stark increase from the 6-hour depletion (L2FC = 0.04) suggesting that the sigma factor RpoH may contribute to the observed changes in associated with nutrient uptake and metabolism during cell wall stress.

Interestingly, the six most downregulated genes in the 16-hour timepoint, with the exception of *mrcA*, encoding PBP1a, were *yciC* (Atu3181), *zinT* (Atu1049), *troC* (Atu3180), *troB* (Atu3179), *troA* (Atu3179), and Atu3184, all of which are major components of cytoplasmic zinc uptake in *A. tumefaciens* (Fig 2A, bottom) [22].

We also observed large increases and decreases in the transcript abundance of signal transduction genes. Transcription of *exoR* (Atu1715), *chvG* (Atu0033), and *chvI* (Atu0034) were upregulated at both the 6-hour (L2FC = 0.995, 1.42, and 2.18) and 16-hour (L2FC = 2.20, 1.41, and 2.27) depletions of PBP1a. Transcription of genes encoding additional signalling systems were also upregulated (S3 Fig, S1 Table).

Transcriptome changes during PBP1a depletion mimic activation of the ChvG-ChvI two-component system.

Transcription of *virG*, encoding a TCS response regulator, was also strongly upregulated in both the 6-hour (L2FC = 2.61) and 16-hour (L2FC = 4.02) timepoints (S3 Fig, S1 Table). Transcription of *virG* has been reported to be upregulated under both host-invasion and virulence-inducing conditions [11]. Because *virG* was also upregulated during depletion of PBP1a, we reasoned that PBP1a depletion may be mimicking one of these two conditions. Using comparative transcriptomics, we compared the 150 most differentially expressed genes (DEGs) against published datasets that simulate host-invasion conditions (Δ*exoR* & pH 5.5) and virulence-inducing conditions (acetosyringone treatment & growth on AB media) [23,24]. We found that L2FC values of the 6-hour PBP1a depletion RNA-seq dataset correlated with the two host-invasion conditions and not with the virulence-inducing datasets, as indicated by the spearmen rho correlation coefficient for each comparison (Δ*exoR*, rho = 0.875; pH 5.5, rho = 0.766) (Fig 3A and S4 Fig). Rho values near 1 indicate similar DEGs between

each dataset. Rho values near 0 would indicate no similar DEGs between each dataset (Fig 3A). Interestingly, each of these two datasets have been implicated in activation of the ChvG-ChvI pathway [9,11]. Correlation with each strongly implicates ChvG-ChvI activation in our RNA-seq dataset, suggesting that depletion of PBP1a may provide a signal leading to changes similar to those described to occur during the transition to a host-invasion lifestyle. While this trend was maintained in the 16-hour timepoint, we observed additional genes that were differentially expressed under depletion of PBP1a, but not in the Δ*exoR* and pH 5.5 datasets (Fig 3A, S4B Fig). Indeed, the rho values for the 16-hour depletion of PBP1a compared to the host-invasion datasets (Δ*exoR*, rho = 0.529; pH 5.5, rho = 0.739 were lower than the 6-hour comparisons. Additionally, we found 215 more genes with L2FC > 2.0 in the 16-hour depletion than in the 6-hour depletion (Fig 3B). Together, these findings suggest that longer depletions of PBP1a may result in the activation of additional regulons beyond ChvG-ChvI.

Overall, a large number and variety of genes are regulated in response to depletion of PBP1a. Although many of these changes in gene expression have been reported previously in response to low pH or deletion of the ChvG-ChvI negative regulator ExoR, these changes have never been associated with loss of a cell wall synthase in *A. tumefaciens*. These observations indicate that there are additional mechanisms that can activate the ChvG-ChvI TCS.

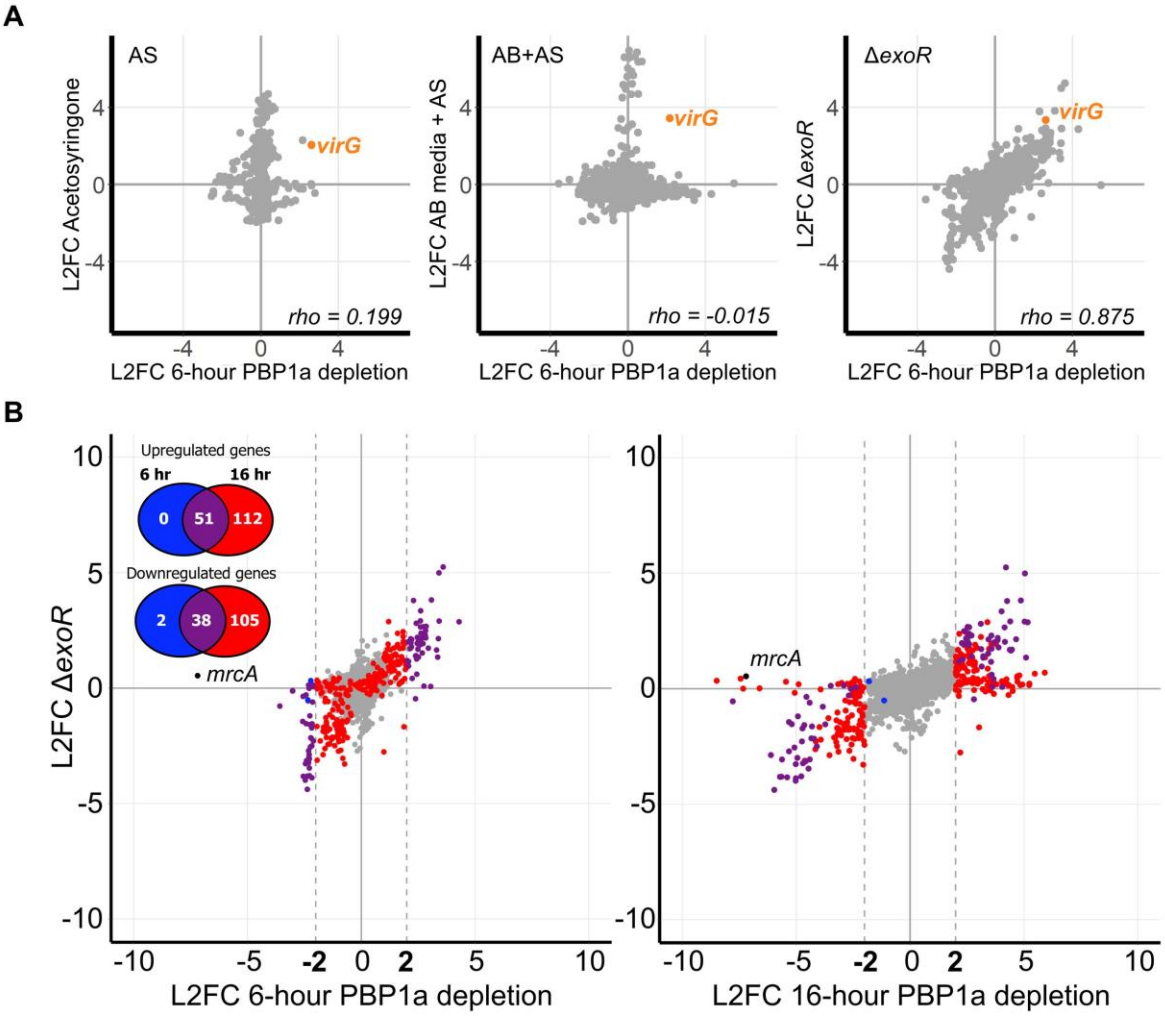

Figure 2.3. The response to the depletion of PBP1a mimics transcriptional changes associated with host invasion. **A.** Correlation scatterplots depicting relationships between the log2fold-change (L2FC) values in the 6-hour PBP1a depletion and transcriptomic data sets taken under simulated virulence-inducing conditions (AS and AB+AS) and under simulated host-invading conditions (Δ*exoR*). Each point represents a unique transcript. AS, acetosyrinogone; AB, Agrobacterium minimal media; rho, Spearman correlation coefficient. **B.** Correlation scatterplots comparing L2FC values of transcripts in the Δ*exoR* microarray to either the 6-hour or 16-hour PBP1a depletion. Each transcript is

colored according to its change in L2FC values from 6 hours of PBP1a depletion to 16 hours of depletion. Gray, no change; Blue, transcript has |L2FC| > 2.0 in the 6-hour but not in the 16-hour depletion; Red, |L2FC| > 2.0 in the 16-hour but not in the 6-hour depletion; Purple, |L2FC| > 2.0 in both the 6-hour and 16-hour depletion.

Succinoglycan overproduction is required for cell spreading

Previous work has clearly associated activation of ChvG-ChvI to a specific transcriptomic pattern involving downregulation of flagellar motility genes and upregulation of T6SS and succinoglycan biosynthesis genes [9,11,25]. Indeed, this same pattern was observed in the 6- and 16-hour PBP1a depletion datasets (Fig 4A). To confirm that the spreading phenotype is unrelated to flagella-dependent motility, we made an in-frame deletion of *rem*, which encodes a transcriptional regulator of genes encoding structural flagella proteins [26,27], in the PBP1a depletion strain. Deletion of *rem* prevents swimming in *A. tumefaciens* and does not impact microcolony formation on agarose pads (Fig 4B). Upon depletion of PBP1a, *rem* mutants continued to spread, suggesting that the cause of this phenotype is independent of flagella-mediated swimming motility (Fig 4B).

All genes in the *imp* and *hcp* operons, which are located on the linear chromosome and encode the structural and toxin proteins of T6SS respectively, are upregulated at both timepoints (Fig 4A). In *A. tumefaciens*, activation of the T6SS results in the production of a contractile nanomachine which delivers effector proteins to antagonize and compete with other bacteria [28]. Among agrobacteria, T6SS is activated by different signals, is important during different stages of the lifecycle, and may be used to acquire nutrients [29]. To determine if the T6SS contributes to the spreading response observed during PBP1a depletion we deleted the intergenic gap between the *hcp* and *imp* operons (ΔT6SSpro). This deletion prevented expression of proteins from both the *hcp* and *imp* operons (S5 Fig) [30]. Cell spreading persisted in ΔT6SSpro during

depletion of PBP1a suggesting that the activation of T6SS is not responsible for this behavior (Fig 4B).

Another possibility is that spreading might be caused by sliding motility, where secretion of a surfactant gives the cells a slippery surface to “slide” across. Notably, *S. meliloti* has been reported to undergo entropy-driven surface spreading during the overproduction of succinoglycan [31]. Succinoglycan is a β-1,4-linked sugar made of glucose and galactose, and is the most abundant exopolysaccharide produced by *A. tumefaciens* and related bacteria [32]. Genes associated with the biosynthesis and secretion of succinoglycan were strongly upregulated in both timepoints. To test if entropy-driven surface spreading is causing PBP1a-depleted *A. tumefaciens* cells to spread, we used a microscopy-based assay to observe succinoglycan production in *A. tumefaciens*. Cells were spotted on agarose pads containing calcofluor white and grown overnight, then imaged using the DAPI filter to detect succinoglycan production (Fig 4C). Wild-type *A. tumefaciens* and the PBP1a replete strains secrete some succinoglycan that enriched near the center of the microcolony (Fig 4C). In comparison, depletion of PBP1a triggers secretion of a large quantity of succinoglycan that defines the boundary of where the cells spread. An in-frame deletion of *exoA*, which encodes a glycosyltransferase required for succinoglycan production in *A. tumefaciens* [33], prevents succinoglycan production (Fig 4D). During PBP1a depletion, microcolony formation is restored in the Δ*exoA* mutant (Fig 4D).

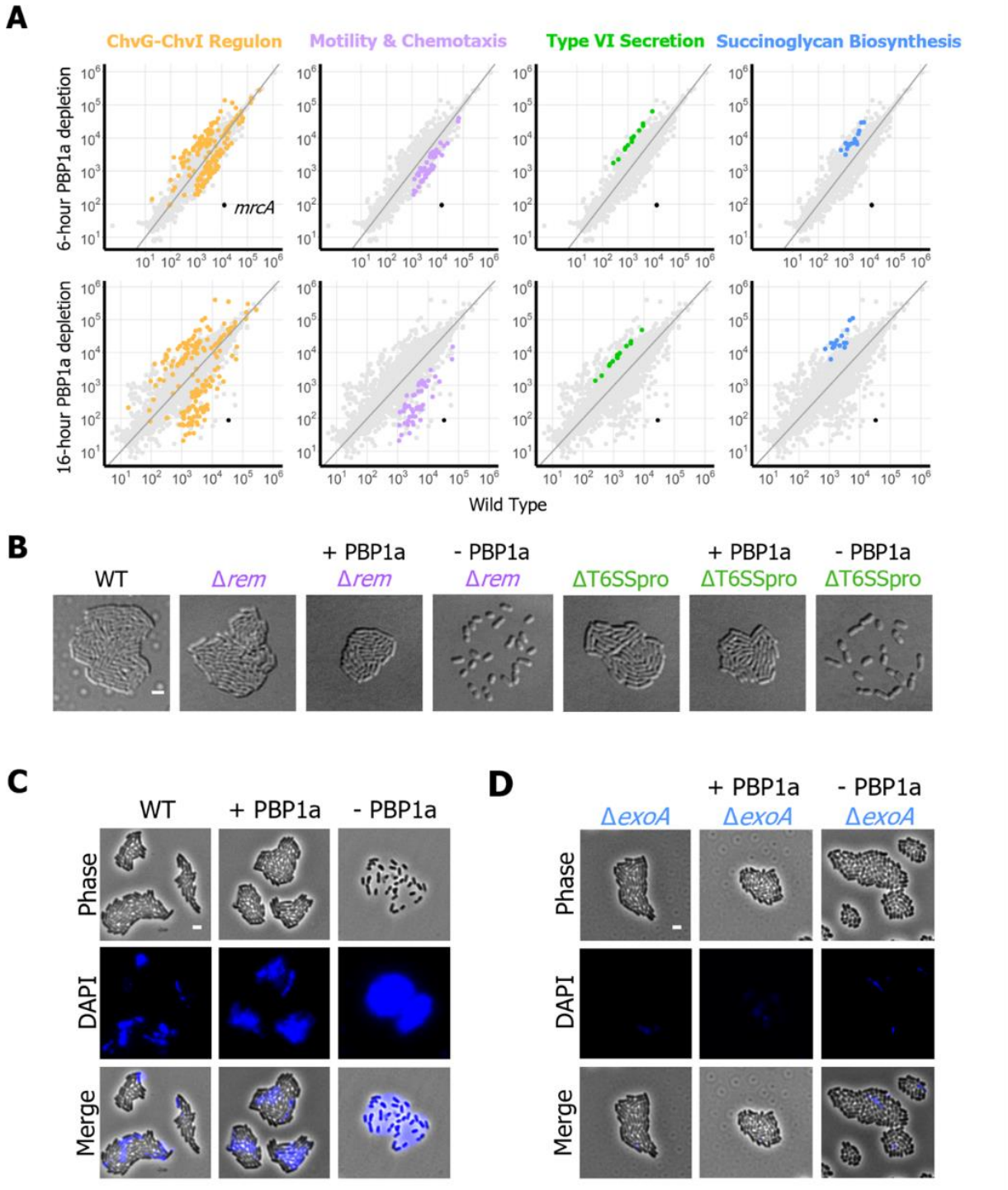

Figure 3.4. Succinoglycan overproduction is a conserved response to PBP1a depletion and results in failed microcolony formation. **A.** Scatter plots depicting RPKM values of the 6-hour and 16-hour compared to wild type. Each point

represents a unique transcript. Points are colored by category. Gold, ChvG-ChvI regulon; Lavender, Motility and Chemotaxis; Green, Type VI Secretion; Blue, Succinoglycan Biosynthesis; Black, *mrcA* (encoding PBP1a). **B.** Micrographs of wild type, Δ*rem*, PBP1a replete Δ*rem*, PBP1a depleted Δrem, ΔT6SSpro, PBP1a replete ΔT6SSpro, and PBP1a depleted ΔT6SSpro. Each strain was grown to exponential phase, spotted on a 1% ATGN agar pad containing 1mM IPTG if inducing *mrcA*, allowed to grow for 16 hours, and imaged by DIC microscopy. The scale bar depicts 2μm. **C.** Micrographs of wild type, and PBP1a depletion with or without IPTG inducer. Each strain was grown to exponential phase and spotted on a 1% ATGN agar pad containing 25μg/mL calcofluor white and 1mM IPTG if inducing *mrcA*. Each was allowed to grow for 16 hours and imaged by phase microscopy with and without the DAPI filter for visualizing calcofluor-stained succinoglycan. **D.** Micrographs of Δ*exoA* and PBP1a depletion Δ*exoA*, with or without IPTG inducer. Strains were grown and imaged as described for panel C.

Together, these data illustrate that succinoglycan overproduction contributes to the surface spreading of the PBP1a depletion.

Deletion of *chvG* or *chvI* results in hypersensitivity to β-lactam antibiotics

Since activation of succinoglycan production is known to be part of the ChvG-ChvI regulon, we next wanted to test if the PBP1a depletion is activating SGN production through the ChvG-ChvI signaling pathway. We made an in-frame deletion of *chvI* in the PBP1a depletion background and found *chvI* mutants replete with PBP1a appear morphologically wild-type when grown in minimal media (S6A Fig). However, PBP1a-depleted Δ*chvI* cells were extremely sick. Previously we reported that the PBP1a depletion produces viable daughter cells for up to 5-6 generations [16], however, the PBP1a-depleted Δ*chvI* strain was incapable of a single division event. Instead, the cells exhibited growth arrest and cell lysis shortly after depletion initiation (S6A Fig, S2 Movie).

To further assess the enhanced sensitivity of Δ*chvI* to PBP1a depletion, we identified an antibiotic that likely targets PBP1a enzymatic activity. Treatment with cefsulodin at a concentration of 20 μg/mL resulted in a cell spreading phenotype similar to the PBP1a depletion (Fig 5A). The presence of cefsulodin induces spreading in the triple PBP mutant (Δ3*pbp*) which lacks all of the high molecular weight PBPs other than PBP1a [16] suggesting that targeting of PBP1a is sufficient to cause this phenotype (Fig 5A). Treatment with cefsulodin

results in short, round cells, phenocopying the PBP1a depletion (Fig 5B). In addition, the ∆3*pbp* mutant does not have obvious resistance to cefsulodin as would be expected if a primary drug target was absent (Fig 5C and S6C Fig). Together, these data suggest that cefsulodin targets the transpeptidase activity of PBP1a in *Agrobacterium tumefaciens*, similar to reported cefsulodin specificity in *E. coli* [34]. Next, we observed relative cefsulodin sensitivities in WT, ∆*chvI*, and Δ*exoR* strains. Remarkably treatment with 10 μg/mL of cefsulodin deceases viability of Δ*chvG* and Δ*chvI* cells by 5 orders of magnitude compared to either WT or Δ*exoR* cells (S6B Fig). Furthermore, growth curve analysis reveals that Δ*chvI* cells are unable to grow within an hour of exposure to cefsulodin at concentrations that are sublethal for WT cells (Fig 5C and S6C Fig). Overall, these findings suggest that the ChvG-ChvI TCS is essential for growth when the activity of the major PG synthase is inhibited either chemically or genetically.

We broadened our investigation by testing Δ*chvG* and Δ*chvI* against ten additional antibiotics: four that block protein synthesis (chloramphenicol, tetracycline, erythromycin, and gentamicin); one that blocks DNA replication (nalidixic acid); one that blocks transcription (rifampin); and four other cell wall synthesis inhibiting β-lactam antibiotics (meropenem, cefoxitin, ampicillin, and ticarcillin). To measure changes in sensitivity to each antibiotic compared to wildtype, Δ*chvG* and Δ*chvI* were spread on ATGN minimal media and disks containing each antibiotic were applied. Diameters of the zones of inhibition (ZOI)

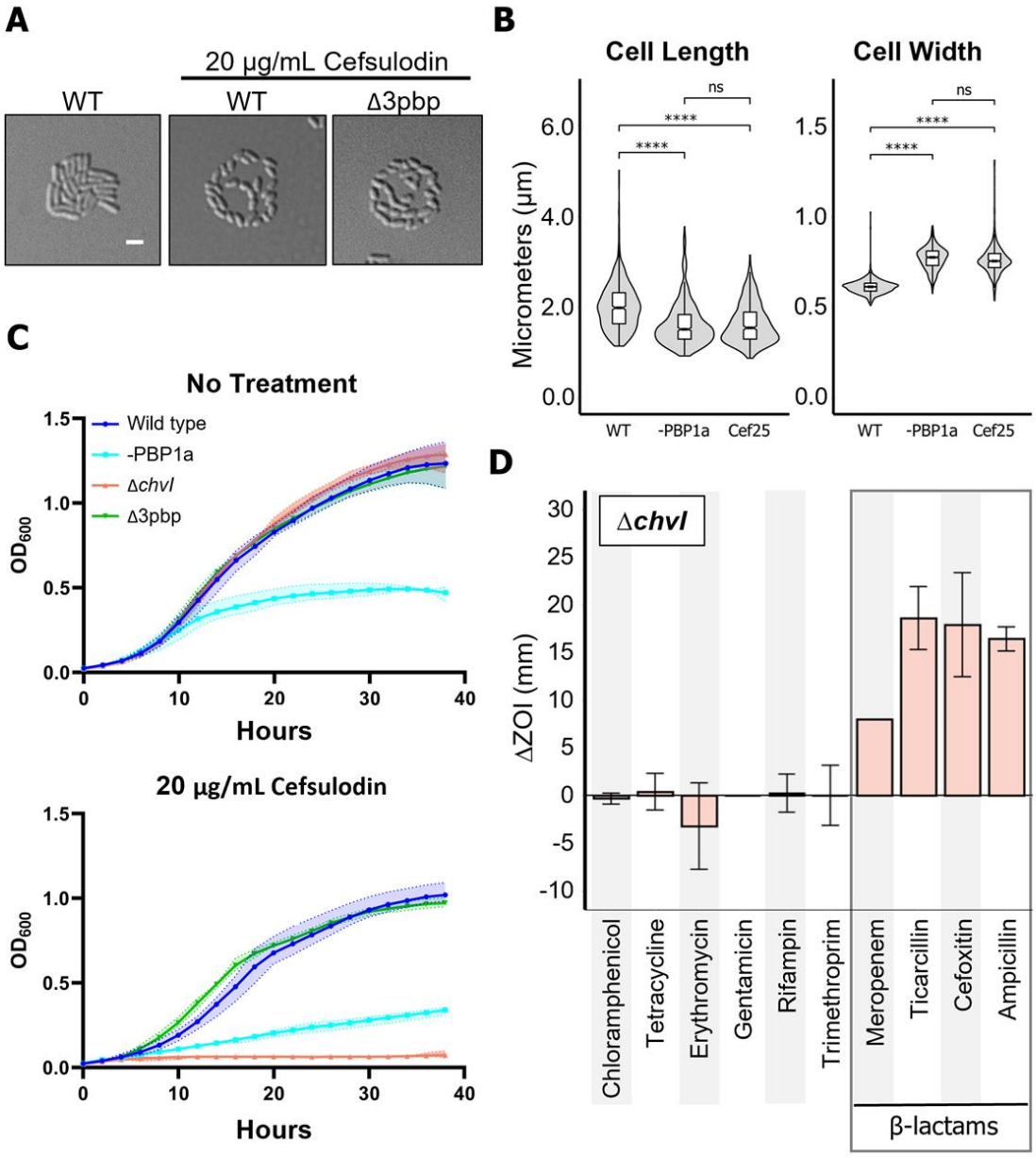

Figure 3.5. The ChvG-ChvI TCS is conditionally essential under treatment with β-lactam antibiotics. A. Micrographs of untreated and cefsulodin-treated cells. Wild-type and Δ3pbp cells were grown to exponential phase, spotted on a 1% ATGN agar pad with or without 20 µg/mL cefsulodin and allowed to grow for 16 hours. Each strain was imaged by DIC microscopy. B. Box plots comparing cell length and width between wild-type, PBP1a-depleted, and cefsulodin-treated

cells. ns, not significant; ****, p < 0.00005. C. Growth curves of WT, -PBP1a, ΔchvI, and Δ3pbp in the absence (top) and presence of 20 μg/mL cefsulodin (bottom). D. Graph depicting the change in zone of inhibition from wildtype in ΔchvI against ten different antibiotic disks. Error bars represent +/- 1 standard deviation from the mean.

were measured and the difference in ZOIs for each mutant strain compared to wildtype are shown (Fig 5D and S6D Fig). Of the antibiotics tested, Δ*chvG* and Δ*chvI* showed increased sensitivity only to β-lactam antibiotics, suggesting specificity of the ChvG-ChvI pathway in conferring resistance to this antibiotic class.

ChvG and ChvI are conserved in Alphaproteobacteria but the presence of ExoR is more constrained

The absence of PBP1a activity at the growth pole during elongation activates ChvG-ChvI, the canonical host-invasion pathway of *Agrobacterium tumefaciens*. The ChvG-ChvI pathway is most well known to be activated by environmental changes associated with conditions favorable for plant association, yet this TCS is retained in many non-plant-associated Alphaproteobacteria (Fig 6). Remarkably, while ChvG-ChvI is conserved in a large proportion of Alphaproteobacteria, ExoR is not (Fig 6) [6]. Predicted structures of the sensor domains of ChvG in bacteria with ChvG-ChvI orthologs show two structural loops (L1 and L2; Fig 6, S7-8 Fig). While L2 is conserved across the orthologous structures, L1 is expanded solely in the Rhizobiales (S8 Fig). This expansion coincides with the retention of ExoR, making it a compelling target for ExoR-ChvG association studies (Fig 6). Structural loops are often sites of protein-protein interaction and can be vital to protein function [35]. To explore the possibility that these loops may play a role in the docking of ExoR we used AlphaFold-Multimer to detect the interaction interface between ExoR and ChvG

[36]. Indeed, an interaction site in L1 comprised of hydrogen bonding and an electrostatic pocket was revealed (Fig 7A). This may indicate that ExoR-dependent repression of ChvG is dependent on L1. Chen et al. identified suppressor mutants in *S. meliloti* to a ChvI mutant displaying decreased activity (S9 Fig) [37]. Two suppressors were substitutions that disrupted ExoR interaction with ChvG (also known as ExoS in *S. meliloti*), G76C and S156Y. S156Y falls near the predicted interaction site between L1 and ExoR (S9 Fig). A computational study by Wiech et al. proposed three possible interaction interfaces between ChvG (ExoS) and ExoR, of which site B is in agreement with our putative interaction interface (S9 Fig) [38].

Either proteolysis of ExoR or deletion of *exoR* is sufficient to elicit transcriptional changes associated with activation of ChvG-ChvI, including the upregulation in genes associated with succinoglycan biosynthesis [6,7,11,39]. We reasoned that if ChvG-ChvI activation initiates surface spreading, we should be able to detect the spreading in an *exoR* mutant. While Δ*exoR* microcolonies appear slightly less crowded than wild type microcolonies, they do not phenocopy the PBP1a depletion nor treatment with cefsulodin (Fig 7B). Remarkably, cell spreading is induced by the Δ*exoR* mutant by the presence of cefsulodin (Fig 7B). To monitor ExoR proteolysis we introduced a C-terminal FLAG-tagged copy of ExoR into the wild type and PBP1a depletion strains (S10 Fig). While elevated levels of the ExoR cleavage product ($ExoR_{C20}$) were readily detected by acid-induction (pH 5.5), depletion of PBP1a for 6 hours and 16 hours in neutral conditions (pH 7.0)

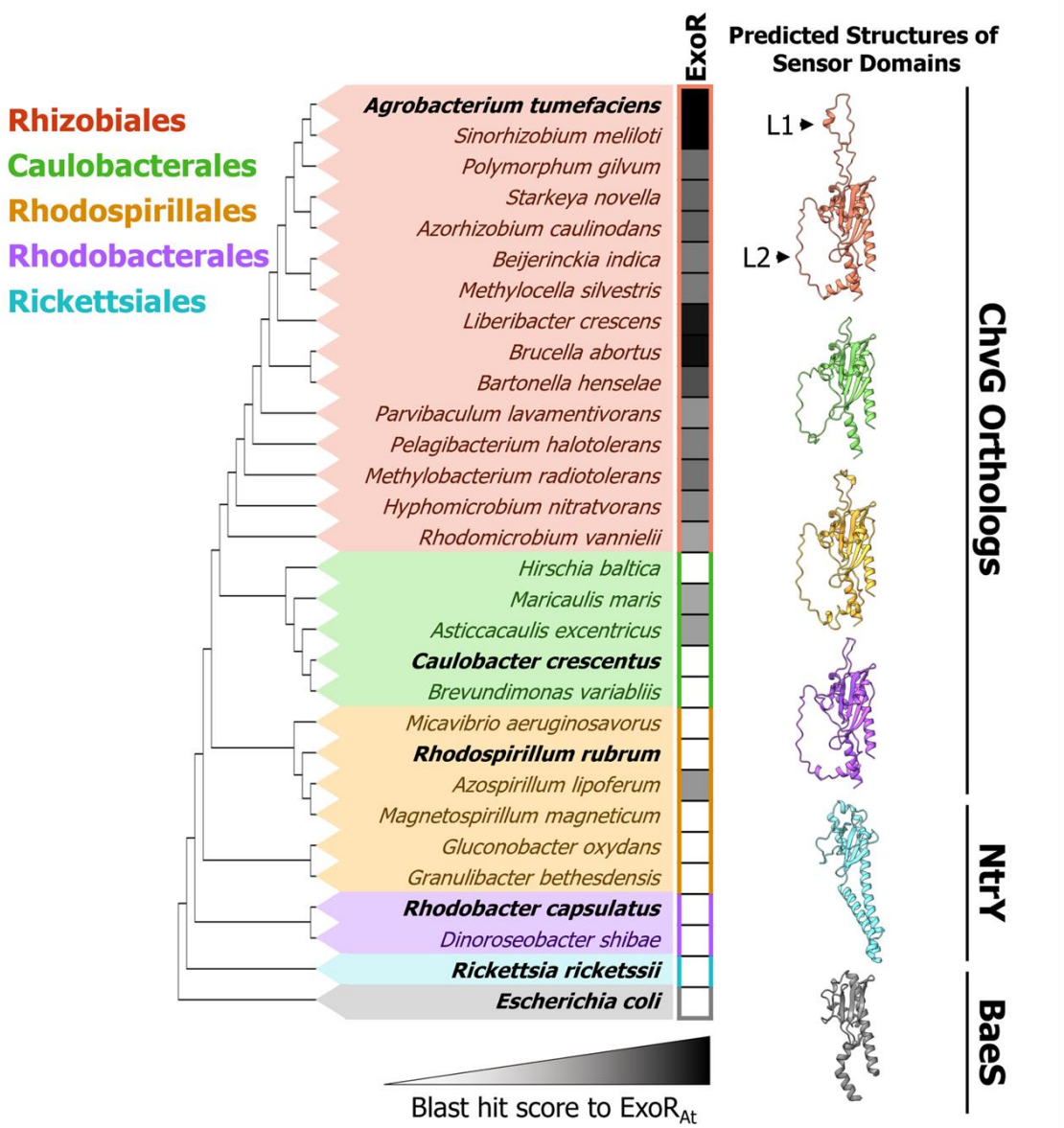

Figure 3.6. Conservation constraints of ExoR suggest conserved ChvG-ChvI response is independent of ExoR. Maximum parsimony tree constructed using MUSCLE sequence alignment [67] on the periplasmic regions of ChvG orthologs. In clades that don't have a ChvG ortholog, the protein with the highest sequence similarity to ChvG was used instead. Conservation of ExoR was calculated using blast max scores from top hits when protein blasting [66] ExoR from Agrobacterium tumefaciens against each species in the tree. Phyre2 [71]

predicted structures of periplasmic domains of ChvG orthologs from representatives (bold) in each genus are shown. Conserved structural loops are denoted as L1 and L2.

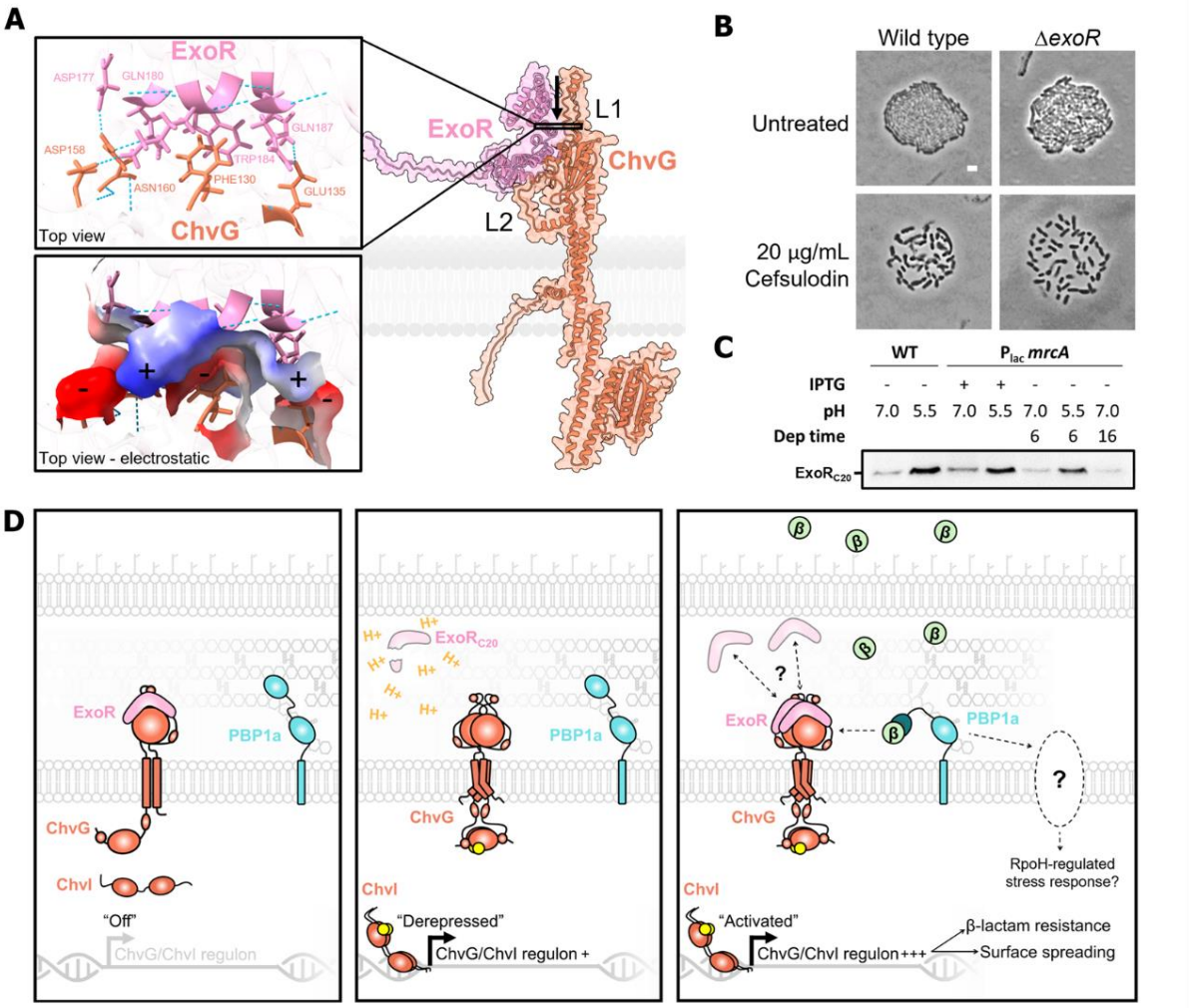

Figure 7. Activation of ChvG-ChvI can proceed independently of ExoR derepression. **A.** Predicted interaction site between ExoR and ChvG through AlphaFold-Multimer structure prediction. Insets show the top-down view of the interaction site with hydrogen bonding and electrostatic surface display. **B.** Microcolonies of wild type and ΔexoR with and without 20 μg/mL cefsulodin treatment. **C.** Western blot detection of ExoR proteolysis (ExoRC20) with anti-FLAG against ExoR-FLAG. **D.** Working model of activation of ChvG-ChvI in *A. tumefaciens*. H+, free proton representing an acidic environment; β, β-lactam antibiotic.

does not result in accumulation of ExoR$_{C20}$ (Fig 7C, S10C Fig). These data are consistent with the phenotypic characterization of Δ*exoR* and together these results suggest that cell wall stress activates the ChvG-ChvI two-component system independently of ExoR.

We hypothesized that the ChvG-ChvI pathway may confer resistance to cell wall stress in other host-associated Rhizobiales. Indeed, depletion of PBP1a in *Sinorhizobium meliloti* causes cells to spread suggest activation of ChvG-ChvI (ExoS-ChvI) pathway (S11A Fig). Like *A. tumefaciens*, this response is specific to depletion of PBP1a and is not triggered by deletion of the 5 other high molecular weight PBPs. These results suggest that cell wall stress may be a well conserved trigger for activation of ChvG-ChvI pathways in the Rhizobiales. Notably, *C. crescentus* does not spread upon treatment with 80 μg/mL of cefsulodin (S11B Fig), despite recent findings that ChvGI likely confers resistance at this concentration [12]. While *S. meliloti* and *A. tumefaciens* encode succinoglycan biosynthesis operons, *C. crescentus* does not. These findings support the hypothesis that the ChvG-ChvI response to cell wall stress is conserved across Alphaproteobacterial species that have orthologs of ChvG-ChvI.

DISCUSSION

Why is ChvG-ChvI TCS activated upon inhibition of polar PG synthesis in *A. tumefaciens*? PBP1a depletion results in a compositional shift in cell wall

muropeptide composition and cell wall crosslinking [16]. Here we find that PBP1a depletion causes upregulation in transcription of $_{LD}$-transpeptidases, endopeptidases, and soluble lytic transglycosylase, indicating cells are attempting to compensate for compromised cells walls. Remarkably, transcripts from these same genes are upregulated in the Δ*exoR* and pH 5.5 datasets, suggesting that remodeling of the cell wall is a part of the ChvG-ChvI regulon. While the role of cell wall remodeling during host-invasion is unclear it is possible that these modifications may be protective for the bacterium when host associated. The upregulation in transcription of genes encoding AopB and the Tol/Pal system may indicate that PBP1a-depleted cells are succumbing to osmotic pressure, a possible explanation for the increase in cell width in PBP1a-depleted and cefsulodin-treated cells (Fig 5B). The increased sensitivity to mecillinam, vancomycin, cefsulodin, and moenomycin in *C. crescentus* ChvGI mutants [12] along with our observation that ChvG-ChvI mutants in *A. tumefaciens* are hypersensitive to β-lactam antibiotics suggests that this pathway may confer resistance to antibiotics inhibiting cell wall synthesis. This aligns well with previous studies in *S. meliloti* demonstrating that *chvG-chvI* mutants have a unique lipopolysaccharide profile [40] and increased sensitivity to detergents [41]. In addition, the *Brucella abortus* ChvG-ChvI orthologs (BvrS-BvrR) initiate extensive transcriptional changes associated with the outer membrane [42–44]. Together, these findings indicate a conserved role within the Alphaproteobacteria for the ChvG-ChvI TCS in sensing and responding to envelope stress. Possible signals may include the accumulation of cytoplasmic peptidoglycan precursors

such as lipid II, increased levels of naked glycan strands in the cell wall, or more conventional stress responses due to osmotic sensitivity [45]. Notably, Gieger et al. found that a phospholipid mutant of *S. meliloti* activates ChvG-ChvI (ExoS-ChvI) in an ExoR-independent manner [46]. The authors proposed that absence of phosphatidylcholine, a major membrane phospholipid causes a conformational change in ChvG, initiating autophosphorylation. It is tempting to consider a similar type of activation during depletion of PBP1a, but our observation that the depletion of *A. tumefaciens* RgsM does not induce surface spreading (Fig 1A) hints that increased cell wall hydrolysis may be responsible for activation of the ChvG-ChvI pathway. While our findings suggest a conserved signal in ChvG-ChvI activation, further studies will need to be conducted to identify the signal(s), determine if they are species-specific, and explore the conditions which lead to signal production.

If there is a conserved role in sensing cell wall stress, why would this pathway be required for host invasion within *Agrobacterium tumefaciens*? One explanation could be that during plant colonization, *A. tumefaciens* decreases cell wall biogenesis to form cells which are relatively persistent in order to evade host recognition and survive the harsh *in plantae* environment [47]. Alternatively, perhaps the integrity and composition of the cell wall is routinely monitored and used as a signal for the activation of pathways associated with lifestyle choice. Decreased activity of PBP1a may mimic one or more of the conditions *A. tumefaciens* and *S. meliloti* encounter during host-invasion, leading to the

activation of ChvG-ChvI. Another possibility is that the absence of PBP1a activity leads to a destabilization of the polar growth complex leading to decreased cell envelope integrity. It will be of interest to determine if other components of the polar growth complex such as GPR [48], RgsP [49], or PopZ [50,51] have increased sensitivity to β-lactam antibiotics and induce surface spreading. This possibility is in agreement with the observation in *C. crescentus* that resistance to cell wall targeting antibiotics is dependent on factors such as TipN that maintain the integrity of the cell envelope [13].

The overproduction of succinoglycan provides cells with passive protection against several stresses *A. tumefaciens* may encounter during host invasion including detergents, salt, acidity, heat, antimicrobial peptides, and reactive oxygen species [32,33]. Production of succinoglycan may also help protect against cell-wall-synthesis targeting antibiotics produced by competing bacteria and fungi in the soil. However, succinoglycan production is taxonomically constrained within plant-host-associated bacteria, indicating that there are other conserved mechanisms regulated by ChvG-ChvI in resistance to these cell envelope stressors. The surface spreading phenomenon that we connected to overproduction of succinoglycan and that has been previously described in *S. meliloti* [31], may be involved in cell dispersal during host invasion.

The role of ExoR regulation is well established for the acid-induction of ChvG-ChvI [9,11,25]. While deletion of *exoR* upregulates expression of succinoglycan

biosynthesis genes [11], it is insufficient to initiate surface spreading. Three pieces of evidence indicate that activation of ChvG-ChvI during cell wall stress proceeds independently of ExoR. First, ExoR conservation is a characteristic of Rhizobiales, but the ChvG-ChvI two-component system is more broadly conserved in Alphaproteobacteria. Second, Δ*exoR* is not more resistant to cefsulodin than wild type. Finally, proteolysis of ExoR occurs in low pH conditions, but not during depletion of PBP1a. One possibility is that derepression of ChvG alone is not sufficient and an alternative mechanism of ChvG activation results in a more robust response. Cell wall stress (ie PBP1a depletion, β-lactam treatment) may cause a signal for ChvG activation to accumulate. Alternatively, ChvI binding to DNA may be enhanced by an unknown mechanism under cell wall stress conditions. The observation that both *ΔchvG and ΔchvI* are hypersensitive to cefsulodin (S6B Fig) and other β-lactam antibiotics (Fig 5D and Fig S6C) suggests that ChvG plays an important role in sensing and responding to cell wall stress and not that ChvI is activated through an alternative histidine kinase. The observation that sublethal concentrations of cefsulodin result in a complete block in growth of Δ*chvI* cells (Fig 5C) indicates that ChvI is required for survival during cell wall stress through activation of the ChvGI regulon. Future experiments will be needed to identify the signals which accumulate during cell wall stress, determine if the signal is sensed directly or indirectly by ChvG, and how activation of ChvI is achieved.

Together our findings support a model in which ChvG-ChvI is repressed by ExoR (Fig 7D, left) but can be derepressed by acid through dissociation and proteolysis of ExoR in a Rhizobiales-specific response (Fig 7D, middle). We posit that ChvG-ChvI is activated through a more broadly conserved cell envelope stress response (Fig 7D, right). Lastly, longer periods of PBP1a depletion result in a more general stress response beyond the ChvG-ChvI regulon (Fig 7D, right), which may be mediated by Atu2445, an ortholog of sigma factor RpoH.

Overall, the data presented here are in agreement with recent works in *Caulobacter* [12,13] which suggest that ChvGI activation is important in oligotrophic free-living bacteria as a cell envelope or osmotic stress response. Remarkably, it seems that the ChvG-ChvI pathway has a dual purpose in protecting the bacterium and invading its host in *A. tumefaciens*, and other host-associated Rhizobiales.

MATERIALS AND METHODS

Bacterial strains, plasmids, and growth conditions. A list of all bacterial strains and plasmids used in this study is provided in the Strains and Plasmids Table. *Agrobacterium tumefaciens* C58 and derived strains were grown in ATGN minimal media [52] without exogenous iron at 28°C with shaking. When appropriate, kanamycin (KAN) was used at the working concentration of 300 μg/ml. When indicated, isopropyl β-D-1-thio-galactopyranoside (IPTG) was used as an inducer at a concentration of 1 mM. *Sinorhizobium meliloti* stains were

grown in TY medium [53] at 28°C. When appropriate, KAN was used at the working concentration of 200 μg/ml, gentamycin (GM) was used at 20 μg/ml, and IPTG was used at a concentration of 2 mM. *C. crescentus* strains were grown in PYE medium [54] at 28°C. *E. coli* DH5α and S17-1 λ pir were grown in Lysogeny Broth medium at 37°C and when appropriate 50 μg/ml or 30 μg/ml of KAN were added, respectively.

Construction of plasmids and strains. A list of all primers and synthetic DNAs used in this study is provided in S3 Table. Vectors for gene deletion by allelic exchange were constructed using recommended methods for *A. tumefaciens* [55]. Briefly, 500-bp fragments upstream and 500 bp downstream of the target gene were amplified using primer pairs P1/P2 and P3/P4 respectively. Amplicons were spliced together by SOEing using primer pair P1/P4. The amplicon was digested and ligated into pNTPS139. The deletion plasmids were introduced into *A. tumefaciens* by mating using an *E. coli* S17 conjugation strain to create kanamycin resistant, sucrose sensitive primary integrants. Primary integrants were grown overnight in media with no selection. Secondary recombinants were screened by patching for sucrose resistance and kanamycin sensitivity. Colony PCR with primers P5/P6 for the respective gene target was used to confirm deletion. PCR products from P5/P6 primer sets were sequenced to further confirm deletions.

The ExoR-FLAG expression vector was constructed by amplifying *exoR* without a stop codon using *exoR* Forward and Reverse primers. The PCR amplicon was digested and ligated into pFLGC-2, generating pFLGC-2*exoR-flag,* containing a copy of *exoR* with an in-frame c-terminal flag tag behind a vanillate-inducible promoter which functions constitutively in *A. tumefaciens* [56]. pFLGC-2*exoR-flag* was sequenced using Plasmidsaurus. pFLGC-2*exoR-flag* was introduced into *A. tumefaciens* by mating using the S17 conjugation strain to create kanamycin resistant colonies. Transformation was verified by colony PCR using pVMCS Forward and Reverse primers.

Phase and fluorescence microscopy. A small volume (~1 µl) of cells in exponential phase (OD600 = 0.2 - 0.4) was applied to a 1% ATGN agarose pad as described previously [57]. DIC, phase contrast and epifluorescence microscopy were performed with an inverted Nikon Eclipse TiE and a QImaging Rolera em-c2 123 1K EMCCD camera with Nikon Elements Imaging Software. For time-lapse microscopy, images were collected every ten minutes, unless otherwise stated. For calcofluor agar pad assays, calcofluor was added to agarose pads at a concentration of 25 µg/mL and exposed to DAPI filter for 50 ms. When appropriate agar pads were supplemented with 1mM IPTG. For quantitative image analysis, live cells were imaged using phase-contrast microscopy, and cell length and width distributions of the indicated number of cells per strain were determined as measured using MicrobeJ software [58]. T-

tests were performed using the compare_means() function of the ggpubr R library.

RNA isolation, sequencing and analysis. Four cultures each of WT, WT + IPTG and 12 cultures of + PBP1a depletion cells were grown overnight in 2 ml of ATGN minimal media at 28°C with shaking; the + PBP1a strains and WT + IPTG strains were supplemented with 1mM IPTG. Cells were then pelleted by centrifugation at 7000 x g for 5 minutes. Cell pellets were washed three times with ATGN by centrifugation and resuspension to remove IPTG. After the final wash the cell pellets from WT, WT + IPTG, and four of the 12 + PBP1a strains were resuspended to an OD600 of 0.05 in 6mL ATGN, or ATGN with 1mM IPTG. The other eight + PBP1a strains were resuspended to an OD600 of 0.05 in 6 ml ATGN without IPTG. This resulted in 4 replicate cultures each of WT, WT +IPTG, + PBP1a, - PBP1a_6hr and - PBP1a_16hr. Growth of the cultures was monitored and supplemented with fresh medium as needed so that the OD600 never went over 0.3. RNA was isolated from the -PBP1a_6hr strains after 6 hours of growth, and RNA was isolated from all other strains after 16 hours of growth. To prepare samples, a culture volume equivalent to 6 ml at an optical density at 600 nm (OD600) of 0.2-0.3 was pelleted by centrifugation at 7000 x g for 5 minutes and pellets were resuspended in 1mL of ATGN media and incubated with 2 mL of RNAProtect reagent (QIAgen) for 15 min at room temperature. Cells were lysed with 10 mg lysozyme, and RNA was extracted using the QIAgen RNEasy kit.

DNA libraries for sequencing were constructed following the manufacturer's protocol with reagents supplied in Illumina's TruSeq mRNA stranded sample preparation kit without the steps to enrich for poly-A mRNA. The sample concentration was determined by Qubit flourometer (Invitrogen) using the Qubit HS RNA assay kit, and the RNA integrity was checked using the Fragment Analyzer automated electrophoresis system. Briefly, RNA is fragmented, double-stranded cDNA is generated from fragmented RNA, and the index containing adapters are ligated to the ends. The amplified cDNA constructs were purified by addition of Axyprep Mag PCR Clean-up beads. The final construct of each purified library was evaluated using the Fragment Analyzer automated electrophoresis system, quantified with the Qubit flourometer using the Qubit HS dsDNA assay kit, and diluted according to Illumina's standard sequencing protocol for sequencing on the NextSeq 500.

For all samples, when adapter sequence was detected, it was removed using cutadapt (0.16) [59]. All samples were purged of reads that mapped to transcripts for rRNA genes using bowtie2 (2.3.4.3) [60]. The reads were then mapped to the *A. fabrum* str. C58 genome using STAR (version 2.5.4b) [61], which also produces the number of read counts per gene. The index files used by STAR were derived from the files *Agrobacterium*_fabrum_str_c58.ASM9202v1.dna.toplevel.fa and *Agrobacterium*_fabrum_str_c58.ASM9202v1.40.gtf, both of which are part of Ensembl release 40 (http://bacteria.ensembl.org/index.html). Pairwise

comparisons were performed to test for differential expression of genes using the Bioconductor package DESeq2 [62]. Gene annotations were collected from the annotations included with the file of cDNAs also at Ensembl *Agrobacterium*_fabrum_str_c58.ASM9202v1.cdna.all.fa.gz.

COG functional annotation. Amino acid sequences for all proteins in *A. tumefaciens* were downloaded in a single FASTA file from GenBank and uploaded to EGGNOG-MAPPER [63,64]. COG terms were outputted, and Python code was written to pull out transcripts from 16-hour depletion of PBP1a with L2FC > 2.0 or < -2.0. Some transcripts had multiple COG annotations and were therefore replicated for visualization according to the number of annotations it had.

Comparative transcriptomics. Transcripts and L2FC values from each dataset were opened in Python code written to screen for and exclude any genes that were not present in both datasets. Statistics and visualization was done in R. Spearman correlation statistical test was run on the L2FC of the 150 most differentially expressed genes in the PBP1a depletion and their corresponding L2FC values in the comparison dataset.

Cell viability assays. For cell viability spot assays, cultures were grown overnight and diluted to an OD_{600} = 0.05 and serially diluted in ATGN and spotted

on ATGN agar plates containing antibiotics as indicated. Four microliters of each dilution was spotted and plates were incubated at 28°C for 48 h before imaging.

Disk diffusion assays. Wild-type, Δ*chvG*, and Δ*chvI* cells were overnight and then knocked down to an OD_{600} of 1.0. Cells were then lawned on ATGN minimal media. Sterile paper disks either soaked in concentrations of each antibiotic or not (blank controls) were applied to the plate. Each plate was grown for ~48 hours at 28°C before being imaged. Zone of inhibition diameters were measured from each image using ImageJ software.

Phylogenetics and structure prediction. A seed of 22 amino acid sequences containing the annotated ChvG sensor domain (PF13755) were initially downloaded from Pfam [65]. Each was blasted against its corresponding proteome to retrieve the full protein sequence [66]. Additional sequences of relevant bacteria such as *S. meliloti, Brucella melitensis,* and *C. crescentus,* were added by blasting the amino acid sequence from *A. tumefaciens* ChvG (Atu0033) against each organism's proteome. All sequences were aligned using MUSCLE and trimmed in Jalview according to Uniprot predicted periplasmic region of Atu0033 [67–69]. A maximum parsimony phylogenetic tree of these sequences was generated using MEGA-X [70].

Each trimmed sequence underwent one-to-one threading in Phyre2 with the complete structure of Atu0033 predicted by AlphaFold as a template [71,72].

Local alignment and a secondary structure weight of 0.1 was used. Structural analysis and structure alignment was done in ChimeraX [73].

The amino acid sequence of *A. tumefaciens* ExoR (Atu1715) was blasted against each organism's proteome and max score values of top hits were recorded. Max score values under 50 were deemed too different and were therefore not considered an ExoR ortholog. Additionally, sequences of each top hit were blasted against the proteome of *A. tumefaciens.* If the top hit was not ExoR, it was also not considered an ExoR ortholog in this analysis.

ExoR-ChvG interaction predictions were made in AlphaFold-Multimer through the Google Colab service [36]. Hydrogen-bonding and electrostatic predictions were made using the ChimeraX software.

Western blot analysis. Two cultures of wild type were grown overnight in 1 mL ATGN each supplemented with 300 µg/mL kanamycin and six cultures of PBP1a depletion were grown in 1 mL ATGN each supplemented with 300 µg/mL kanamycin and 1mM IPTG. Overnight cells were knocked down to an OD600 of 0.1 and allowed to grow in fresh media supplemented with kanamycin and if necessary IPTG for four hours. Cells were pelleted and washed 3 times. One WT pellet and three PBP1a depletion pellets were resuspended in 25 mL ATGN supplemented with 300 µg/mL kanamycin. One of these resuspended PBP1a pellets was also supplemented with 1mM IPTG. The other WT pellet and three

PBP1a pellets were resuspended in 25 mL of ATGN buffered to pH 5.5 with 200 mM MES supplemented with 300 µg/mL kanamycin. One of these resuspended PBP1a pellets was also supplemented with 1mM IPTG. All resuspensions were placed in a shaking incubator at 28^{o}C. WT and +PBP1a cultures were removed when OD600 reached 0.3 - 0.4. The 6-hour PBP1a depletion cultures were monitored for 6 hours, and fresh media was added so that they never rose above an OD600 of 0.4. The 16-hour depletions were monitored for 16 hours with fresh media added so that they never rose above 0.4. No growth was detected in the 16-hour depletion grown at pH 5.5 and this culture was not processed further. All cultures were pelleted at 5000 x g for 15 minutes and resuspended in 1 mL of Qiagen B1 Lysis Buffer and 100 ug/mL of lysozyme was added to each sample. The samples were vortexed at max speed and incubated for 30 minutes at 37^{o}C.

Protein concentrations were measured using a Pierce BCA Protein Assay Kit. Each sample was normalized to 1 µg/mL of protein. 10 µL of 4X loading buffer was added to 30 µL of each sample. All nine protein samples with 4X loading buffer were boiled for five minutes and added to a 4-20% Bis-Tris GenScript *SurePAGE* gel. BlueStain Protein ladder (P007-500) was loaded into the first well. Proteins were transferred to a PVDF membrane cut to the size of the gel using a BioRad Thermo-Blot-Turbo-Transfer device. The membrane was blocked for 1 hour in 20 mL of 5% milk in TBS + 0.05% Tween 20. 1:1000 dilution of HRP-conjµgated Anti-DYKDDDDK mouse monoclonal antibody (Invitrogen) was added, and the membrane was gently shaken overnight at 4^{o}C. The membrane

was washed 3 times with fresh TBS + 0.05% Tween 20 for 5 minutes each. Immediately after wash steps, membranes were transferred to TBS + 0.05% Tween 20 with 1:10000 dilution of goat anti-mouse IgG secondary antibody (Invitrogen) and gently shaken for 1 hour. The membrane was washed 3 times with fresh TBS + 0.05% Tween 20 and then developed for 5 minutes using SuperSignal West Femto Maximum Sensitivity Substrate (34095). The membrane was imaged using a BioRad ChemiDoc Imager.

DATA AVAILABILITY

Raw RNA-seq read files (.fastq) and complete list of differentially expressed genes for each comparison are publicly available through the NCBI Gene Expression Omnibus (GEO) under the accession GSE173921.

ACKNOWLEDGEMENTS

We thank Elizaveta Krol and Anke Becker for providing *Sinorhizobium meliloti* strains and micrographs and Erh-Min Lai for providing antibodies used in this work. We thank Amelia Randich, Alex Quintero, Regis Hallez and members of the Brown lab for critical feedback on this manuscript.

REFERENCES

1. Venturi V, Keel C. Signaling in the rhizosphere. Trends Plant Sci. 2016;21: 187–198. doi:10.1016/j.tplants.2016.01.005

2. Capra EJ, Laub MT. Evolution of two-component signal transduction systems. Annu Rev Microbiol. 2012;66: 325–347. doi:10.1146/annurev-micro-092611-150039
3. Yuan Z-C, Haudecoeur E, Faure D, Kerr KF, Nester EW. Comparative transcriptome analysis of *Agrobacterium tumefaciens* in response to plant signal salicylic acid, indole-3-acetic acid and γ-amino butyric acid reveals signalling cross-talk and *Agrobacterium* -plant co-evolution. Cell Microbiol. 2008;10: 2339–2354. doi:10.1111/j.1462-5822.2008.01215.x
4. Cho H, Winans SC. VirA and VirG activate the Ti plasmid *repABC* operon, elevating plasmid copy number in response to wound-released chemical signals. Proceedings of the National Academy of Sciences. 2005;102: 14843–14848. doi:10.1073/pnas.0503458102
5. Xue S, Biondi EG. Coordination of symbiosis and cell cycle functions in *Sinorhizobium meliloti*. Biochimica et Biophysica Acta (BBA) - Gene Regulatory Mechanisms. 2019;1862: 691–696. doi:10.1016/j.bbagrm.2018.05.003
6. Heavner ME, Qiu W-G, Cheng H-P. Phylogenetic co-occurrence of ExoR, ExoS, and ChvI, components of the RSI bacterial invasion switch, suggests a key adaptive mechanism regulating the transition between free-living and host-invading phases in Rhizobiales. Mergaert P, editor. PLoS One. 2015;10: e0135655. doi:10.1371/journal.pone.0135655
7. Wells DH, Chen EJ, Fisher RF, Long SR. ExoR is genetically coupled to the ExoS-ChvI two-component system and located in the periplasm of

Sinorhizobium meliloti. Mol Microbiol. 2007;64: 647–664. doi:10.1111/j.1365-2958.2007.05680.x

8. Lu H-Y, Luo L, Yang M-H, Cheng H-P. *Sinorhizobium meliloti* ExoR is the target of periplasmic proteolysis. J Bacteriol. 2012;194: 4029–4040. doi:10.1128/JB.00313-12
9. Yuan ZC, Liu P, Saenkham P, Kerr K, Nester EW. Transcriptome profiling and functional analysis of *Agrobacterium tumefaciens* reveals a general conserved response to acidic conditions (pH 5.5) and a complex acid-mediated signaling involved in *Agrobacterium*-plant interactions. J Bacteriol. 2008;190. doi:10.1128/JB.01387-07
10. Alakavuklar MA, Heckel BC, Stoner AM, Stembel JA, Fuqua C. Motility control through an anti-activation mechanism in *Agrobacterium tumefaciens*. Mol Microbiol. 2021;116: 1281–1297. doi:10.1111/mmi.14823
11. Heckel BC, Tomlinson AD, Morton ER, Choi JH, Fuqua C. *Agrobacterium tumefaciens* ExoR controls acid response genes and impacts exopolysaccharide synthesis, horizontal gene transfer, and virulence gene expression. J Bacteriol. 2014;196. doi:10.1128/JB.01751-14
12. Quintero-Yanes A, Mayard A, Hallez R. The two-component system ChvGI maintains cell envelope homeostasis in *Caulobacter crescentus*. bioRxiv. 2022; 2022.01.18.476748. doi:10.1101/2022.01.18.476748
13. Vallet SU, Hansen LH, Bistrup FC, Laursen SA, Chapalay JB, Chambon M, et al. Loss of bacterial cell pole stabilization in *Caulobacter crescentus*

sensitizes to outer membrane stress and peptidoglycan-directed antibiotics. mBio. 2020;11. doi:10.1128/mBio.00538-20

14. Brown PJB, de Pedro MA, Kysela DT, van der Henst C, Kim J, de Bolle X, et al. Polar growth in the Alphaproteobacterial Order Rhizobiales. Proc Natl Acad Sci U S A. 2012;109. doi:10.1073/pnas.1114476109
15. Margolin W. Sculpting the bacterial cell. Current Biology. 2009. doi:10.1016/j.cub.2009.06.033
16. Williams MA, Aliashkevich A, Krol E, Kuru E, Bouchier JM, Rittichier J, et al. Unipolar peptidoglycan synthesis in the Rhizobiales requires an essential class A penicillin-binding protein. mBio. 2021;12. doi:10.1128/mBio.02346-21
17. Figueroa-Cuilan WM, Randich AM, Dunn CM, Santiago-Collazo G, Yowell A, Brown PJB. Diversification of LytM protein functions in polar elongation and cell division of *Agrobacterium tumefaciens*. Front Microbiol. 2021;12. doi:10.3389/fmicb.2021.729307
18. Krol E, Yau HCL, Lechner M, Schäper S, Bange G, Vollmer W, et al. Tol-pal system and Rgs proteins interact to promote unipolar growth and cell division in *Sinorhizobium meliloti*. mBio. 2020;11. doi:10.1128/MBIO.00306-20
19. Tatusov RL, Koonin VE, Lipman DJ. A genomic perspective on protein families. Science. 1997;278: 631–637. doi:10.1126/SCIENCE.278.5338.631

20. Galperin MY, Kristensen DM, Makarova KS, Wolf YI, Koonin VE. Microbial genome analysis: the COG approach. Brief Bioinform. 2019;20: 1063. doi:10.1093/BIB/BBX117

21. de Lucena DK, Pühler A, Weidner S. The role of sigma factor RpoH1 in the pH stress response of *Sinorhizobium meliloti*. BMC Microbiol. 2010;10: 265. doi:10.1186/1471-2180-10-265

22. Chaoprasid P, Dokpikul T, Johnrod J, Sirirakphaisarn S, Nookabkaew S, Sukchawalit R, et al. *Agrobacterium tumefaciens* Zur regulates the high-affinity zinc uptake system TroCBA and the putative metal chaperone YciC, along with ZinT and ZnuABC, for survival under zinc-limiting conditions. Appl Environ Microbiol. 2016;82: 3503. doi:10.1128/AEM.00299-16

23. Yuan Z-C, Edlind MP, Liu P, Saenkham P, Banta LM, Wise AA, et al. The plant signal salicylic acid shuts down expression of the *vir* regulon and activates quormone-quenching genes in *Agrobacterium*. Proceedings of the National Academy of Sciences. 2007;104: 11790–11795. doi:10.1073/pnas.0704866104

24. Haryono M, Cho S-T, Fang M-J, Chen A-P, Chou S-J, Lai E-M, et al. Differentiations in gene content and expression response to virulence induction between two *Agrobacterium* Strains. Front Microbiol. 2019;10: 1554. doi:10.3389/fmicb.2019.01554

25. Wu C-F, Lin J-S, Shaw G-C, Lai E-M. Acid-induced type VI secretion system is regulated by ExoR-ChvG/ChvI signaling cascade in

Agrobacterium tumefaciens. Ausubel FM, editor. PLoS Pathog. 2012;8: e1002938. doi:10.1371/journal.ppat.1002938

26. Figueroa-Cuilan W, Daniel JJ, Howell M, Sulaiman A, Brown PJB. Mini-Tn7 insertion in an artificial *att*Tn7 site enables depletion of the essential master regulator *ctrA* in the phytopathogen *Agrobacterium tumefaciens*. Appl Environ Microbiol. 2016;82. doi:10.1128/AEM.01392-16
27. Rotter C, Mühlbacher S, Salamon D, Schmitt R, Scharf B. Rem, a new transcriptional activator of motility and chemotaxis in *Sinorhizobium meliloti*. J Bacteriol. 2006;188: 6932–6942. doi:10.1128/JB.01902-05
28. Wu C-F, Smith DA, Lai E-M, Chang JH. The *Agrobacterium* type VI secretion system: A contractile nanomachine for interbacterial competition. Current Topics in Microbiology and Immunology. Berlin, Heidelberg: Springer; 2018. pp. 215–231. doi:10.1007/82_2018_99
29. Wu C-F, Weisberg AJ, Davis EW, Chou L, Khan S, Lai E-M, et al. Diversification of the type VI secretion system in Agrobacteria. Comstock LE, editor. mBio. 2021;12: e01927–21. doi:10.1128/mBio.01927-21
30. Lin J-S, Ma L-S, Lai E-M. Systematic dissection of the *Agrobacterium* type VI secretion system reveals machinery and secreted components for subcomplex formation. PLoS One. 2013;8: e67647. doi:10.1371/journal.pone.0067647
31. Dilanji GE, Teplitski M, Hagen SJ. Entropy-driven motility of *Sinorhizobium meliloti* on a semi-solid surface. Proceedings of the Royal Society B: Biological Sciences. 2014;281: 20132575. doi:10.1098/rspb.2013.2575

32. Mendis HC, Madzima TF, Queiroux C, Jones KM. Function of succinoglycan polysaccharide in *Sinorhizobium meliloti* host plant invasion depends on succinylation, not molecular weight. Winans SC, editor. mBio. 2016;7. doi:10.1128/mBio.00606-16

33. Schmid J, Sieber V, Rehm B. Bacterial exopolysaccharides: biosynthesis pathways and engineering strategies. Front Microbiol. 2015;6: 496. doi:10.3389/fmicb.2015.00496

34. Curtis NA, Orr D, Ross GW, Boulton MG. Affinities of penicillins and cephalosporins for the penicillin-binding proteins of *Escherichia coli* K-12 and their antibacterial activity. Antimicrob Agents Chemother. 1979;16: 533–539. doi:10.1128/AAC.16.5.533

35. Espadaler J, Querol E, Aviles FX, Oliva B. Identification of function-associated loop motifs and application to protein function prediction. Bioinformatics. 2006;22: 2237–2243. doi:10.1093/bioinformatics/btl382

36. Evans R, O'Neill M, Pritzel A, Antropova N, Senior A, Green T, et al. Protein complex prediction with AlphaFold-Multimer. bioRxiv. 2022; 2021.10.04.463034. doi:doi:10.1101/2021.10.04.463034

37. Chen EJ, Sabio EA, Long SR. The periplasmic regulator ExoR inhibits ExoS/ChvI two-component signalling in *Sinorhizobium meliloti*. Mol Microbiol. 2008;69: 1290–1303. doi:10.1111/j.1365-2958.2008.06362.x

38. Wiech EM, Cheng H-P, Singh SM. Molecular modeling and computational analyses suggests that the *Sinorhizobium meliloti* periplasmic regulator protein ExoR adopts a superhelical fold and is controlled by a unique

mechanism of proteolysis. Protein Science. 2015;24: 319–327. doi:10.1002/pro.2616

39. Ratib NR, Sabio EY, Mendoza C, Barnett MJ, Clover SB, Ortega JA, et al. Genome-wide identification of genes directly regulated by ChvI and a consensus sequence for ChvI binding in *Sinorhizobium meliloti*. Mol Microbiol. 2018;110: 596–615. doi:10.1111/mmi.14119

40. Wang C, Kemp J, da Fonseca IO, Equi RC, Sheng X, Charles TC, et al. *Sinorhizobium meliloti* 1021 loss-of-function deletion mutation in *chvI* and its phenotypic characteristics. Molecular Plant-Microbe Interactions®. 2010;23: 153–160. doi:10.1094/MPMI-23-2-0153

41. Charles TC, Nester EW. A chromosomally encoded two-component sensory transduction system is required for virulence of *Agrobacterium tumefaciens*. J Bacteriol. 1993;175: 6614–6625. doi:10.1128/jb.175.20.6614-6625.1993

42. Lamontagne J, Butler H, Chaves-Olarte E, Hunter J, Schirm M, Paquet C, et al. Extensive cell envelope modulation is associated with virulence in *Brucella abortus*. J Proteome Res. 2007;6: 1519–1529. doi:10.1021/pr060636a

43. Manterola L, Moriyón I, Moreno E, Sola-Landa A, Weiss DS, Koch MHJ, et al. The lipopolysaccharide of *Brucella abortus* BvrS/BvrR mutants contains lipid A modifications and has higher affinity for bactericidal cationic peptides. J Bacteriol. 2005;187: 5631–5639. doi:10.1128/JB.187.16.5631-5639.2005

44. Viadas C, Rodríguez MC, Sangari FJ, Gorvel J-P, García-Lobo JM, López-Goñi I. Transcriptome analysis of the *Brucella abortus* BvrR/BvrS two-component regulatory system. Bereswill S, editor. PLoS One. 2010;5: e10216. doi:10.1371/journal.pone.0010216

45. Piepenbreier H, Diehl A, Fritz G. Minimal exposure of lipid II cycle intermediates triggers cell wall antibiotic resistance. Nat Commun. 2019;10: 2733. doi:10.1038/s41467-019-10673-4

46. Geiger O, Sohlenkamp C, Vera-Cruz D, Medeot DB, Martínez-Aguilar L, Sahonero-Canavesi DX, et al. ExoS/ChvI two-component signal-transduction system activated in the absence of bacterial phosphatidylcholine. Front Plant Sci. 2021;12. doi:10.3389/fpls.2021.678976

47. Erbs G, Silipo A, Aslam S, de Castro C, Liparoti V, Flagiello A, et al. Peptidoglycan and muropeptides from pathogens *Agrobacterium* and *Xanthomonas* elicit plant innate immunity: Structure and activity. Chem Biol. 2008;15: 438–448. doi:10.1016/j.chembiol.2008.03.017

48. Zupan JR, Grangeon R, Robalino-Espinosa JS, Garnica N, Zambryski P. GROWTH POLE RING protein forms a 200-nm-diameter ring structure essential for polar growth and rod shape in *Agrobacterium tumefaciens*. Proc Natl Acad Sci U S A. 2019;166. doi:10.1073/pnas.1905900116

49. Schäper S, Yau HCL, Krol E, Skotnicka D, Heimerl T, Gray J, et al. Seven-transmembrane receptor protein RgsP and cell wall-binding protein RgsM

promote unipolar growth in Rhizobiales. Copenhaver GP, editor. PLoS Genet. 2018;14: e1007594. doi:10.1371/journal.pgen.1007594

50. Howell M, Aliashkevich A, Salisbury AK, Cava F, Bowman GR, Brown PJB. Absence of the polar organizing protein PopZ results in reduced and asymmetric cell division in *Agrobacterium tumefaciens*. J Bacteriol. 2017;199. doi:10.1128/JB.00101-17

51. Grangeon R, Zupan J, Jeon Y, Zambryski PC. Loss of PopZ $_{At}$ activity in *Agrobacterium tumefaciens* by deletion or depletion leads to multiple growth poles, minicells, and growth defects. mBio. 2017;8. doi:10.1128/mBio.01881-17

52. Morton ER, Fuqua C. Laboratory Maintenance of *Agrobacterium*. Current Protocols in Microbiology. 2012. doi:10.1002/9780471729259.mc03d01s24

53. BERINGER JE. R factor transfer in *Rhizobium leguminosarum*. Microbiology (N Y). 1974;84: 188–198. doi:10.1099/00221287-84-1-188

54. Poindexter JS. Biological properties and classification of the *Caulobacter* group. Bacteriol Rev. 1964;28: 231–295. doi:10.1128/br.28.3.231-295.1964

55. Morton ER, Fuqua C. Genetic manipulation of *Agrobacterium*. Curr Protoc Microbiol. 2012. doi:10.1002/9780471729259.mc03d02s25

56. Thanbichler M, Iniesta AA, Shapiro L. A comprehensive set of plasmids for vanillate- and xylose-inducible gene expression in *Caulobacter crescentus*. Nucleic Acids Res. 2007;35: e137–e137. doi:10.1093/nar/gkm818

57. Howell M, Daniel JJ, Brown PJB. Live cell fluorescence microscopy to observe essential processes during microbial cell growth. Journal of Visualized Experiments. 2017;2017. doi:10.3791/56497

58. Ducret A, Quardokus EM, Brun Y v. MicrobeJ, a tool for high throughput bacterial cell detection and quantitative analysis. Nat Microbiol. 2016;1: 16077. doi:10.1038/nmicrobiol.2016.77

59. Martin M. Cutadapt removes adapter sequences from high-throughput sequencing reads. EMBnet J. 2011;17: 10. doi:10.14806/ej.17.1.200

60. Langmead B, Salzberg SL. Fast gapped-read alignment with Bowtie 2. Nat Methods. 2012;9: 357–359. doi:10.1038/nmeth.1923

61. Dobin A, Gingeras TR. Mapping RNA-seq Reads with STAR. Curr Protoc Bioinformatics. 2015;51: 11.14.1–11.14.19. doi:10.1002/0471250953.bi1114s51

62. Love MI, Huber W, Anders S. Moderated estimation of fold change and dispersion for RNA-seq data with DESeq2. Genome Biol. 2014;15: 550. doi:10.1186/s13059-014-0550-8

63. Sayers EW, Bolton EE, Brister JR, Canese K, Chan J, Comeau DC, et al. Database resources of the national center for biotechnology information. Nucleic Acids Res. 2022;50: D20–D26. doi:10.1093/nar/gkab1112

64. Huerta-Cepas J, Szklarczyk D, Heller D, Hernández-Plaza A, Forslund SK, Cook H, et al. eggNOG 5.0: a hierarchical, functionally and phylogenetically annotated orthology resource based on 5090 organisms

and 2502 viruses. Nucleic Acids Res. 2019;47: D309–D314. doi:10.1093/nar/gky1085

65. Mistry J, Chuguransky S, Williams L, Qureshi M, Salazar GA, Sonnhammer ELL, et al. Pfam: The protein families database in 2021. Nucleic Acids Res. 2021;49: D412–D419. doi:10.1093/nar/gkaa913
66. Johnson M, Zaretskaya I, Raytselis Y, Merezhuk Y, McGinnis S, Madden TL. NCBI BLAST: a better web interface. Nucleic Acids Res. 2008;36: W5–W9. doi:10.1093/nar/gkn201
67. Edgar RC. MUSCLE: multiple sequence alignment with high accuracy and high throughput. Nucleic Acids Res. 2004;32: 1792–1797. doi:10.1093/nar/gkh340
68. Waterhouse AM, Procter JB, Martin DMA, Clamp M, Barton GJ. Jalview Version 2--a multiple sequence alignment editor and analysis workbench. Bioinformatics. 2009;25: 1189–1191. doi:10.1093/bioinformatics/btp033
69. Bateman A, Martin M-J, Orchard S, Magrane M, Agivetova R, Ahmad S, et al. UniProt: the universal protein knowledgebase in 2021. Nucleic Acids Res. 2021;49: D480–D489. doi:10.1093/nar/gkaa1100
70. Kumar S, Stecher G, Li M, Knyaz C, Tamura K. MEGA X: Molecular evolutionary genetics analysis across computing platforms. Battistuzzi FU, editor. Mol Biol Evol. 2018;35: 1547–1549. doi:10.1093/molbev/msy096
71. Kelley LA, Mezulis S, Yates CM, Wass MN, Sternberg MJE. The Phyre2 web portal for protein modeling, prediction and analysis. Nat Protoc. 2015;10: 845–858. doi:10.1038/nprot.2015.053

72. Jumper J, Evans R, Pritzel A, Green T, Figurnov M, Ronneberger O, et al. Highly accurate protein structure prediction with AlphaFold. Nature. 2021;596: 583–589. doi:10.1038/s41586-021-03819-2

73. Pettersen EF, Goddard TD, Huang CC, Meng EC, Couch GS, Croll TI, et al. UCSF ChimeraX: Structure visualization for researchers, educators, and developers. Protein Science. 2021;30: 70–82. doi:10.1002/pro.3943

STRAINS AND PLASMIDS

Strain or Plasmid	Relevant Genotype, Features or Characteristics	Source or Reference
Source Plasmids		
pNTPS139	Km^r; Suicide vector containing *oriT* and *sacB*	D. Alley
pFLGC-2	Km^r, P_{van} expression vector containing *oriV* and MCS with c-terminal *flag* tag	1
Deletion Plasmids		
pNTPS138Δ*chvI*	Km^r Suc^s; deletion plasmid for *chvI*	2
pNTPS138Δ*rem*	Km^r Suc^s; deletion plasmid for *rem*	3
pNTPS139Δ*exoA*	Km^r Suc^s; deletion plasmid for *exoA*	This Study
pNTPS139ΔT6SSpro	Km^r Suc^s; deletion plasmid for T6SSpro	This Study
Expression Plasmids		
pFLGC-2*exoR-flag*	Km^r, P_{van} expression vector containing *exoR* with c-terminal *flag* tag	This Study
***E. coli* strains**		
DH5α	Cloning strain	Life Technologies
S17-1	Smr;RP4-2 TC::MU Km-Tn7; for plasmid mobilization	4
***A. tumefaciens* strains**		
C58	Parent strain	5
C58Δ*exoR*	Δ*exoR*	2
C58Δ*chvG*	Δ*chvG*	6
C58Δ*chvI*	Δ*chvI*	6
C58Δ*tetRA*::a-*att*Tn7 (WT)	Replacement of the *tetRA* locus with an artificial *att*Tn7 site	3

C58Δ*tetRA*::a-*att*Tn7 Δ*rem*	Δ*rem*	3
C58Δ*tetRA*::a-*att*Tn7 Δ*exoA*	Δ*exoA*	This Study
C58Δ*tetRA*::a-*att*Tn7 ΔT6SSpro	ΔT6SSpro	This Study
C58Δ*tetRA*::a-*att*Tn7 Δ*pbp1b1*	Δ*pbp1b1*	7
C58Δ*tetRA*::a-*att*Tn7 Δ*pbp1b2*	Δ*pbp1b2*	7
C58Δ*tetRA*::a-*att*Tn7 Δ*pbp1c*	Δ*pbp1c*	7
C58Δ*tetRA*::a-*att*Tn7 Δ*mtgA*	Δ*mtgA*	7
C58Δ*tetRA*::a-*att*Tn7 Δ*pbp1b1,*Δ*pbp1b2*	Δ*pbp1b1,*Δ*pbp1b2*	7
C58Δ*tetRA*::a-*att*Tn7 Δ*pbp1b1,* Δ*pbp1b2,* Δ*pbp1c*	Δ*pbp1b1,*Δ*pbp1b2,*Δ*pbp1c* (Δ3pbp)	7
C58Δ*tetRA*::mini-Tn7-GM-Plac -pbp1a, Δ*pbp1a*	Chromosome-based complementation of Δ*pbp1a* with C58Δ*tetRA*::mini-Tn7-GM-Plac-pbp1a allowing depletion of PBP1a under control of the lac promoter	7
C58 Δ*tetRA*::mini-Tn7-GM-Plac -pbp1a, Δ*pbp1a,* Δ*rem*	Δ*rem* in PBP1a depletion background	This Study
C58 Δ*tetRA*::mini-Tn7-GM-Plac -pbp1a, Δ*pbp1a,* Δ*exoA*	Δ*exoA* in PBP1a depletion background	This Study
C58 Δ*tetRA*::mini-Tn7-GM-Plac -pbp1a, Δ*pbp1a,* ΔT6SSpro	ΔT6SSpro in PBP1a depletion background	This Study
C58 Δ*tetRA*::mini-Tn7-GM-Plac -pbp1a, Δ*pbp1a,* Δ*chvI*	Δ*chvI* in PBP1a depletion background	This Study
C58Δ*tetRA*::a-*att*Tn7 Δ*pbp1b1,* Δ*pbp1b2,* Δ*pbp1c*	Δ*pbp1b1,*Δ*pbp1b2,*Δ*pbp1c* (Δ3pbp)	7
C58Δ*tetRA*::mini-Tn7-GM-Plac -pbp1a, Δ*pbp1a*	Chromosome-based complementation of Δ*pbp1a* with C58Δ*tetRA*::mini-Tn7-GM-Plac-pbp1a allowing depletion of PBP1a under control of the lac promoter	7
C58Δ*tetRA*::a-*att*Tn7 + pFLGC-2*exoR-flag*	Km^r, Constiuitive expression of ExoR-FLAG	This Study
C58Δ*tetRA*::mini-Tn7-GM-Plac -pbp1a, Δ*pbp1a* + pFLGC-2*exoR-flag*	Km^r, Constiuitive expression of ExoR-FLAG in the PBP1a depletion background	This Study
***S. meliloti* strains**		
Rm2011	Wild type, Str^r	8
Rm2011 *rgsP-egfp*, Δ5pbp	Rm2011 *rgsP*-egfp carrying markerless deletions of *mrcA2, mcrB, pbp, pbpC* and SMc02856 Δ5pbp	7

Rm2011 *rgsP*-egfp *mrcA*1 depletion	Rm2011 *rgsP*-egfp carrying markerless deletion of *mrcA1*, curable complementation plasmid pGCH14-*mrcA1*, and pSRKKm as a source of *lacI* to cure pGCH14-*mrcA1*, Gm^r Km^r	7
***C. crescentus* strains**		
NA1000	Wild type	Hallez Lab

Source References

1. Thanbichler M, Iniesta AA, Shapiro L. A comprehensive set of plasmids for vanillate- and xylose-inducible gene expression in *Caulobacter crescentus*. Nucleic Acids Res. 2007;35: e137–e137. doi:10.1093/nar/gkm818
2. Tomlinson AD, Ramey-Hartung B, Day TW, Merritt PM, Fuqua C. Agrobacterium tumefaciens ExoR represses succinoglycan biosynthesis and is required for biofilm formation and motility. Microbiology (N Y). 2010;156: 2670–2681. doi:10.1099/mic.0.039032-0
3. Figueroa-Cuilan W, Daniel JJ, Howell M, Sulaiman A, Brown PJB. Mini-Tn7 insertion in an artificial attTn7 site enables depletion of the essential master regulator ctrA in the phytopathogen Agrobacterium tumefaciens. Appl Environ Microbiol. 2016;82. doi:10.1128/AEM.01392-16
4. Simon R, Priefer U, Pühler A. A broad host range mobilization system for in vivo genetic engineering: transposon mutagenesis in gram negative bacteria. Bio/Technology. 1983;1: 784–791. doi:10.1038/nbt1183-784

5. Watson B, Currier TC, Gordon MP, Chilton MD, Nester EW. Plasmid required for virulence of Agrobacterium tumefaciens. J Bacteriol. 1975;123: 255–64. doi:10.1128/jb.123.1.255-264.1975
6. Heckel BC, Tomlinson AD, Morton ER, Choi JH, Fuqua C. Agrobacterium tumefaciens ExoR controls acid response genes and impacts exopolysaccharide synthesis, horizontal gene transfer, and virulence gene expression. J Bacteriol. 2014;196: 3221–3233. doi:10.1128/JB.01751-14
7. Williams MA, Aliashkevich A, Krol E, Kuru E, Bouchier JM, Rittichier J, et al. Unipolar peptidoglycan synthesis in the Rhizobiales requires an essential class A penicillin-binding protein. mBio. 2021;12. doi:10.1128/mBio.02346-21
8. Casse F, Bouchier C, Julliot JS, Michel M, Denarie J. Identification and characterization of large lasmids in Rhizobium meliloti using agarose gel electrophoresis. J Gen Microbiol. 1979;113: 229–242. doi:10.1099/00221287-113-2-229

PRIMER LIST

Synthesized DNA	Sequence (5' – 3')
Primers for deletion vectors in *A. tumefaciens*	
exoA P1 Forward SpeI	GCACACTAGTCGAGATCATCCTGCG
exoA P2 Reverse	AAGCTTGGTACCGAATTCAAGACCTTCCATGATTTG
exoA P3 Forward	GAATTCGGTACCAAGCTTAAAGGCTGTCTCATGACC
exoA P4 Reverse BamHI	CTGTCCTAGGCTTCCATCCTGAGAAGCG

exoA P5 Forward	TGCTGGTGACGAGTTCTCCGG
exoA P6 Reverse	AGTACCTGCACCACGCGG
rem P5 Forward	CATTATTTCCACGGCGAAAACTTCACCTC
rem P6 Reverse	GACCCGTGAAGCCATTGACGAC
T6SSpro P1 Forward SpeI	GCACACTAGTGCCTCTCCTGAACTTGTCAGC
T6SSpro P2 Reverse	AAGCTTGGTACCGAATTCATGTCGCATATCGATCTCAATCGCC
T6SSpro P3 Forward	GAATTCGGTACCAAGCTTTTGGATACACAGCATGTTAAAAG
T6SSpro P4 Reverse BamHI	CTAGCCTAGGGCTATCCGGTACAGTTCTTCG
T6SSpro P5 Forward	CGAGGTTCAGCAGGCAGACATTG
T6SSpro P6 Reverse	GCTTTCATCGGTGCCCGC
chvI P5 Forward	CGGCAGCAGGTAGTTCAGCAC
chvI P6 Reverse	CAGTGACAACACGATATTGACCAGCG
exoR Forward NdeI	GCACCATATGCTGAAATGTGAAGCCAACGTTTTAAAG
exoR Reverse AgeI	GCACACCGGTTATCCGGATCGTTGAACTGCAT
pVMCS Forward	GATGGCTTCCATGTCGGCA
pVMCS Reverse	GTAAAACGACGGCCAGTGAATG

SUPPLEMENTAL

S1 Table

Gene Name	GeneID	Description	log_2 FC	p value
Cell wall synthesis and remodeling				
pbp1a	Atu1341	class A penicillin-binding protein 1a	-7.2	0
pbp1b1	Atu0103	class A penicillin-binding protein 1b	0.78	1.19E-45
pbp1b2	Atu0931	class A penicillin-binding protein 1b	0.55	5.50E-14
pbp1c	Atu3694	class A penicillin-binding protein 1c	0.12	0.10308
mtgA	Atu2720	monofunctional glycosyltransferase	-0.19	0.058441
pbp3a	Atu2100	class B penicillin-binding protein 3a	0.71	2.86E-13
pbp3b	Atu1064	class B penicillin-binding protein 3b	-0.14	0.086185
ftsW	Atu2095	SEDS protein	0.94	2.70E-23
rgsM	Atu4178	DD-endopeptidase	1.72	5.40E-132
-	Atu1832	DD-endopeptidase	0.41	0.01114
mepA	Atu0186	DD/LD-endopeptidase	1.93	1.89E-77
-	Atu2133	LD-transpeptidase	1.84	5.47E-85
-	Atu3332	LD-transpeptidase	1.91	2.29E-114
-	Atu0844	LD-transpeptidase	-4.95	4.51E-90
-	Atu2336	LD-transpeptidase	-1.99	5.57E-51
-	Atu0290	soluble lytic transglycosylase	2.46	4.70E-16
-	Atu0572	soluble lytic transglycosylase	-4.65	3.70E-125
-	Atu2112	soluble lytic transglycosylase	5.17	1.10E-104
-	Atu1221	NLpC/p60 superfamily	4.21	9.04E-21
-	Atu0933	beta-lactamase class D	2.37	2.22E-54
Cell envelope homeostasis				
palA	Atu3713	omp16 protein	1.64	2.58E-51
tolB	Atu3714	tolB protein	2.26	1.55E-116
tolA	Atu3715	conserved hypothetical protein	2.06	1.98E-293
tolR	Atu3716	tolR protein	2.06	3.97E-143
tolQ	Atu3717	tolQ Protein	1.74	7.55E-34
ropB	Atu1131	OmpA-like outer membrane protein	5.04	1.40E-149
-	Atu1877	OmpA-like outer membrane protein	3.3	3.50E-159
-	Atu1155	periplasmic sensor creD	4.38	0
-	Atu2760	lipoprotein transporter	2.57	3.40E-108
Signaling				
virA	Atu6166	two component sensor kinase	0.52	1.56E-13
virG	Atu6178	two component response regulator	4.02	0
	Atu4639	two component sensor kinase	2.74	2.90E-99
	Atu4638	two component response regulator	3.21	2.32E-68
rem	Atu0573	OmpR-type transcriptional regulator	-2.58	4.53E-89
visN	Atu0524	LuxR-type transcriptional regulator	-0.17	0.034462
visR	Atu0525	LuxR-type transcriptional regulator	0.16	0.114024
exoR	Atu1715	eps production negative regulator	2.2	1.64E-37
chvG	Atu0033	two component sensor kinase	1.41	4.00E-62
chvI	Atu0034	two component response regulator	2.27	3.60E-95

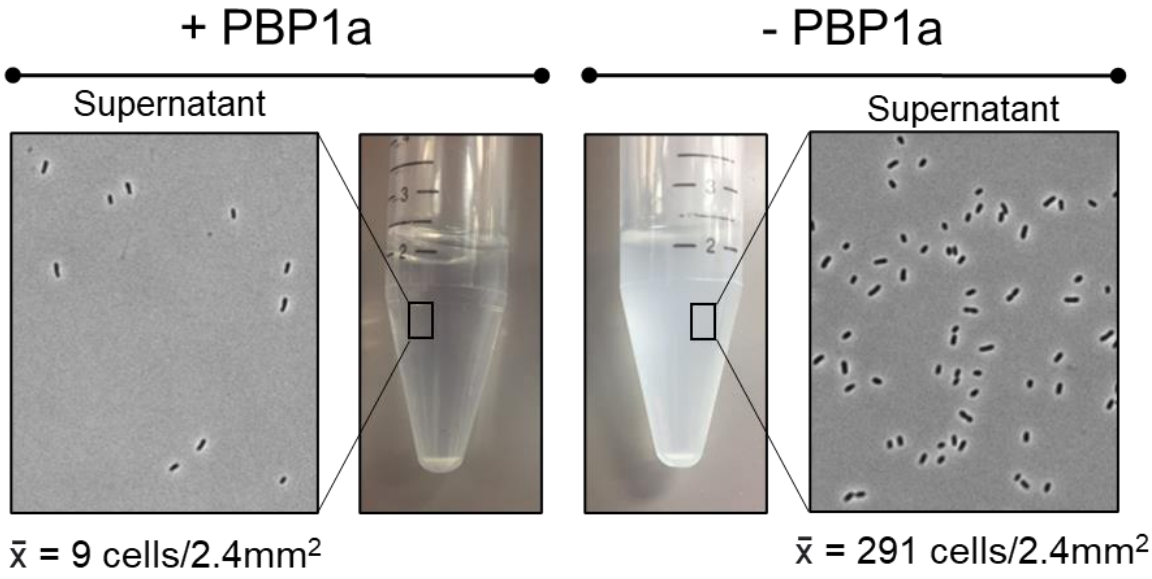

Figure 2.S1. Pelleting of PBP1a-depleted and repleted cells. Conical tubes show turbidity after pelleting cells grown for 16 hours in PBP1a replete (+PBP1a) or depleted (-PBP1a) conditions. Cells were centrifuged at 1690 x g (3000 rpm in TX-400 rotor in a Sorvall Legend X1R centrifuge) for 10 minutes. Supernatants were spotted on a 1.25% ATGN agarose pad. = average number of cells from 10 fields of view.

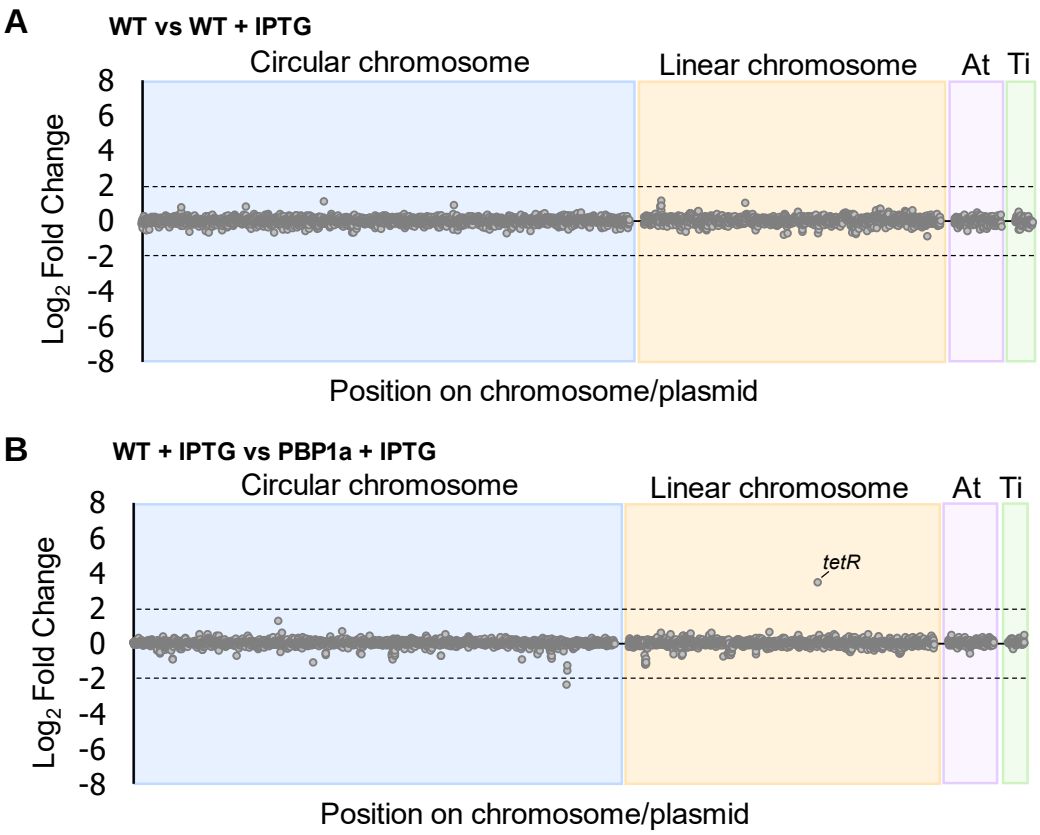

Figure 2.S2. Analysis of the control transcriptomes by RNA-seq. **A.** Plots comparing Log2Fold Change of the WT 6-hour transcriptome to that of the WT +ITPG 6-hour transcriptome. Gray dots represent a single transcript, and the dotted lines represent +/- 2.0 Log2Fold Change threshold. Plots are delimited by chromosomes and mega plasmids. **B.** Plots comparing Log2Fold Change of the WT +IPTG transcriptome to that of the PBP1a depletion strain with ITPG present to drive PBP1a expression. Comparisons shown are of the 6-hour transcriptomes. Gray dots represent a single transcript, and the dotted lines represent +/- 2.0 Log2Fold Change threshold. Plots are delimited by chromosomes and mega plasmids.

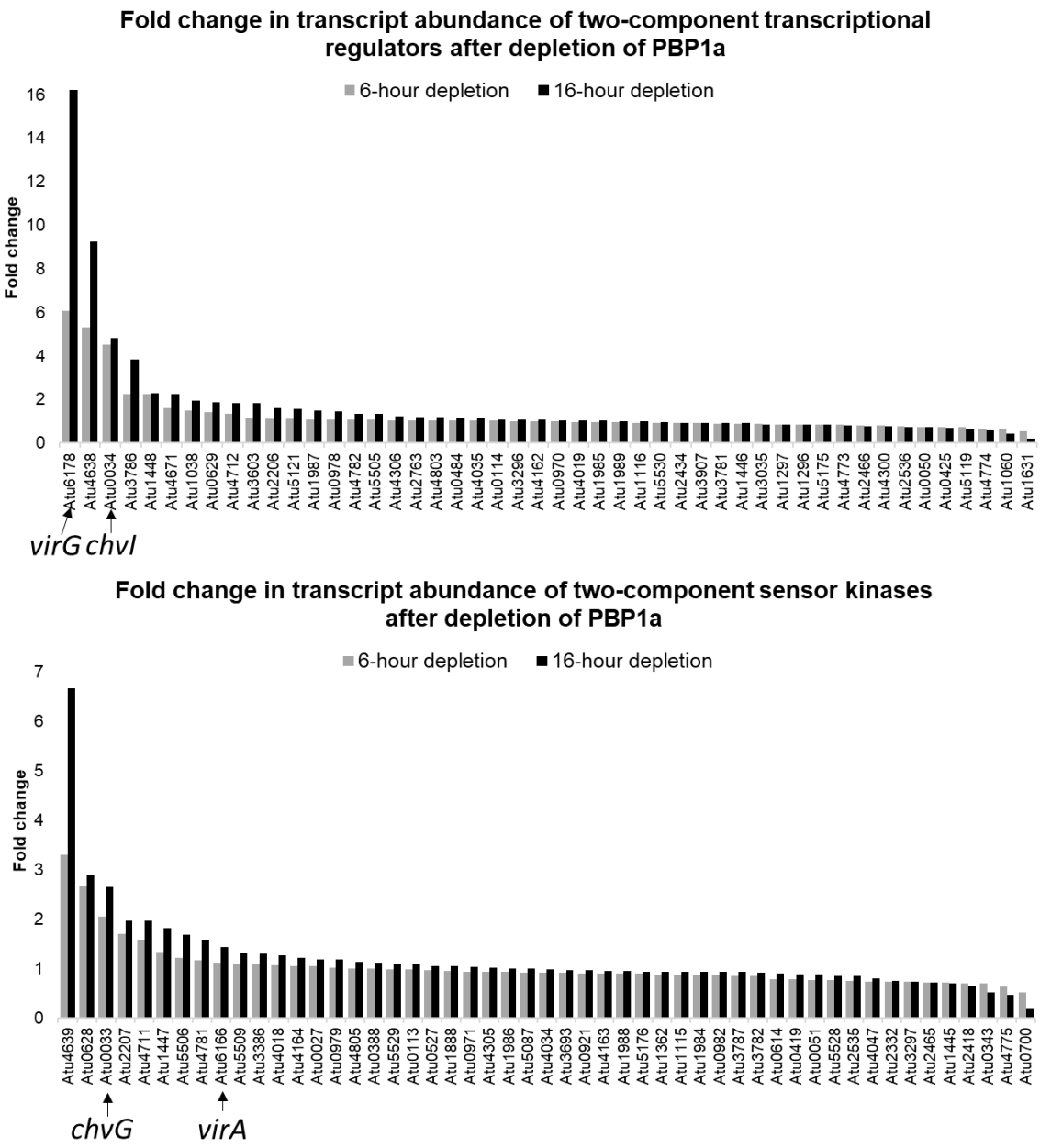

Figure 2.S3. Transcriptional changes of TCS regulators and kinases during PBP1a depletion. The fold change in expression level of TCS regulators and kinases are shown following 6 hours (gray) and 16 hours (black) of PBP1a depletion. The virAG and chvGI TCS pairs are labeled.

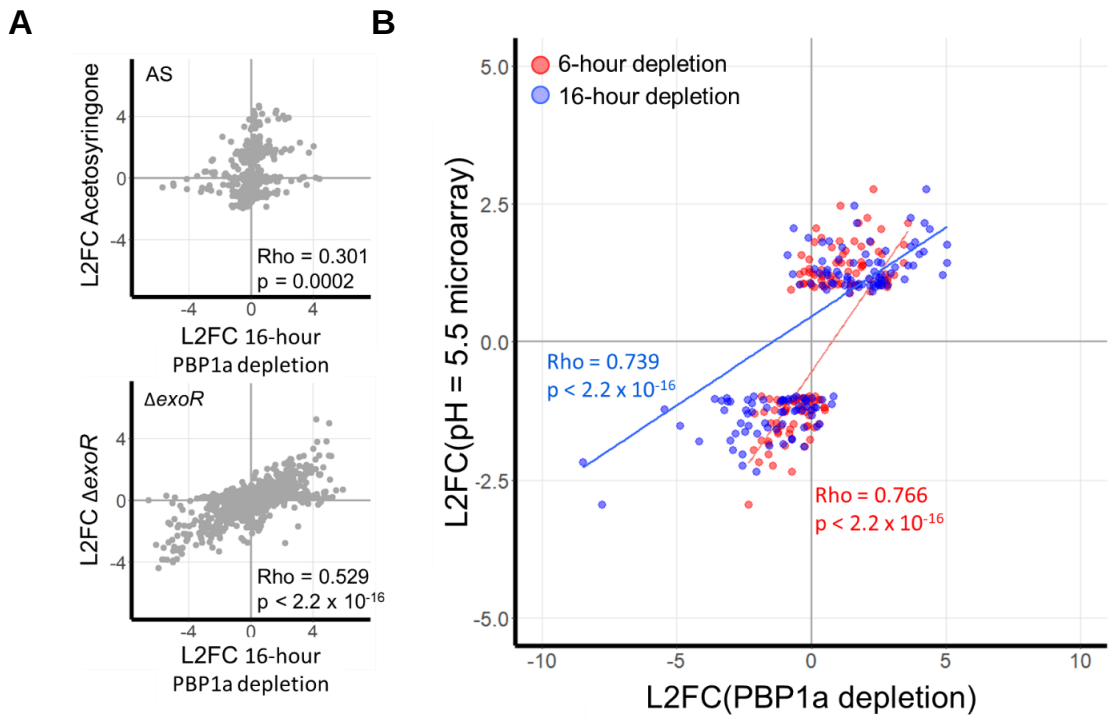

Figure 2.S4. The response to the depletion of PBP1a mimics transcriptional changes associated with host invasion. **A.** Correlation scatterplots depicting relationships between the log2fold-change (L2FC) values in the 16-hour PBP1a depletion and transcriptomic data sets taken under simulated virulence-inducing conditions (AS) and under simulated host-invading conditions (ΔexoR). Each point represents a unique transcript. AS, acetosyrinogone; Rho, Spearman correlation coefficient. **B.** Correlation scatterplots comparing L2FC values of transcripts in the pH 5.5 microarray, a condition known to induce the chvG-chvI regulon, to either the 6-hour (red) or 16-hour (blue) PBP1a depletion. Rho, Spearman correlation coefficient.

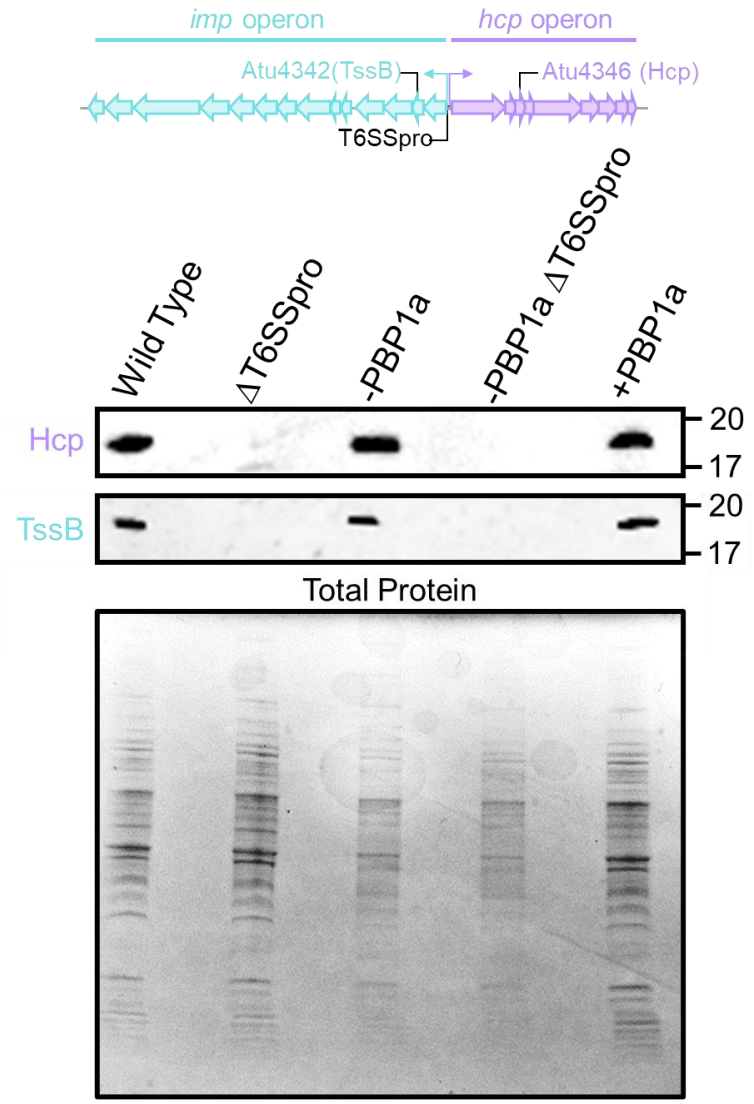

Figure 2.S5. Western blot of proteins expressed from the two type VI secretion system operons in ΔT6SSpro strains. Top panel, diagram of the two operons encoding elements of Type VI Secretion in *A. tumefaciens*. T6SSpro labels the intergenic gap that is deleted in ΔT6SSpro strains. Middle panel, western blots using anti-Hcp and anti-TssB in each of the indicated strains. Protein sizes (kDa) are shown on the right. Bottom panel, Coomassie stained gel showing total protein from each strain. Western blots were performed as described in the methods with the following modifications. Lysates were prepared by pelleting

cells via centrifugation and resuspending in 1X loading buffer. Next, the suspension was run through a 20G needle for lysis. 3 gels were loaded with identical concentrations of sample. BlueStain2 Protein ladder (P008-500) was loaded into the first well of each. One of the three gels was Coomassie stained at room temperature with gentle shaking for 10–15 minutes and imaged for total protein content. The other two gels were transferred to immobilon-FL transfer membranes, blocked with 0.5% milk, and transferred to a solution of TBS + 0.05% Tween 20 with 4 µL of 1:1000 dilution of either anti-TssB or anti-Hcp for 1 hour. Membranes were washed and transferred to TBS + 0.05% Tween 20 with 4 µL of 1:1000 dilution of anti-rabbit HRP goat IgG for 1 hour.

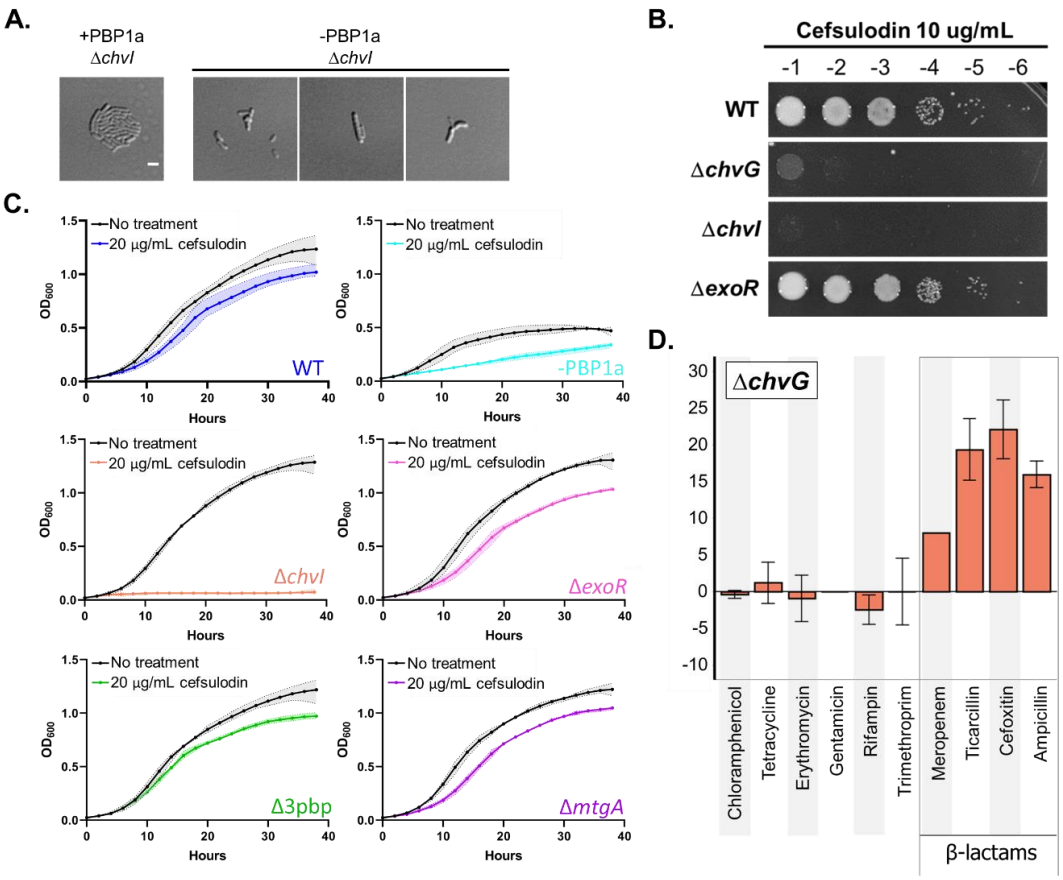

Figure 2.S6. Impact of decreased PG synthesis on *A. tumefaciens*. **A.** Micrographs of PBP1a depletion ΔchvI with (+PBP1A) or without (-PBP1A) IPTG. Cells were grown to exponential phase in ATGN media containing IPTG, spotted on an ATGN agarose pad with or without IPTG, allowed to grow for 16 hours, and imaged by DIC microscopy. **B.** Cell viability of each wild type, ΔchvG, ΔchvI, and ΔexoR spotted on an ATGN agar plate containing 10 µg/mL of cefsulodin. Ten-fold serial dilutions are indicated. **C.** Growth curves of WT, -PBP1a, ΔchvI, and ΔexoR, Δpbp3, ΔmtgA in the absence (black line) and presence of 20 µg/mL cefsulodin (colored line). **D.** Graph depicting the change in zone of inhibition from wildtype in ΔchvG against ten different antibiotic disks. Error bars represent +/- 1 standard deviation from the mean.

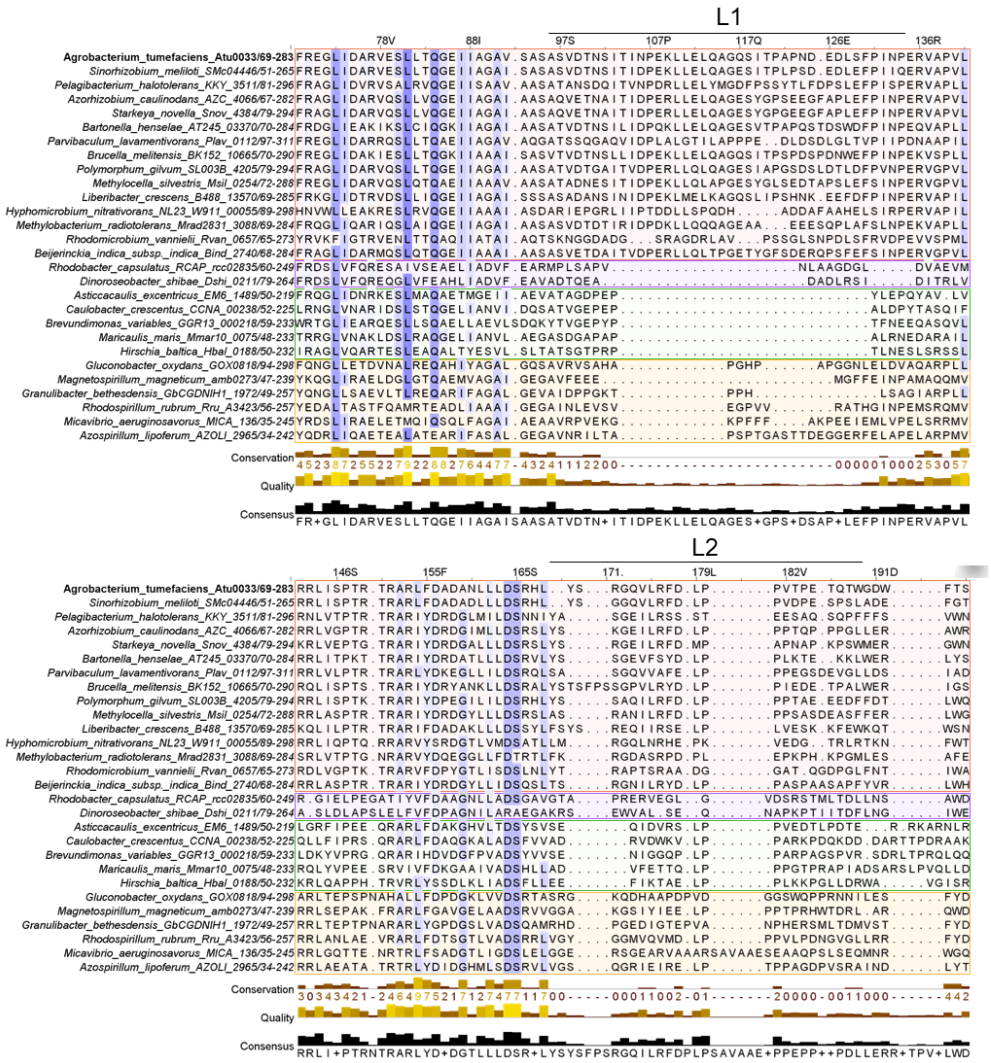

Figure 2.S7. Alignment of periplasmic regions of ChvG orthologs. Partial MUSCLE alignment of ChvG ortholog periplasmic domains. Highlighted columns represent strong conservation across aligned sequences. Atu0033 (ChvG of *A. tumefaciens*) is the reference sequence for this analysis. L1 and L2 correspond to two conserved structural loops. Conservation, quality, and consensus scores for each site are represented as bar graphs under the alignment. Shading indicates Order of the bacterium containing the ChvG ortholog: Orange, Rhizobiales; Purple, Rhodobacterales; Green, Caulobacterales; Gold, Rhodospirales.

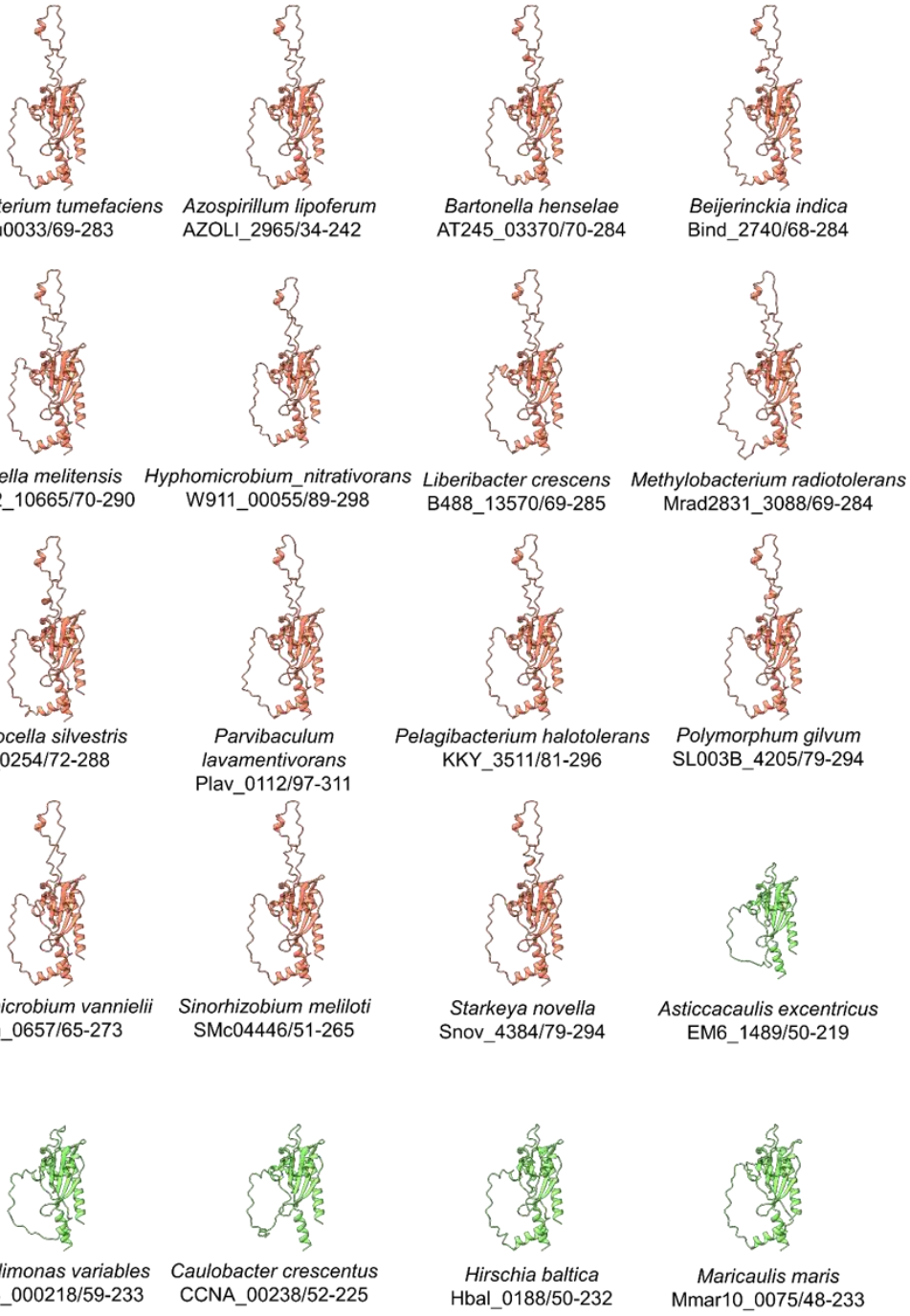
Agrobacterium tumefaciens
Atu0033/69-283
Azospirillum lipoferum
AZOLI_2965/34-242
Bartonella henselae
AT245_03370/70-284
Beijerinckia indica
Bind_2740/68-284
Brucella melitensis
BK152_10665/70-290
Hyphomicrobium_nitrativorans
W911_00055/89-298
Liberibacter crescens
B488_13570/69-285
Methylobacterium radiotolerans
Mrad2831_3088/69-284
Methylocella silvestris
Msil_0254/72-288
Parvibaculum lavamentivorans
Plav_0112/97-311
Pelagibacterium halotolerans
KKY_3511/81-296
Polymorphum gilvum
SL003B_4205/79-294
Rhodomicrobium vannielii
Rvan_0657/65-273
Sinorhizobium meliloti
SMc04446/51-265
Starkeya novella
Snov_4384/79-294
Asticcacaulis excentricus
EM6_1489/50-219
Brevundimonas variables
GGR13_000218/59-233
Caulobacter crescentus
CCNA_00238/52-225
Hirschia baltica
Hbal_0188/50-232
Maricaulis maris
Mmar10_0075/48-233

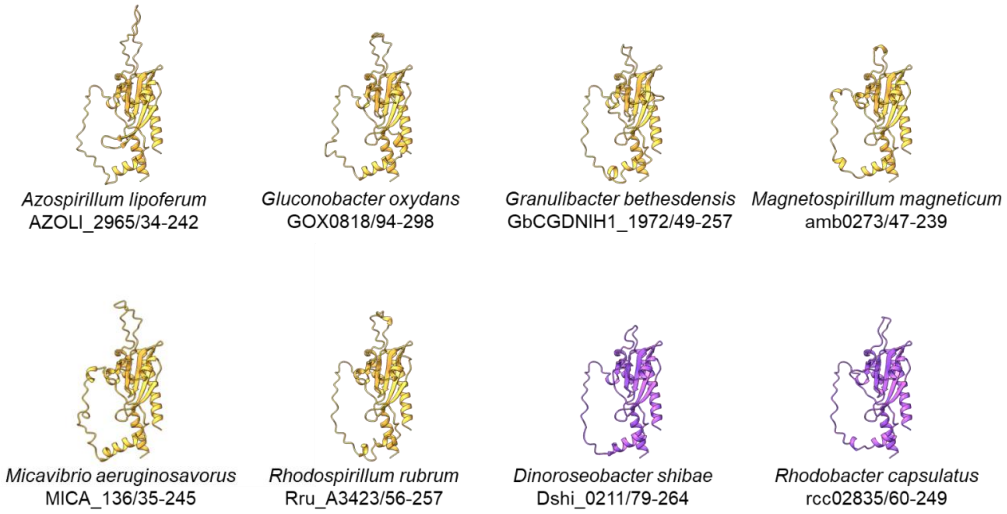

Figure 2.S8. Structure predictions for the periplasmic regions of ChvG orthologs. Phyre2 structural predictions for each organism displayed in Fig 6A of this work. Genus and species names as well as locus tags for each ChvG ortholog are provided. Range of numbers following the back slash are the amino acid sites used in structure prediction. Colors indicates order of the bacterium containing the ChvG ortholog: Orange, Rhizobiales; Purple, Rhodobacterales; Green, Caulobacterales; Gold, Rhodospirales.

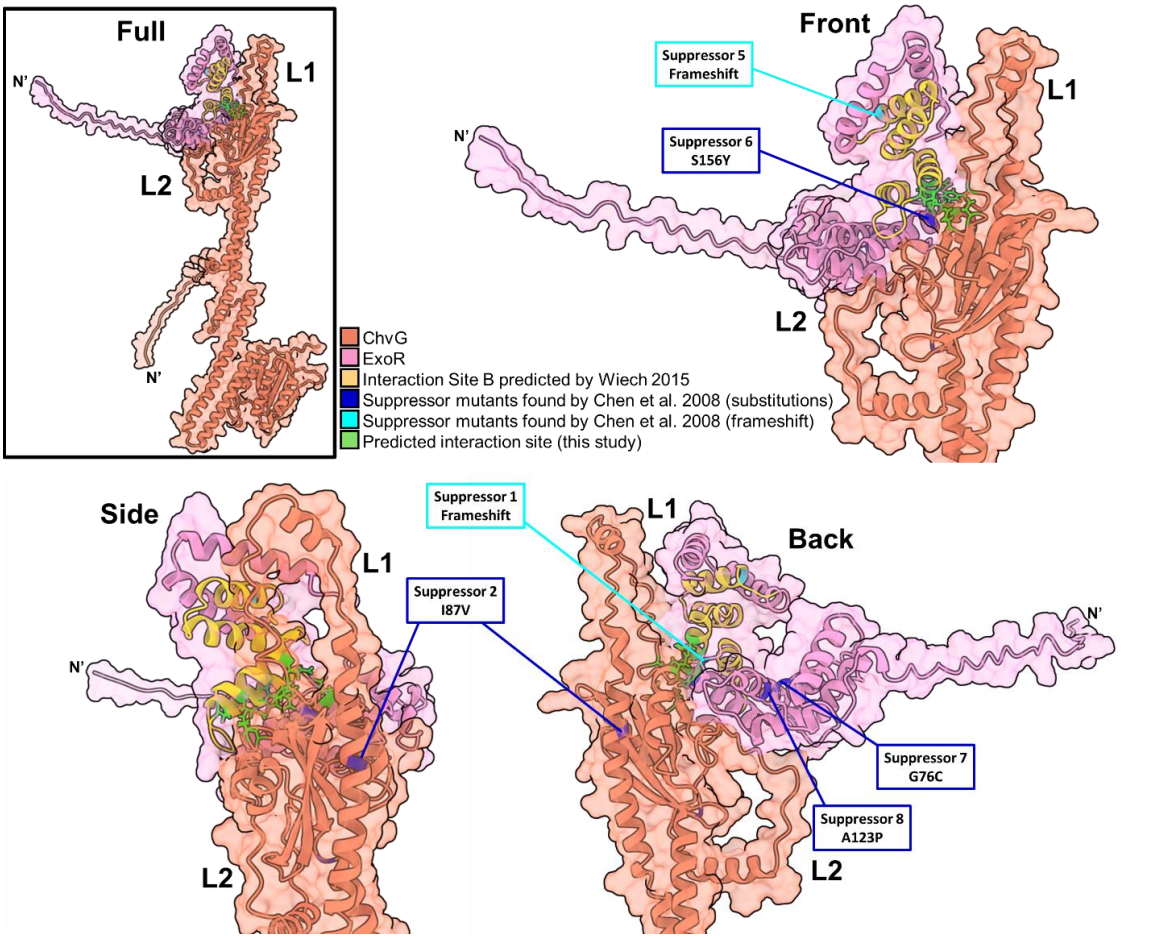

Figure 2.S9. Comparisons of putative interaction sites between ExoR and ChvG. Previously characterized suppressor mutants (Chen et al. 2008) or predicted interaction sites (Wiech et al. 2014) are mapped onto the ExoR-ChvG AlphaFold Multimer structure presented here. The full structure is shown at the top left with detailed views of the ExoR-ChvG interface shown as the protein complex is rotated (front, side, and back).

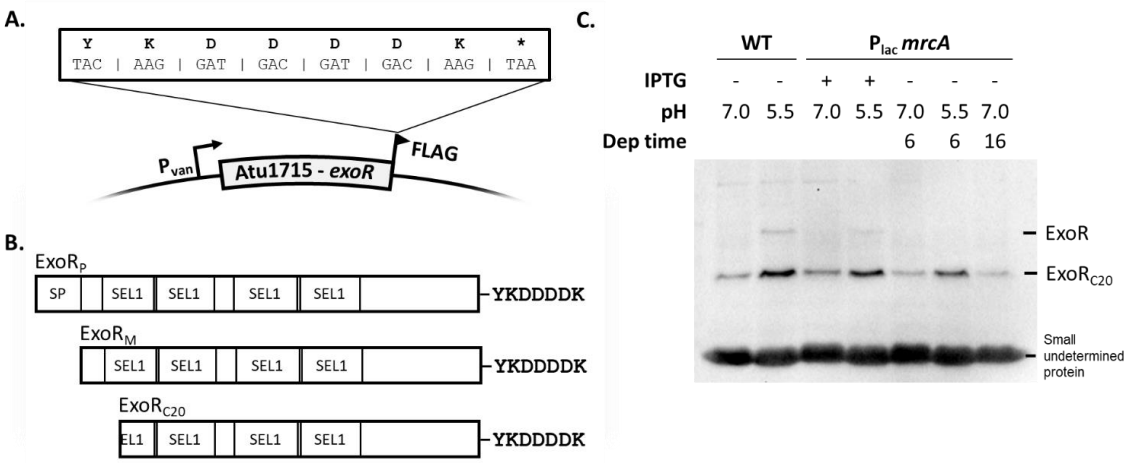

Figure 2.S10. ExoR-FLAG proteolysis. **A.** Schematic of Pvan driven expression of a ExoR-FLAG fusion protein. The sequence of the FLAG tag is shown above. The plasmid was introduced in the WT and PBP1a depletion strains to enable monitoring of ExoR proteolysis. **B.** Potential ExoR products are shown, including the pro-ExoR (ExoRP), mature ExoR (ExoRM), and cleaved ExoR (ExoRC20). ExoRP and ExoRM were indistinguishable and therefore denoted as ExoR. **C.** Western blot demonstrating ExoR-FLAG cleavage following acid treatment but not PBP1a depletion. Bands corresponding to ExoRC20 are labeled. Resolution of the ExoR on the blot does not allow for distinguishing between ExoRP and ExoRM.

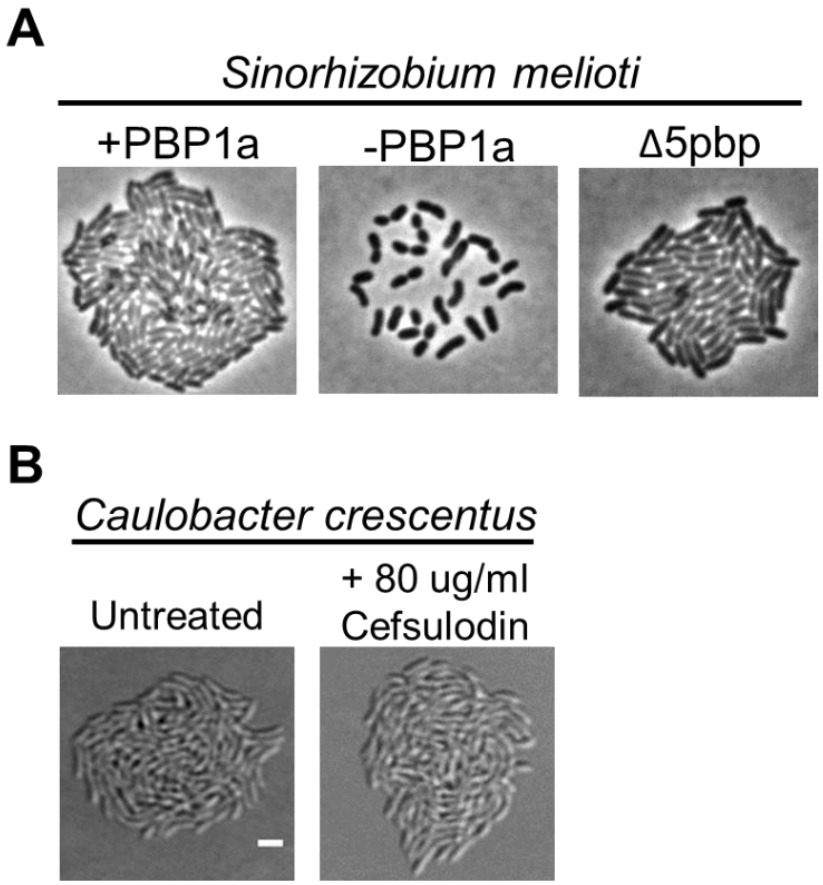

Figure 2.S11. Surface spreading is taxonomically constrained to succinoglycan producing bacteria. **A.** Micrographs of *Sinorhizobium meliloti* Rm2011 PBP1a replete, PBP1a depleted, and a strain with deletions of genes encoding all other high molecular weight PBPs (Δ5pbp). Each strain was grown to exponential phase, spotted on a 1% TY agar pad containing 1mM IPTG if inducing mrcA, allowed to grow for 16 hours, and imaged with phase microscopy. **B.** Micrographs of WT *C. crescentus* cells growth with or without cefsulodin. Cells were grown to exponential phase in PYE media, spotted on a PYE agar pad with or without cefsulodin, allowed to grow for 16 hours, and imaged by DIC microscopy. All scale bars depict 2 μm.

CHAPTER 3

The ChvG-ChvI Two-component System Senses and Protects Against Cell Wall Damage in *A. tumefaciens*

Author Contributions

Jacob Bouchier, Carli McCurry, Amara Mason, Cooper Barnes, Michelle Williams, Emily Knebel conducted experiments and analyzed data, Jacob Bouchier, Michelle Williams, Emily Knebel, and Pamela Brown designed experiments, Jacob Bouchier wrote the original draft and designed the figures, Jacob Bouchier and Pamela Brown reviewed and edited this dissertation chapter

ABSTRACT

For bacteria with complex life cycles involving several environmental niches, adaptability is key. The plant pathogen *Agrobacterium tumefaciens* freely lives in the soil in a benign state. In this environment, *A. tumefaciens* encounters many environmental stressors such as salinity, antibiotics, nutrient availability, changes in pH, and temperature that it must adapt to in order to survive. Upon encountering a potential host plant, *A. tumefaciens* must completely transform its lifestyle from a free-living benign one, to a host-invading state capable of surviving the barrage of host defenses. This transformation is driven by activation of the two-component system ChvG-ChvI. However, recent work has also shown that ChvG-ChvI may function as a more generalized stress response with activity that can be tailored to day-to-day stresses that the bacterium encounters. For example, ChvG-ChvI activation is required for growth in complex media, suggesting that growth on these medias is stressful for *A. tumefaciens*. Here we demonstrate how ChvG-ChvI is important for growth during treatment with cell-wall targeting antibiotics and for growth in complex media. We also demonstrate that biosynthesis of an exopolysaccharide controlled by ChvG-ChvI activation helps protect *A. tumefaciens* against cell-wall targeting antibiotics.

INTRODUCTION

Bacteria must be able to sense and respond to changes in their environment to thrive and survive in diverse habitats. One mechanism bacteria use to sense and respond to changes in the extracellular environment are two-component systems

(TCS). When a sensor histidine kinase detects a stimulus, it dimerizes and undergoes cross-phosphorylation. The kinase dimer subsequently phosphorylates and activates its corresponding response regulator, which also dimerizes. The response regulator dimer then binds to a specific DNA sequence motifs and recruits RNA polymerase, leading to differential expression of genes within the regulon.

The ChvG-ChvI TCS is a characteristic of many, but not all Alphaproteobacteria [1]. It is best studied as an initiator of host invasion in the plant symbiont *Sinorhizobium meliloti* and the plant pathogen *Agrobacterium tumefaciens*. However, recent work in *Caulobacter crescentus* and *A. tumefaciens* has demonstrated ChvG-ChvI functionality beyond association with plants [1,2]. Indeed, ChvG-ChvI is required for survival under various cell envelope stresses. For instance, *chvG* and *chvI* mutants are hypersensitive to treatment with β-lactam antibiotics and in *A. tumefaciens* are unable to grow in rich media containing either yeast extract or tryptone [1–3].

In *A. tumefaciens* activation of ChvG-ChvI results in a complete transformation in lifestyle, resulting in differential expression of hundreds of genes, including those associated with metabolism, nutrient uptake, type VI secretion, and motility. Among the genes with upregulated expression are those required for the biosynthesis of succinoglycan (SGN), an exopolysaccharide synthesized and secreted by plant-associated Rhizobia. The function of SGN remains obscure,

but it is required for plant-host invasion. Notably, secretion of SGN results in a form of flagellar-independent surface spreading motility [1,4]. SGN also binds and inhibits at least one type of anti-microbial peptide known to generate cell-envelope stress [5].

Although evidence continues to accumulate to support the role of ChvG-ChvI TCS in envelope stress tolerance, crucial questions remain unanswered. For example, how does ChvG-ChvI sense stress, and how does the activation of the TCS lead to stress tolerance? Obtaining answers to these questions will aid in our understanding of the types of stresses that these bacteria experience in their natural environments and how they have evolved to overcome them.

Our findings reveal that cell wall-targeting antibiotics and cell wall mutants activate the ChvG-ChvI promoter, directly linking cell-wall stress to pathway activation. We also report on a point mutant in PBP1a that overcomes the hypersensitivity of the *chvI* mutant to cefsulodin, demonstrating that activation of ChvG-ChvI results from antibiotic activity and not direct molecule sensing. Next, we demonstrate that SGN is secreted polarly and that loss of succinoglycan biosynthesis leads to increased sensitivity to cell-wall-targeting antibiotics, linking components of the ChvG-ChvI regulon directly to stress tolerance. Finally, we observed variable localization patterns of ChvG in response to different media conditions, suggesting that ChvG may be targeted to subcellular locations impacted by stress.

RESULTS

Treatment with cell-wall-targeting antibiotics activates the ChvG-ChvI promoter through indirect antibiotic activity

We previously reported that *chvG* and *chvI* mutants are hypersensitive to β-lactam antibiotics, but not to other classes of antibiotics [1]. To test if treatment with these antibiotics results in activation of ChvG-ChvI, we generated pMR15-P_{chvGI}*lacZ*, that expresses *lacZ* during activation of the *chvG-chvI* promoter. Since ChvG-ChvI form a positive feedback loop and regulate expression of themselves [1,3,6], we can use this vector to detect activation of the pathway. Using ONPG as a hydrolytic substrate for β-galactosidase, encoded by *lacZ*, we performed Miller assays to measure the rate of hydrolysis [7,8] (Figure 1A). As expected, β-lactam antibiotics that specifically target activate the ChvG-ChvI TCS. An exception is that cephalexin did not activate the *chvG-chvI* promoter. Cephalexin targets penicillin-binding protein 3 (PBP3) in other bacteria [9] and *A. tumefaciens* expresses two paralogous copies of PBP3 (PBP3a and PBP3b). This redundancy may account for this discrepancy in ChvG-ChvI activation or alternatively loss of PBP3 activity may not activate the ChvG-ChvI. Notably, activation of the pathway was also detected upon treatment with bacitracin, that targets dephosphorylation of the phospholipid carrier of lipid II, preventing incorporation into the existing peptidoglycan macromolecule [10]. This unexpected finding suggests that activation of ChvG-ChvI by antibiotics is not β-

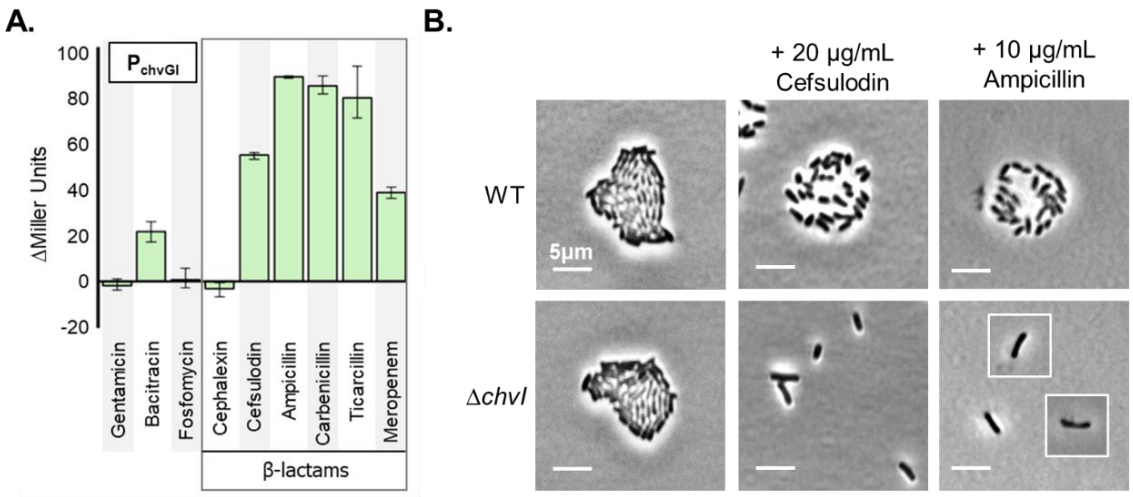

Figure 3.1. Treatment with β-lactam antibiotics activates the *chvGI* promoter. **A.** Panel displays β-galactosidase assay results as change in Miller units for each antibiotic treatment compared to no treatment control. **B.** Micrographs of wild-type and *chvI* mutant cells grown overnight on an ATGN agarose pad without treatment, with treatment of 20 μg/mL cefsulodin, and with treatment of 10μg/mL ampicillin. Insets outlined in white represent additional cells from the same field of view. Scale bar is 5μm for each micrograph.

lactam antibiotic specific, but instead more broadly activated by many types of cell-wall-targeting antibiotics. As reported previously, cefsulodin-treated cells grown overnight on an agarose pad displayed failed microcolonies and spread out cells, characteristic of ChvG-ChvI activation [1] (Figure 1B). Ampicillin-treated cells also failed to form microcolonies. Unsurprisingly, the *chvI* mutant died quickly in the presence of either 20μg/mL of cefsulodin or 10μg/mL of ampicillin overnight and no cell growth or division occurred (Figure 1B). While these results were convincing that treatment with cell-wall targeting antibiotics activates ChvG-ChvI, we had no evidence to speculate if activation occurred through direct sensing of the antibiotics or through activity of the antibiotics.

To address this gap in our understanding, we subjected the *chvI* mutant to a 30-day selective evolution series against cefsulodin treatment. We reasoned that a mutation in the target of cefsulodin that restored cefsulodin resistance in the *chvI* mutant background would suggest that ChvG senses and responds to antibiotic activity, instead of direct sensing of the antibiotic molecule. After 30 days, we had three *chvI* mutants that were resistant to cefsulodin at concentrations over 100μg/mL, a more than 100x increase in minimum-inhibitory concentration compared to the unevolved *chvI* mutant. Whole genome sequencing found that resistance was the result of the same mutation in all three strains. A substitution mutation in the transpeptidase domain of PBP1a (V659M), the target of cefsulodin. AlphaFold2 structure prediction [11] was performed on the point mutant and a cefsulodin docking analysis was performed using AutoDock Vina

[12]. In the wild-type PBP1a, AutoDock Vina predicted a binding affinity of -7.3 kcal/mol for cefsulodin docking to the catalytic pocket of the PBP1a transpeptidase domain (Figure 2A). However, AutoDock Vina was unable to predict even low affinity docking of cefsulodin to the same catalytic pocket in PBP1a^{V659M}, suggesting that the substitution blocks cefsulodin docking completely. By using surface models in ChimeraX [13] of both PBP1a and PBP1a^{V659M}, we were able to identify the cefsulodin-binding catalytic pocket of the transpeptidase domain (Figure 2B). Characterization of the PBP1a^{V659M} predicted structure found a decrease in localized charge within the pocket (Figure 2C), as well as decrease width of the pocket by a predicted 0.493 Å (Figure 2D). Further, the suppressor restored microcolony formation under treatment with cefsulodin (Figure 2E). The observation that a mutation in PBP1a can circumvent cefsulodin hypersensitivity in the *chvI* mutant suggests that activation of ChvG-ChvI is through indirect and occurs due to the loss of PBP1a activity. Next, we sought to understand how ChvG-ChvI activation results in resistance to cell-wall targeting antibiotics.

Secretion of succinoglycan is polarly located and protects against β-lactam antibiotics

SGN is an acidic heteropolysaccharide with a large oligosaccharide repeating unit of β-linked glucose and galactose with several modifications including acetylation, succinylation, and pyruvalation. SGN is produced in copious amount, up to 20% of the total cell dry weight, thus it has been suggested that this

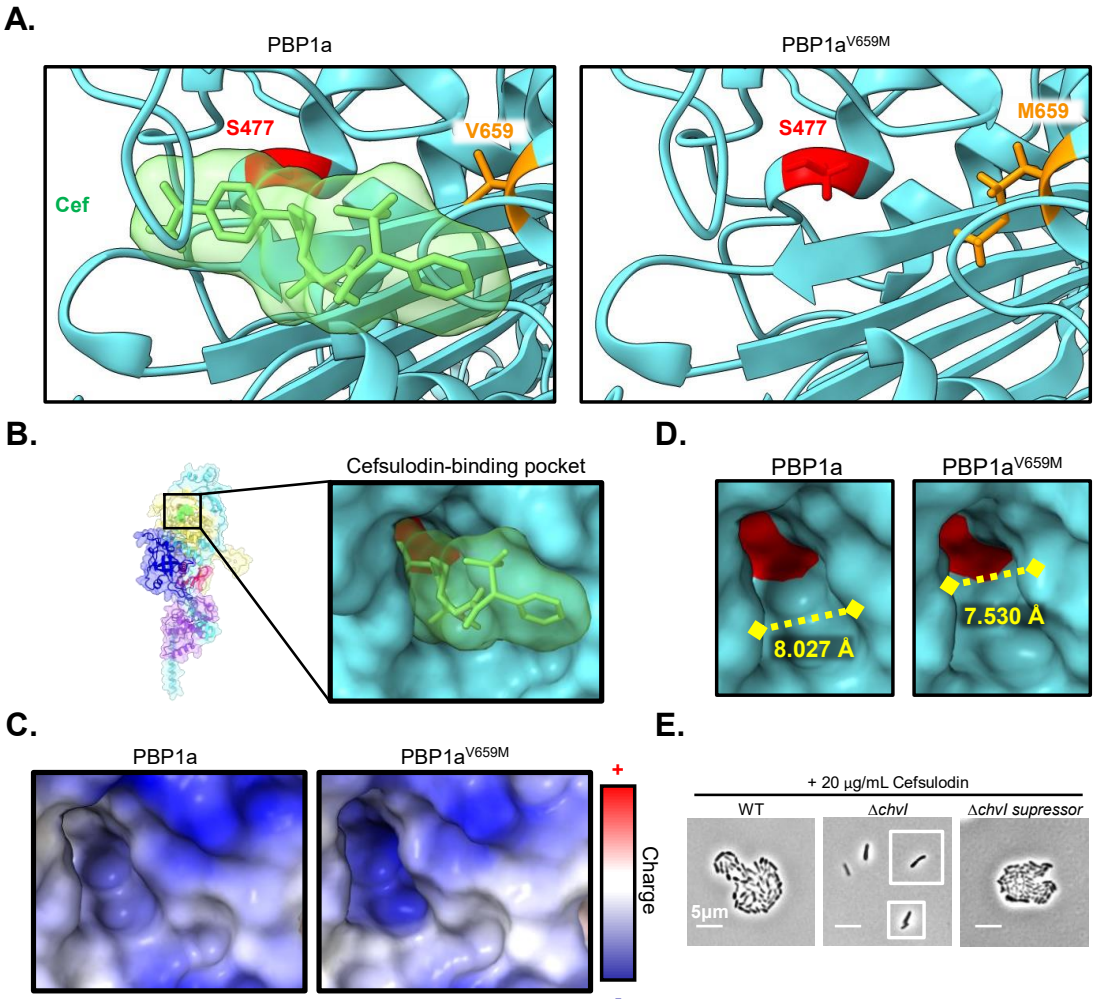

Figure 3.2. Structural characterization of the ΔchvI suppressor. **A.** Ribbon structures of PBP1a and PBP1a^{V659M}. Green, cefsulodin molecule; Red, catalytic transpeptidase residue S477; Orange, substitution V659M. **B.** Surface model of the cefsulodin-binding pocket of PBP1a as predicted using AutoDock Vina. Red, catalytic transpeptidase residue S477. **C.** Charge comparison between the catalytic transpeptidase pockets of PBP1a and PBP1a^{V659M}. **D.** Width comparison between the catalytic transpeptidase pockets of PBP1a and PBP1a^{V659M}. **E.** Micrographs of wild-type, chvI mutant, and chvI mutant suppressor cells grown overnight on an ATGN agarose pad containing 20 µg/mL of cefsulodin. Insets outlined in white represent additional cells from the same field of view.

polysaccharide is required in large amounts for normal growth or survival [20]. The observation that secretion of SGN was further increased by activation of ChvG-ChvI during treatment with cell-wall targeting antibiotics as indicated by cell spreading (Figure 1A) led us to suspect that SGN may have a protective role against these antibiotics. We reasoned that since *A. tumefaciens* grows polarly, meaning peptidoglycan is both metabolized and expanded at a single pole [1,14], cells would be most susceptible to cell-wall stress at the growth pole and thus, the SGN machinery may localize to the growth pole. SGN biosynthesis is mediated by a Wzx/Wzy dependent pathway encoded by 19 *exo* genes (Figure 3A). The ExoP, ExoQ, and ExoT proteins comprise the translocation machinery. Thus, to localize the SGN secretion complex we generated pSRKKm-P_{cym}*exoT-sfGFP* to express a cumate-inducible copy of ExoT-GFP in the wild-type and PBP1a depletion backgrounds. As expected, localization of ExoT-GFP was polar in both wild-type and PBP1a-depleted cells, however, unexpectedly some cells displayed bipolar localization (Figure 3B). To test if succinoglycan secretion was also polar, we briefly co-incubated wild-type and PBP1a-depleted cells with 25 μM of the SGN stain calcofluor white (CFW) and then immediately made a wet-mount slide with each culture. Succinoglycan was imaged using an emission wavelength of 460 nm. Using this technique polar succinoglycan secretion was detected (Figure 3C) in both wild-type and PBP1a-depleted cells, however a much smaller proportion of the cells were labeled with CFW in the wild-type cells than in the PBP1a-depleted cells (data not shown).

To test if SGN contributes to resistance to cell-wall targeting antibiotics we subjected wild-type cells and *exoA* mutant cells to different antibiotics (Table 1). ExoA is a protein involved in SGN biosynthesis and is required for the first committed step in this process. Deletion of *exoA* prevents all SGN biosynthesis [1,15]. We assayed sensitivity to each antibiotic by using disk diffusions with various antibiotic-soaked disks on ATGN. Plates lawned with wild-type or *exoA* mutant cells were co-incubated with each antibiotic disk for two days at 28^{o}C. Zones of inhibition surrounding each antibiotic disk were measured (Figure 3D). Disks containing the β-lactam antibiotics meropenem, cefoxitin, and ampicillin exhibited the largest difference in zones of inhibition between wild-type and *exoA* mutant cells, suggesting that succinoglycan protects against these antibiotics.

PBPs localize to new pole, midcell, and old pole in cells grown in minimal media

To better understand where cells treated with β-lactam antibiotics would experience cell wall stress, we treated wild-type cells grown in both the defined media ATGN (*Agrobacterium tumefaciens* glucose and nitrogen growth media) and the rich, undefined media LB (lysogeny broth) with Bocillin-FL. Bocillin-FL is a fluorescent penicillin that binds penicillin-binding proteins (PBPs) like PBP1a. We confirmed a previous report that Bocilin-FL labels the midcell and new growth pole of *A. tumefaciens* when grown in LB [16] (Figure 4A) but made the surprising discovery that it also labeled the old pole in about a third of the cells when grown in ATGN (Figure 4B), reminiscent of the localization of ExoT-GFP in

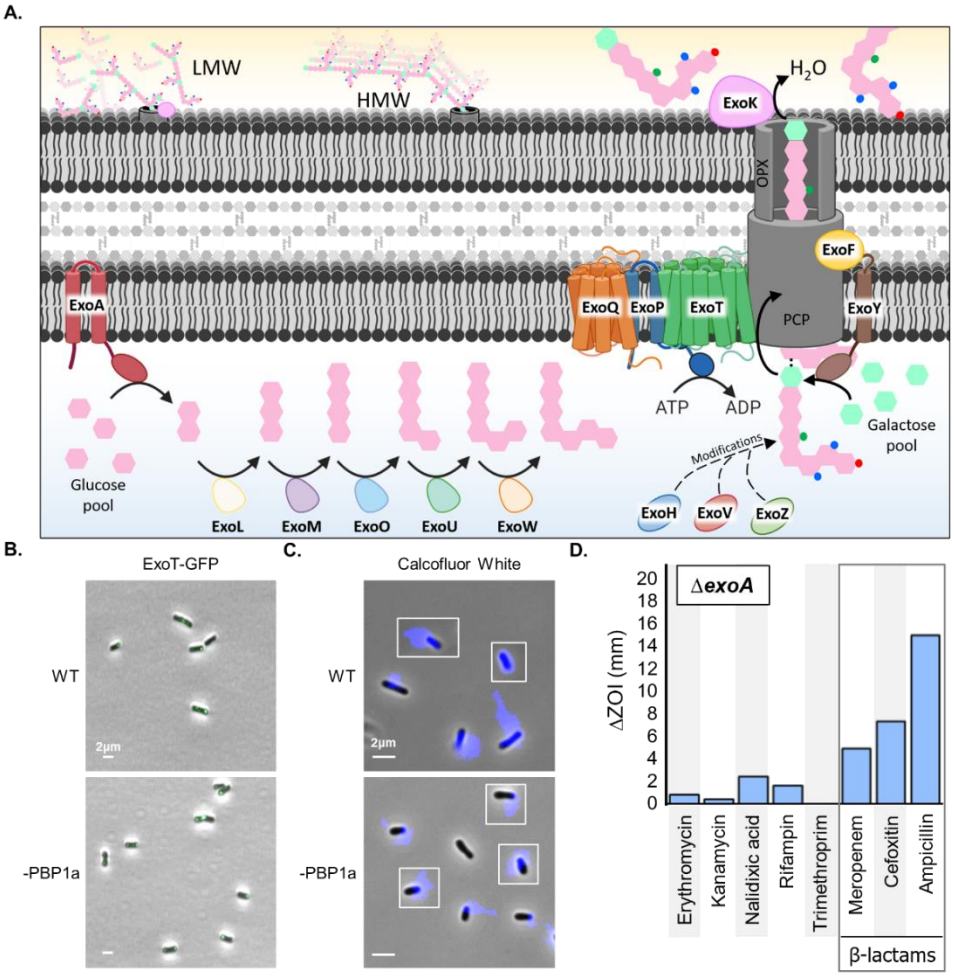

Figure 3.3. Succinoglycan is secreted polarly and protects against β-lactam antibiotics. **A.** Schematic depicting succinoglycan biosynthesis and secretion proteins. **B.** Micrographs showing localization of plasmid-driven ExoT-GFP in wild-type and PBP1a-depleted cells grown in ATGN and spotted onto an agarose pad. **C.** Wet mounts of wild-type and PBP1a-depleted cells grown in ATGN and incubated with 25μM calcofluor white for 5 minutes immediately before imaging. Calcofluor-stained succinoglycan was imaged with an emission wavelength of 460nm. Insets outlined in white represent additional cells from the same field of view. **D.** Panel summarizing the disk diffusion results as a change in zone of inhibition (ΔZOI) between ΔexoA and Wild Type.

PBP1a-depleted cells (Figure 3B). This observation suggests that under certain conditions a subset of PBPs localize bipolarly and may indicate that bacteria experience different stressors between media types.

ChvG displays variable subpolar localization patterns

We postulated that if differential PBP localization was indicative of different envelope stressors that *A. tumefaciens* encounters during growth on different medias, then ChvG would localize to these sites of stress. To test this hypothesis, we replaced the native *chvG* with *chvG-sfGFP* on the chromosome using allelic exchange [17] in our wild-type background. Cells expressing ChvG-sfGFP as the sole copy of ChvG in the cell retain rod-shaped morphology (Figure 5A) and are capable of growth in the presence of cefsulodin (Figure 5B) and on LB (LB10, Figure 5D) suggesting that ChvG-sfGFP is a functional fusion. After multiple attempts to localize ChvG-GFP in cells grown in liquid ATGN with and without treatment with cefsulodin, we concluded that ChvG-GFP has a dispersed localization (Figure 5A, only no treatment data shown). Next, we incubated our ChvG-GFP strain overnight on an ATGN agarose pad with and without cefsulodin. To our surprise, both showed polar localization. Notably, not all polar localization was at the new pole. Some cells displayed old pole foci and others were bipolar. Further, some foci were off-center suggesting that the localization of ChvG-GFP molecules may be dynamic or have an atypical asymmetric localization pattern (Figure 5B). While cefsulodin-treated cells were easier to see because they are wider and spread apart, we didn’t observe any obvious

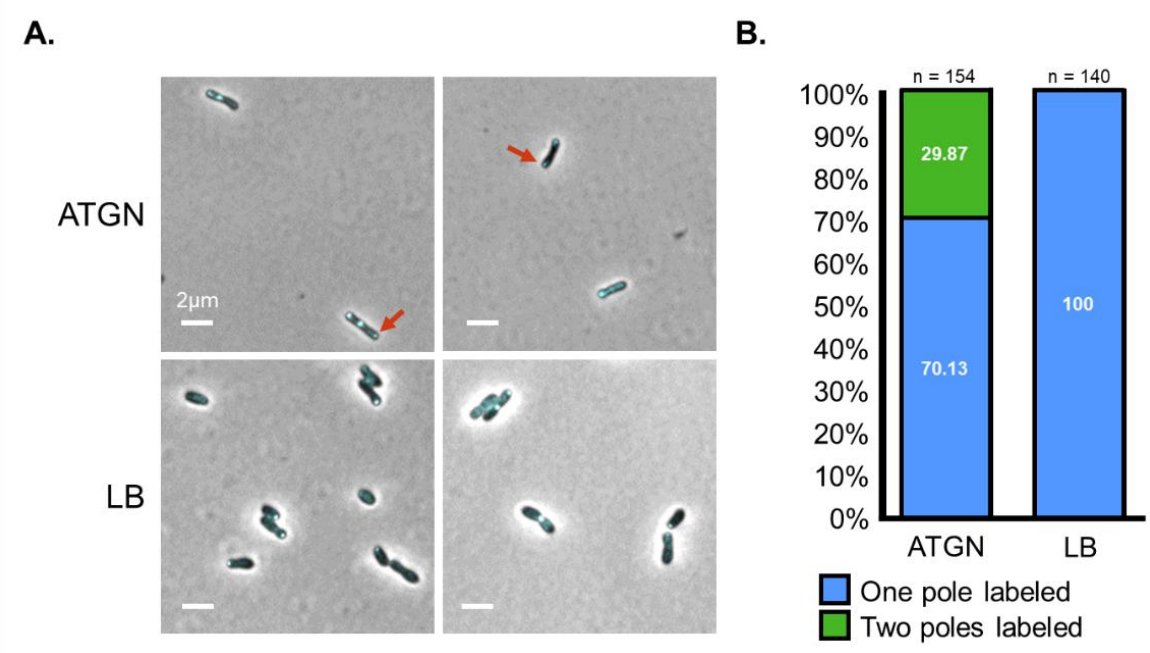

Figure 3.4. Bocillin-FL treatment labels cells differently depending on growth medium. **A.** Cells grown in corresponding growth media and then incubated with 20μg/mL of Bocillin-FL for 30 minutes at 28ºC without shaking. **B.** Quantification of pole labeling in Bocillin-FL treated cells. Cells labeled at midcell were ignored for this analysis.

differences in localization between treated and untreated cells grown on overnight pads made with ATGN. The observation that cells grown in liquid ATGN don't localize ChvG-GFP, but those grown on ATGN agarose pads do, suggests that the presence of agarose introduces a stress that is different than growing in liquid media.We hypothesized that growth on LB media may be stressful for *A. tumefaciens* due to the inability of *chvG* mutants to grow on it. Supporting this hypothesis, we observed a clear localization pattern in ChvG-GFP cells grown in LB, which is a mixture of yeast extract, tryptone, NaCl, and water (LB10, Figure 5C-5D). As ChvG senses cell envelope stresses, we hypothesized that different NaCl concentrations could impact the osmotic stresses experienced by the cells. We tested this by varying the NaCl concentration in three batches of LB and growing ChvG-GFP cells in each. We observed clear localization in a subpolar region near the new pole of cells in all batches, even in one with no NaCl added (LB0, Figure 5C and 5D), indicating that NaCl is not strictly required for ChvG-GFP localization. However, higher NaCl concentrations reduced pattern variability and increased the overall density of foci within the subpolar region near the new pole (LB5 and LB10, Figure 5C and 5D). These findings suggest that ChvG localization depends on the growth conditions and ChvG may be monitoring the cell wall integrity and responding to local sites of cell wall damage.

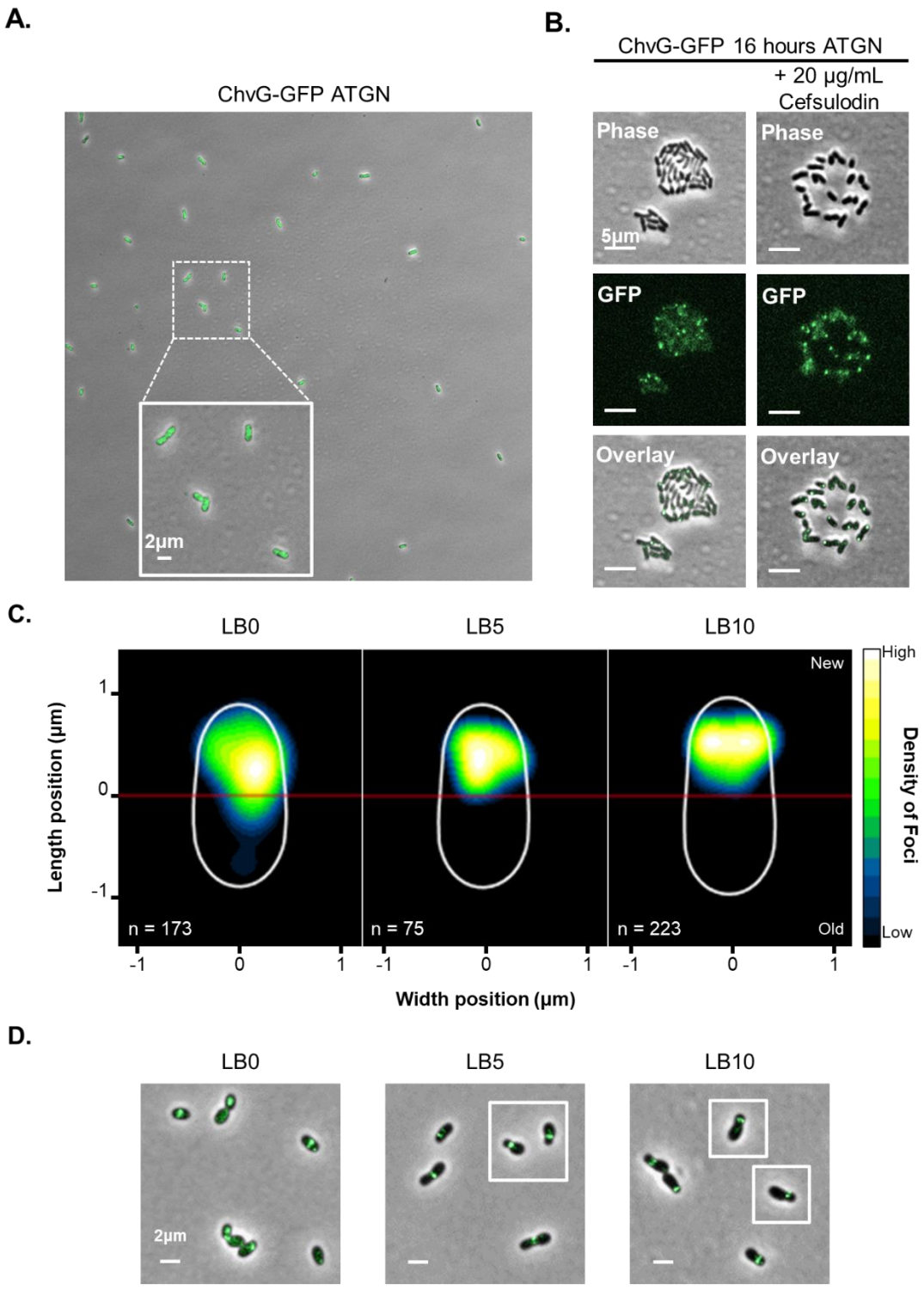

Figure 3.5. ChvG-GFP localization exhibits unique localization patterns between ATGN and LB. **A.** Full field micrograph of ChvG-GFP strain grown overnight to expoential in ATGN and then spotted onto an agarose pad. **B.** ChvG-GFP strain

grown overnight on an ATGN agarose pads with and without 20 μg/mL of cefsulodin. **C.** Heatmap of foci density for each LB media type. LB0 has 0% NaCl, LB5 has 5% NaCl, and LB10 has 10% NaCl. White cell shape contour represents the average morphology of all cells used in the analysis. Sample size is number of foci used in the analysis. **D.** Micrographs of cells grown overnight to exponential in either LB0, LB5, or LB10 and then spotted on an agar pad for imaging. Insets outlined in white represent additional cells from the same field of view.

DISCUSSION

Bacteria must be able to overcome the stress caused during cell growth. Naturally, growth in different environments will intensify or relieve these stresses. To this end, bacteria rely on dynamic mechanisms that tailor responses to the severity of the stress. *A. tumefaciens* uses the ChvG-ChvI TCS to sense and respond to cell-envelope stress. Morphological differences along with differences in Bocillin-FL labeling between media types suggests that we have yet to fully understand the complex nature of polar growth in this organism, let alone the stresses that distinct media types can induce during growth. Notably, treatment with FDAADs on cells grown in ATGN only labels the new pole and midcell, suggesting that PBPs localized to the old pole may be nonfunctional [18]. ChvG likely localizes to areas of active cell-wall metabolism and synthesis as these areas are the most likely sites cell envelop stress to occur. Activation of the pathway results in differential expression of genes involved in stress tolerance, including genes associated with the biosynthesis of SGN.

SGN preferentially protects *A. tumefaciens* cells from the activity of cell-wall targeting antibiotics. However, how it confers this protection remains a mystery. Perhaps SGN forms a protective barrier analogous to a capsule, but this doesn't explain the specificity of its protection. Another possibility is that it directly binds these antibiotics. In *Sinorhizobium meliloti,* SGN binds the cell-envelope-stress-causing antimicrobial peptide NCR247, preventing it from ever entering the cell

[5]. Another possibility is that SGN functions in the periplasm of *A. tumefaciens,* blocking targets for antibiotics. It could also be both possibilities. SGN exists in two forms, a high-molecular weight (HMW) and a low-molecular weight (LMW) form. While both HMW SGN and LMW SGN are likely secreted outside of the cell, some LMW SGN may remain in the periplasm. ExoT has been proposed as a flippase [19], transporting LMW SGN synthesized in the cytoplasm to the periplasm. Future work will be needed to determine if extracellular or periplasmic SGN is important for protection during cell wall stress. In addition, while the pyruvate is present in stoichiometric amounts, the succinate and acetate modification of SGN is variable in different culture conditions [21]. Thus, the role of chain length and modification of SGN should be a direction for future studies to understand the contributions of SGN to antibiotic tolerance in *A. tumefaciens*.

MATERIALS AND METHODS

Bacterial strains, plasmids, and growth conditions. A list of all bacterial strains and plasmids used in this study is provided in the Strains and Plasmids Table. *Agrobacterium tumefaciens* C58 and derived strains were grown in ATGN minimal media [23] without exogenous iron or in Lysogeny Broth as stated at 28°C with shaking. When appropriate, kanamycin (KAN) was used at the working concentration of 300 µg/ml. When indicated, isopropyl β-D-1-thio-galactopyranoside (IPTG) was used as an inducer at a concentration of 1 mM. *E. coli* DH5α and S17-1 λ pir were grown in Lysogeny Broth medium at 37°C and when appropriate 50 µg/ml or 30 µg/ml of KAN were added, respectively.

Construction of plasmids and strains. Vector for allelic exchange with ChvG-GFP were constructed using recommended methods for *A. tumefaciens* [22]. Briefly, 500-bp fragments upstream and 500 bp downstream of the c-terminal end of ChvG, excluding the stop codon were amplified using primer pairs P1/P2 and P3/P4 respectively. Amplicons were spliced together by SOEing using primer pair P1/P4. The amplicon was digested and ligated into pNTPS139. The deletion plasmids were introduced into *A. tumefaciens* by mating using an *E. coli* S17 conjugation strain to create kanamycin resistant, sucrose sensitive primary integrates. Primary integrates were grown overnight in media with no selection. Secondary recombinants were screened by patching for sucrose resistance and kanamycin sensitivity. Colony PCR with primers P5/P6 for the respective sequence target was used to confirm insertion. PCR products from P5/P6 primer sets were sequenced to further confirm insertion.

The ExoT-GFP expression vector was constructed by amplifying *exoT* without a stop codon using *exoT* Forward and Reverse primers. The PCR amplicon was digested and ligated into pSRKKm-P_{cym} with a copy of sfGFP, generating pSRKKm-P_{cym}*exoT*-sfGFP*,* containing a copy of *exoT* with an in-frame c-terminal GFP tag behind a cumate-inducible promoter. pSRKKm-P_{cym}*exoT*-sfGFP was sequenced and was introduced into *A. tumefaciens* using the S17 conjugation strain to create kanamycin resistant colonies. Transformation was verified by colony PCR using Cumate Forward and pSRK Reverse primers.

The vector for Miller assays pMR15 P_{chvGI}-*lacZ* was constructed by amplifying the 338 bp intergenic region just upstream of the *chvI-chvG-hprK* operon of Agrobacterium tumefaciens with primers flanked with the restriction digestion sites PstI and NheI. Restriction digestion of the pMR15-*lacZ* and the intergenic region amplicon was performed and the fragments were ligated and transformed as described above.

Miller assays. Ten 1 mL cultures of wild-type cells carrying the pMR15 P_{chvGI}-*lacZ* plasmid were grown up overnight in 300 ug/mL of kanamycin for selection and diluted to an OD_{600} of 0.2. Nine of the diluted cultures were supplemented with 20 ug/mL of each corresponding antibiotic. Cells were grown in the presence of the antibiotic for 6 hours at 28^{o}C. The OD_{600} of each culture was monitored and fresh media supplemented with the appropriate antibiotic was added so that the OD_{600} never grew to above 0.8. After incubation, the ten cultures were diluted down to match the OD_{600} of the least concentrated culture. The Miller assays were performed in a BioTek Synergy H1 Hybrid plate reader using a protocol described previously [25]. BugBuster (Millipore; 70921-4) was substituted for PopCulture reagent.

Cefsulodin adaptive evolution experiment. One Δ*chvI* colony was inoculated in 1 mL of ATGN media and grown overnight at 28^{o}C in a shaking incubator. Overnight culture was diluted to an OD_{600} of 0.1 and grown to an OD_{600} of ~0.7.

Culture was diluted to an OD_{600} of 0.05 split into two 500 uL cultures. Cefsulodin was added to each culture to a final concentration of 4 µg/mL. Cultures were grown overnight and each morning were saved in a frozen stock and diluted back down to an OD_{600} of 0.05, adding 25% more cefsulodin each subsequent day for 15 days. DNA of day 15 cultures was extracted using a GeneJet Genomic Purification Kit (K0722) and submitted for whole genome sequencing at SeqCenter (https://www.seqcenter.com/).

Disk diffusion assays. Wild-type and Δ*exoA* cells were overnight and then knocked down to an OD_{600} of 1.0. Cells were then lawned on ATGN minimal media. Sterile paper disks either soaked in concentrations of each antibiotic or not (blank controls) were applied to the plate. Each plate was grown for ~48 hours at 28°C before being imaged. Zone of inhibition diameters were measured from each image using ImageJ software.

Phase and fluorescence microscopy. A small volume (~1 µl) of cells in exponential phase (OD600 = 0.2 - 0.4) was applied to 1.5% agarose pads made with either ATGN, LB not supplemented with NaCl (LB0), LB supplemented with 5 g/L NaCl (LB5), or LB supplemented with 10 g/L NaCl (LB10, the standard LB concentration). When appropriate agar pads were also supplemented with 1mM IPTG. Phase contrast and epifluorescence microscopy were performed with an inverted Nikon Eclipse TiE and a QImaging Rolera em-c2 123 1K EMCCD camera with Nikon Elements Imaging Software.

For calcofluor staining of succinoglycan, exponential cells were incubated with 5mM calcofluor white for 30 minutes, cells were imaged as wet mounts by immediately spotting cells onto a glass slide and covering with a glass coverslip. Calcofluor-stained succinoglycan was imaged using the DAPI filter with an exposure time of 40 ms. GFP fusion strains were imaged using the FITC filter with an exposure time of 300ms.

For cell labeling with Bocillin-FL, bacterial cells were grown overnight in either LB or ATGN and then diluted to an OD_{600} of 0.1. When cells reached an OD_{600} of 0.5 they were incubated with 15 µg/mL of Bocillin-FL for 30 minutes at 28^{o}C. Immediately after incubation, cells were spotted on agarose pads made with the corresponding media. Cells were imaged with an emission wave length of 488 nm. Quantification was done by manually counting foci.

Image analysis of ChvG-GFP localization. Cells grown for 12 hours in either LB0, LB5, or LB10 were imaged. Images were opened in MicrobeJ [24] and localization of peak GFP fluorescence for each cell was identified as maxima foci. Cell polarity is oriented using max cell width for each pole. Average cell shape and density plots were generated for each media condition using the maxima localization data.

REFERENCES

1. Williams MA, Bouchier JM, Mason AK, Brown PJB. Activation of ChvG-ChvI regulon by cell wall stress confers resistance to β-lactam antibiotics and initiates surface spreading in Agrobacterium tumefaciens. PLOS Genet. 2022;18: e1010274. doi:10.1371/JOURNAL.PGEN.1010274
2. Quintero-Yanes A, Mayard A, Hallez R. The two-component system ChvGI maintains cell envelope homeostasis in *Caulobacter crescentus*. PLOS Genet. 2022;18: e1010465. doi:10.1371/JOURNAL.PGEN.1010465
3. Heckel BC, Tomlinson AD, Morton ER, Choi JH, Fuqua C. Agrobacterium tumefaciens ExoR controls acid response genes and impacts exopolysaccharide synthesis, horizontal gene transfer, and virulence gene expression. J Bacteriol. 2014;196: 3221–3233. doi:10.1128/JB.01751-14
4. Dilanji GE, Teplitski M, Hagen SJ. Entropy-driven motility of *Sinorhizobium meliloti* on a semi-solid surface. Proc R Soc B Biol Sci. 2014;281. doi:10.1098/RSPB.2013.2575
5. Arnold MFF, Penterman J, Shabab M, Chen EJ, Walker GC. Important Late-Stage Symbiotic Role of the *Sinorhizobium meliloti* Exopolysaccharide Succinoglycan. J Bacteriol. 2018;200. doi:10.1128/JB.00665-17
6. Yuan ZC, Liu P, Saenkham P, Kerr K, Nester EW. Transcriptome profiling and functional analysis of Agrobacterium tumefaciens reveals a general conserved response to acidic conditions (pH 5.5) and a complex acid-mediated signaling involved in Agrobacterium-plant interactions. J Bacteriol. 2008;190: 494–507. doi:10.1128/JB.01387-07

7. Schaefer J, Jovanovic G, Kotta-Loizou I, Buck M. Single-step method for β-galactosidase assays in Escherichia coli using a 96-well microplate reader. Anal Biochem. 2016;503: 56. doi:10.1016/J.AB.2016.03.017
8. Zubay G, Morse DE, Schrenk WJ, Miller JH. Detection and Isolation of the Repressor Protein for the Tryptophan Operon of Escherichia coli. Proc Natl Acad Sci. 1972;69: 1100–1103. doi:10.1073/PNAS.69.5.1100
9. Yao Z, Kahne D, Kishony R. Distinct Single-Cell Morphological Dynamics under Beta-Lactam Antibiotics. Mol Cell. 2012;48: 705–712. doi:10.1016/J.MOLCEL.2012.09.016
10. Stone KJ, Strominger JL. Mechanism of Action of Bacitracin: Complexation with Metal Ion and C55-Isoprenyl Pyrophosphate. Proc Natl Acad Sci. 1971;68: 3223–3227. doi:10.1073/PNAS.68.12.3223
11. Jumper J, Evans R, Pritzel A, Green T, Figurnov M, Ronneberger O, et al. Highly accurate protein structure prediction with AlphaFold. Nat 2021 5967873. 2021;596: 583–589. doi:10.1038/s41586-021-03819-2
12. Eberhardt J, Santos-Martins D, Tillack AF, Forli S. AutoDock Vina 1.2.0: New Docking Methods, Expanded Force Field, and Python Bindings. J Chem Inf Model. 2021;61: 3891–3898. doi:10.1021/ACS.JCIM.1C00203/SUPPL_FILE/CI1C00203_SI_002.ZIP
13. Pettersen EF, Goddard TD, Huang CC, Meng EC, Couch GS, Croll TI, et al. UCSF ChimeraX: Structure visualization for researchers, educators, and developers. Protein Sci. 2021;30: 70–82. doi:10.1002/PRO.3943
14. Brown PJB, De Pedro MA, Kysela DT, Van Der Henst C, Kim J, De Bolle

X, et al. Polar growth in the Alphaproteobacterial order Rhizobiales. doi:10.1073/pnas.1114476109

15. Tomlinson AD, Ramey-Hartung B, Day TW, Merritt PM, Fuqua C. Agrobacterium tumefaciens ExoR represses succinoglycan biosynthesis and is required for biofilm formation and motility. Microbiology. 2010;156: 2670. doi:10.1099/MIC.0.039032-0
16. Cameron TA, Anderson-Furgeson J, Zupan JR, Zik JJ, Zambryski PC. Peptidoglycan Synthesis Machinery in Agrobacterium tumefaciens During Unipolar Growth and Cell Division. 2014 [cited 19 May 2020]. doi:10.1128/mBio.01219-14
17. Blomfield IC, Vaughn V, Rest RF, Eisenstein BI. Allelic exchange in Escherichia coli using the Bacillus subtilis sacB gene and a temperature-sensitive pSC101 replicon. Mol Microbiol. 1991;5: 1447–1457. doi:10.1111/J.1365-2958.1991.TB00791.X
18. Williams MA, Aliashkevich A, Krol E, Kuru E, Bouchier JM, Rittichier J, et al. Unipolar Peptidoglycan Synthesis in the Rhizobiales Requires an Essential Class A Penicillin-Binding Protein. MBio. 2021;12. doi:10.1128/MBIO.02346-21/SUPPL_FILE/MBIO.02346-21-S0001.DOCX
19. González JE, Semino CE, Wang LX, Castellano-Torres LE, Walker GC. Biosynthetic control of molecular weight in the polymerization of the octasaccharide subunits of succinoglycan, a symbiotically important exopolysaccharide of Rhizobium meliloti. Proc Natl Acad Sci U S A. 1998;95: 13477. doi:10.1073/PNAS.95.23.13477

20. Wu D, Li A, Ma F et al (2016) Genetic control and regulatory mechanisms of succinoglycan and curdlan biosynthesis in genus Agrobacterium. Appl Microbiol Biotechnol 100:6183–6192

21. Stredansky M. (2005). Succinoglycan. Biopolym. Online 5 10.1002/3527600035.bpol5007

22. Morton ER, Fuqua C. Genetic manipulation of Agrobacterium. Curr Protoc Microbiol. 2012. doi:10.1002/9780471729259.mc03d02s25

23. Morton ER, Fuqua C. Laboratory Maintenance of *Agrobacterium*. Current Protocols in Microbiology. 2012. doi:10.1002/9780471729259.mc03d01s24

24. Ducret A, Quardokus EM, Brun Y v. MicrobeJ, a tool for high throughput bacterial cell detection and quantitative analysis. Nat Microbiol. 2016;1: 16077. doi:10.1038/nmicrobiol.2016.77

25. Shaefer J, Jovanovic G, Kotta-Loizou I, Buck M. Single-step method for β-galactosidase assays in *Escherichia coli* using a 96-well microplate reader. Anal Biochem. 2016;503:56-57. doi:10.1016/j.ab.2016.03.017

STRAINS AND PLASMIDS

Strain or Plasmid	Relevant Genotype, Features or Characteristics	Source or Reference
Source Plasmids		
pNTPS139	Km^r; Suicide vector containing *oriT* and *sacB*	D. Alley
pSRKKm-P_{cym}	Km^r, CymR expression, P_{lac} expression vector with cymR operators replacing lacI operators. Contains *oriV* and MCS with c-terminal GFP.	
Exchange Plasmids		
pNTPS139-*chvG-sfGFP*	Km^r Suc^s; allelic exchange plasmid for tagging native copy of *chvG* with GFP	This Study
Expression Plasmids		
pMR15-P_{chvGI}*lacZ*	Plasmid-driven expression of *lacZ* under control of the ChvG-ChvI promoter	This Study
pSRKKm-P_{cym}*exoT-sfGFP*	Km^r, Cumate-inducible copy of the ExoT-GFP	This Study
***E. coli* strains**		
DH5α	Cloning strain	Life Technologies
S17-1	Sm^r;RP4-2 TC::MU Km-Tn7; for plasmid mobilization	1
***A. tumefaciens* strains**		
C58ΔtetRA::a-attTn7 (WT)	Replacement of the tetRA locus with an artificial attTn7 site	2
C58	Parent strain	3
C58 Δ*chvI*	*chvI* deletion in the C58 parent strain background	4
C58 Δ*chvI,* $PBP1a^{V659M}$	PBP1a point mutation in the *chvI* deletion background that circumvents hypersensitivity to cefsulodin.	This Study
C58ΔtetRA::a-attTn7 Δ*exoA*	*exoA* deletion in the WT background	5
C58ΔtetRA::mini-Tn7-GM-Plac -pbp1a, Δpbp1a	Gm^r, Chromosome-based complementation of Δpbp1a with C58ΔtetRA::mini-Tn7-GM-Plac-pbp1a allowing depletion of PBP1a under control of the lac promoter	6
C58ΔtetRA::a-attTn7 + pSRKKm-P_{cym}*exoT-sfGFP*	Km^r, WT strain carrying a cumate-inducible copy of ExoT-GFP	This Study
C58ΔtetRA::mini-Tn7-GM-Plac -pbp1a, Δpbp1a + pSRKKm-P_{cym}*exoT-sfGFP*	Gm^r, Km^r, PBP1a depletion strain carrying a cumate-inducible copy of ExoT-GFP	This Study
C58ΔtetRA::a-attTn7 + pMR15-P_{chvGI}*lacZ*	Km^r, WT background carrying a copy of *lacZ* under control of the ChvG-ChvI promoter	This Study

Source References

1. Simon R, Priefer U, Pühler A. A broad host range mobilization system for in vivo genetic engineering: transposon mutagenesis in gram negative bacteria. Bio/Technology. 1983;1: 784–791. doi:10.1038/nbt1183-784
2. Figueroa-Cuilan W, Daniel JJ, Howell M, Sulaiman A, Brown PJB. Mini-Tn7 insertion in an artificial attTn7 site enables depletion of the essential master regulator ctrA in the phytopathogen Agrobacterium tumefaciens. Appl Environ Microbiol. 2016;82. doi:10.1128/AEM.01392-16
3. Watson B, Currier TC, Gordon MP, Chilton MD, Nester EW. Plasmid required for virulence of Agrobacterium tumefaciens. J Bacteriol. 1975;123: 255–64. doi:10.1128/jb.123.1.255-264.1975
4. Heckel BC, Tomlinson AD, Morton ER, Choi JH, Fuqua C. Agrobacterium tumefaciens ExoR controls acid response genes and impacts exopolysaccharide synthesis, horizontal gene transfer, and virulence gene expression. J Bacteriol. 2014;196: 3221–3233. doi:10.1128/JB.01751-14
5. Williams MA, Bouchier JM, Mason AK, Brown PJB. Activation of ChvG-ChvI regulon by cell wall stress confers resistance to β-lactam antibiotics and initiates surface spreading in Agrobacterium tumefaciens. PLoS Genet. 2022;18: e1010274. doi:10.1371/journal.pgen.1010274
6. Williams MA, Aliashkevich A, Krol E, Kuru E, Bouchier JM, Rittichier J, et al. Unipolar peptidoglycan synthesis in the Rhizobiales requires an

essential class A penicillin-binding protein. mBio. 2021;12. doi:10.1128/mBio.02346-21

PRIMER LIST

Synthesized DNA	Sequence (5' – 3')
Primers for deletion vectors in *A. tumefaciens*	
chvI-chvG-hprK Promoter PstI Forward	GCACCTGCAGGACGCGTTCCTTGTAAATGACG
chvI-chvG-hprK Promoter NheI Reverse	GCACGCTAGCGGTCTCCATCGTCATTTTCTCGT
exoT Forward NdeI	CTACGTCATATGCCCCCAGCGCCAAATGTAAAG
exoT Reverse BamHI	CAGTACGGATCCACCTTGGGTTGCGGTATC
pNPTS139 Reverse	GGATCCACGATATCCTGCAGGAAGC
chvG pNPTS139 Overlap Forward	gcttcctgcaggatatcgtggatccGTGTTGAAGAAAACGCCGG
chvG sfGFP_Linker Overlap Reverse	cagcggatccGCGTTCATGGGTTTCGGC
sfGFP_Linker *chvG* Overlap Forward	ccatgaacgcGGATCCGCTGGCTCCGCT
sfGFP *chvG*_500ds Overlap Reverse	cagcgttcatTTATTTGTAGAGTTCATCCATGCCGTGCG
*chvG*_500ds sfGFP Overlap Forward	ctacaaataaATGAACGCTGAACGCTTC
*chvG*_500ds pNPTS139 Overlap Reverse	aagctacgtaatacgactcactagtGATGAGGAAAATGCGAATCGC
pNPTS139 Forward	ACTAGTGAGTCGTATTACGTAGCTTGGC

CHAPTER 4

Dissection of PBP1a structure, function, and interacting protein partners reveals a putative elongasome in *Agrobacterium tumefaciens*

Author Contributions

Jacob Bouchier, Robert Kazmierczak, Wanda Figueroa-Cuilan, and Laurie Agosto conducted experiments, Jacob Bouchier, Robert Kazmierczak, Wanda Figueroa-Cuilan, and Pamela Brown designed experiments, Jacob Bouchier and Robert Kazmierczak analyzed data, Jacob Bouchier wrote the original draft and was responsible for visualizations and Jacob Bouchier, Robert Kazmierczak, and Pamela Brown reviewed and edited this dissertation chapter.

ABSTRACT

In contrast to many rod-shaped bacteria, *Agrobacterium tumefaciens* lacks a canonical elongasome comprised of MreB-RodA-PBP2 to drive cellular elongation. Instead, *A. tumefaciens* uses a bifunctional penicillin binding protein, PBP1a, as the primary driver of elongation. Here, we sought to characterize the structure and function of PBP1a domains. We find that the enzymatic domains are necessary for PBP1a to function in elongation. In addition, we find that the OB-fold likely interacts with a negative regulator of PBP1a activity. To identify candidate regulators of PBP1a activity, we used PBP1a as a bait protein and identified proteins that complex with PBP1a. These efforts have revealed several proteins involved in the synthesis and regulation of peptidoglycan metabolism. Overall, this work has improved our understanding of the *A. tumefaciens* elongasome and its regulation.

INTRODUCTION

To withstand osmotic stresses, most bacteria rely on the cell wall, a robust and rigid structure composed of a mesh-like network of glycan strands and short cross-linked peptides that form a macromolecule called peptidoglycan. This structure not only defines bacterial cell shape but is also essential for bacterial cell elongation and division. Bacterial growth and division have been extensively studied in model organisms such as *Escherichia coli*, *Bacillus subtilis*, and *Caulobacter crescentus*, leading to the emergence of a canonical model for bacterial growth in rod-shaped bacteria. In these bacteria, a molecular machine

known as the elongasome containing MreB, RodA, and PBP2 function together to drive elongation (for review [1]). Yet, the insights gained from these studies are not universal.

The genomes of members of the Rhizobiales clade of the Alphaproteobacteria do not encode MreB, RodA, or PBP2 suggesting that alternative mechanisms can drive peptidoglycan biosynthesis in these bacteria. Indeed, *Agrobacterium tumefaciens* relies on the activity of an essential class A penicillin-binding protein PBP1a to confine cell wall synthesis to a single growth pole [2]. While the activity of PBP1a is essential for elongation [2] and an absence of PBP1a activity activates the ChvGI stress response [3], we lack an understanding of how PBP1a activity is regulated through the cell cycle.

In this work, we found that PBP1a interacts with a variety of proteins, many of which are involved in cell wall synthesis and metabolism. These interactions are painting a clearer picture of the regulatory mechanisms governing polar growth dynamics in *A. tumefaciens*.

RESULTS

Both transpeptidase and glycosyltransferase activities of PBP1a are required for elongation in *Agrobacterium tumefaciens*

PBP1a is essential for viability and cellular elongation in *A. tumefaciens* [2]. PBP1a has three discrete domains: a glycosyltransferase domain, a

transpeptidase domain, and an OB-fold extension of unknown function. It also has a flexible linker between the glycosyltransferase and transpeptidase domains, a signal peptide that anchors it into the inner membrane, and an extended structural loop of unknown function that extends out between the transpeptidase domain and linker. Here, we dissected PBP1a and its domains to better understand its essentiality during polar growth. Throughout this work we characterized the impact of PBP1a variants expressed from cumate-inducible plasmids (Figure 1A-B) in both wild-type *A. tumefaciens* cells (WT) and a PBP1a depletion strain under conditions where PBP1a is expressed (+PBP1a) or depleted (-PBP1a).

When chromosomal PBP1a is depleted, the expression of full-length PBP1a from a plasmid is sufficient to restore growth (cyan, Figure 1C). In contrast, expression of PBP1a point mutants in the transpeptidase (S477A) and glycosyltransferase (E87Q) domains failed to restore length in PBP1a-depleted cells to IPTG-induced levels (yellow and purple, Figure 1C). Notably, uninduced PBP1a-depleted cells carrying plasmids with full-length PBP1a were on average longer than those

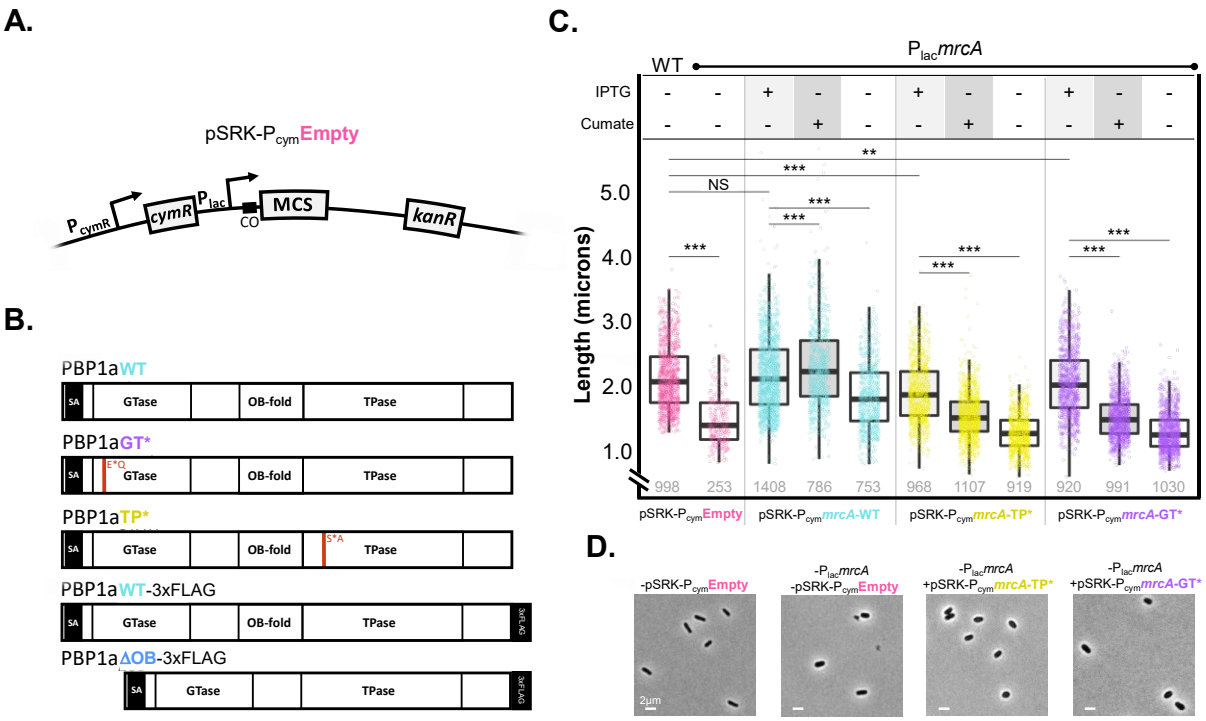

Figure 4.1. Mutagenesis of the catalytic domains reveals dual essentiality in the bifunctional roles of PBP1a. **A.** Plasmid schematic of the cumate-inducible vector used in this study. P_{cymR}cymR, repressor expression cassette; P_{lac}, lac promoter; CO, cumate operator and binding site of CymR; Derepression by cumate; MCS, multiple cloning site; kanR, kanamycin selection cassette. **B.** Schematic of PBP1a variants cloned into the MCS of pSRK-P_{cym}Empty. Red-orange lines denote point mutations. **C.** Length analysis of constructs expressing corresponding PBP1a variants. PBP1a is encoded by the gene mrcA. **D.** Micrographs showing cell morphology of cells expressing the corresponding PBP1a variant from panel C. Statistical significance was determined using an ANOVA and pairwise comparisons was determined using a post hoc TukeyHSD test. NS, Not significant; * , $p_{adj} < 0.05$; ** , $p_{adj} < 0.005$; *** , $p_{adj} < 0.0005$.

carrying plasmids with either mutant (Figure 1C), suggesting that there may be a degree of leakiness associated with the cumate-induced promoter. When induced with cumate, these same cells were also longer than IPTG-induced cells. Plasmid-driven expression of genes tends to be higher than chromosomal expression, due to the higher copy number. These data indicate that overexpression of PBP1a results in increased elongation prior to division, presumably due to increased PBP1a activity. Expression of either the transpeptidase or the glycosyltransferase mutant in PBP1a-depleted cells morphologically phenocopies the PBP1a depletion with an empty pSRK, resulting in shorter, rounder cells (Figure 1D). Together, these findings suggest that both transpeptidase and glycosyltransferase activities of PBP1a are required for polar growth.

Expression of PBP1aΔOB has a dominant lethal phenotype

To assess the role of the OB-fold in the regulation of PBP1a we generated a cumate-inducible pSRK-P_{cym}-*mrcA*ΔOB-3xFLG vector (Figure 1B) and conjugated it and an empty pSRK into our IPTG-inducible PBP1a depletion background. Growth in liquid ATGN with the uninduced pSRK-P_{cym}-*mrcA*ΔOB-3xflag vector was noticeably impaired compared to growth with the empty pSRK, suggesting that weak expression of PBP1aΔOB from the leaky *cym* promoter is toxic. Consistent with this observation, we find that expression of PBP1aΔOB as the only copy of PBP1a in the cell not only fails to rescue -PBP1a growth, but it exasperated the growth phenotype (Figure 2). Together, these data suggest that

+PBP1aΔOB is toxic to growth. Since growth is restored to +PBP1a levels when a complete PBP1a is expressed from a plasmid (Figure 1D), this toxicity is unlikely to be due to excess PBP1a activity. Thus, we hypothesized that the OB-fold is required for regulation of PBP activity as in *E. coli* [4–6] and expression of PBP1aΔOB may therefore result in misregulation or inhibition of PBP1a activity.

To test this possibility, we treated WT cells with and without the plasmid to express +PBP1aΔOB with 25 μg/mL of cefsulodin for 16 hours. Cefsulodin is known to target PBP1a in *A. tumefaciens* [3], thus we can use this drug to determine if PBP1aΔOB remains active. In WT cells, induction of +PBP1aΔOB or treatment with cefsulodin resulted in shorter cells compared to untreated cells. Further, we observed an additive effect on cell length during treatment cefsulodin and induction of +PBP1aΔOB, resulting in cells that were even shorter than induction of +PBP1aΔOB or treatment with cefsulodin, individually (Figures 3A and D). This observation suggests that only minimal PBP1a activity is retained when PBP1aΔOB is expressed in WT cells. Notably, induction of +PBP1aΔOB does not recapitulate the characteristic increased width associated with cefsulodin treatment (Figure 3B; [3]). Expression of PBP1aΔOB in WT cells are only slightly wider than untreated WT cells. Once again, an additive effect is noted as treatment with cefsulodin further increases the +PBP1aΔOB cell width (Figures 3B and D). Together, these observations suggest not only is PBP1aΔOB

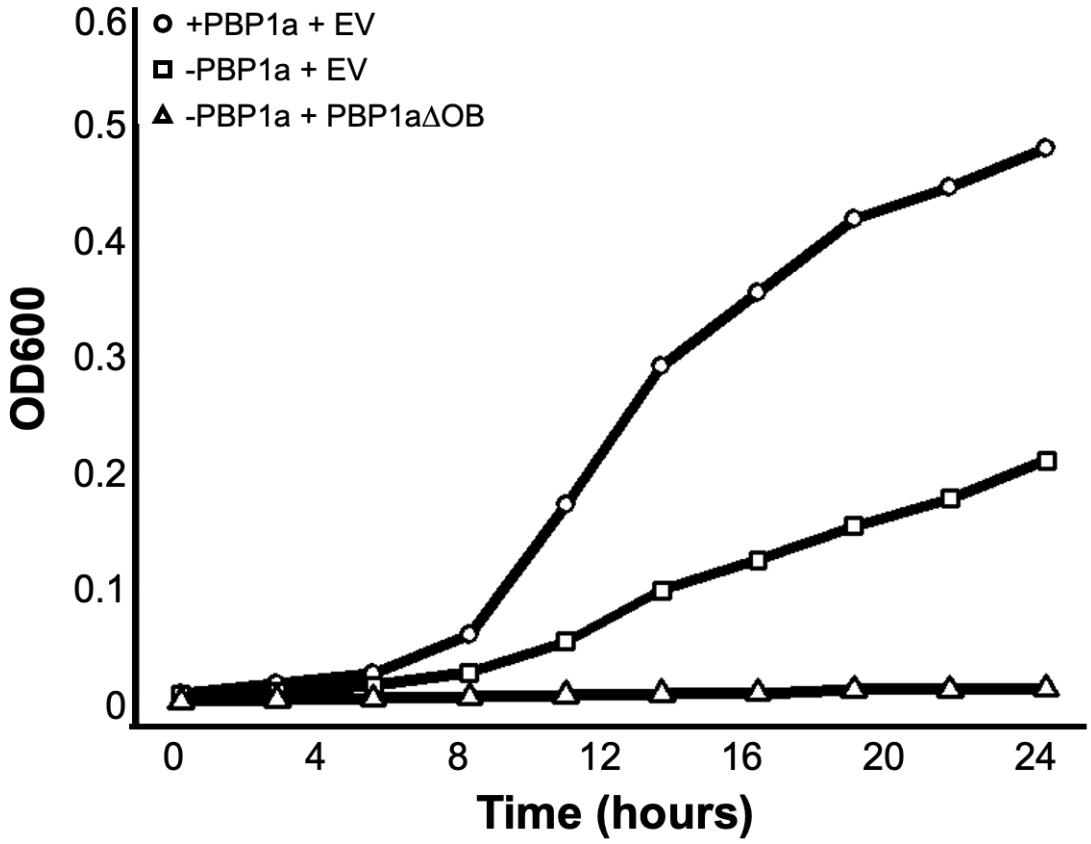

Figure 4.2. Expression of PBP1aΔOB does not rescue growth of PBP1a-depleted cells. Growth curve depicts growth of induced and uninduced PBP1a carry empty vectors, and uninduced PBP1a carrying a cumate-induced pSRK-P_{cym}mrcAΔOB.

likely to be inactive, but its expression compromises WT PBP1a activity. To ensure the PBP1aΔOB protein was expressed and stable, we immunoblotted with anti-FLAG and confirmed expression and stability of PBP1aΔOB (Figure 3C). These data strongly suggest the OB-fold as an essential domain required for proper PBP1a activity and that the presence of misregulated PBP1a activity is toxic.

Immunoprecipitation of PBP1a reveals a putative elongasome complex

Since OB-folds of PBP1a are known to mediate protein-protein interactions with regulators of PBP1a activity [4–6], we sought to identify proteins that interact with PBP1a. To maintain wild-type levels of expression, we replaced the native *mrcA* with *mrcA-3xFLG* in our wild-type background. We crosslinked, immunoprecipitated, and compared mass spectrometric analyses of PBP1a-3xFLAG lysate against lysate from our C58 wild type strain. Briefly, exponentially growing cells (OD=0.4-0.7) of *A. tumefaciens* with *mrcA* or *mrcA*-3xFLAG in ATGN media (28°C, 220rpm) were crosslinked with 0.2% paraformaldehyde for 15 minutes followed by quenching, washing, chemical lysis of cells, and binding of extracts to FLAG-specific monoclonal antibodies bound to agarose resin beads. Proteins were eluted from the FLAG-specific agarose beads, digested, and peptides identified using mass spectrometry. Datasets were analyzed using Fragpipe v19.0 which included a database search against the Uniprot (TrEMBL) database of *Agrobacterium fabrum* (strain C58/ATCC33970) OX=176299, MSFragger v3.6, and Philospher v4.6.0 for peptide spectrum match validation

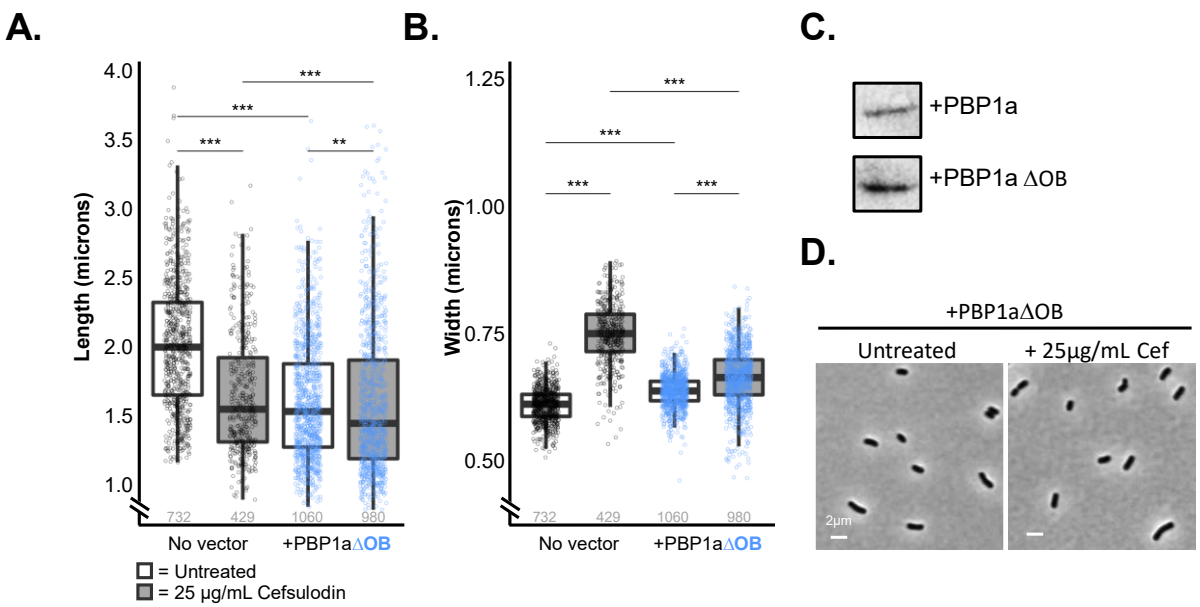

Figure 4.3. Treatment with cefsulodin does not restore average length or width of WT cells with Induced expression of PBP1aΔOB. **A.** Length analysis of no vector control and induced pSRK-P_{cym}mrcAΔOB in wild-type backgrounds with and without 25 µg/mL of cefsulodin. **B.** Width analysis on the same cells from panel A. **C.** Western blot using Anti-3xFLAG antibody. **D.** Micrographs depicting representative cells from the analysis in panels A and B.

and protein inference. Results were the consensus of three independent sample runs.

Using eggNOG-mapper, we revealed functional COG categories for the 239 proteins identified as unique PBP1a binding proteins follow immunoprecipitation and mass spectrometry (Figure 4A). While nearly all these proteins were identified consistently from three independent replicates, many of them had low spectral counts and therefore represent proteins in low abundance in the crosslinked sample. We therefore set a threshold of 10 or more spectral counts (SC > 9) to narrow our focus on the 49 most abundant proteins from the immunoprecipitation. The COG group with the highest number of representatives was “Function Unknown” (S), followed by “Cell wall/membrane/envelope biogenesis” (M). Select proteins of interest were detailed in Table 1.

PBP1a-associated proteins include other periplasmic enzymes involved in peptidoglycan metabolism

As expected, proteins that form a complex with PBP1a include other enzymes that are important for the synthesis, modification, or hydrolysis of peptidoglycan. Other than PBP1a, the most abundant hit was in the lytic tranglycosylase Atu1099. Atu1099 has a 34.58% sequence identity to *E. coli* MltG. In *E. coli*, MltG functions by cleaving nascent PG strands and therefore terminates strand

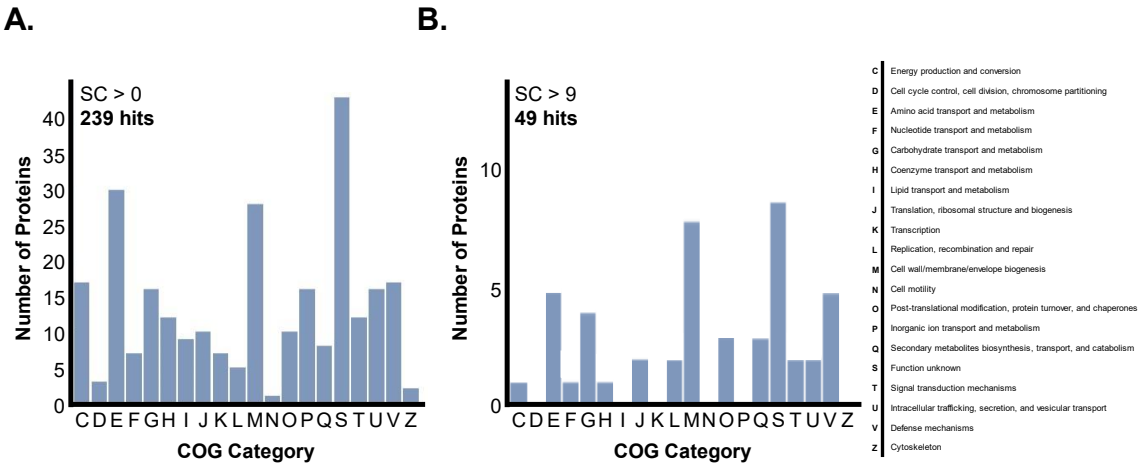

Figure 4.4. Cog analysis results for PBP1a-interacting proteins. **A.** COG categories for the 239 proteins with a spectral count of above 0. **B.** COG categories of the 49 proteins with spectral counts of 10 or higher.

elongation [7,8]. Atu1099 may interact with PBP1a in *A. tumefaciens* to terminate nascent peptidoglycan synthesis.

Among the high-abundance interactors of PBP1a were two LD-transpeptidases (LDTs) Atu2336 (SC = 11) and Atu1164 (SC = 17). Previously we reported differential expression of these LDTs in response to activation of the ChvG-ChvI two-component system by depletion of PBP1a [3]. Atu2336 is strongly down-regulated (L2FC = -1.99) in this condition and Atu1164 is strongly up-regulated (L2FC = 1.72). ChvG and ChvI mutants are hypersensitive to beta-lactam antibiotics and more sensitive to loss of PBP1a activity [9]. We also reported that Atu2336 localizes to the pole, while Atu1164 has a dispersed localization, but localizes to the new pole upon over expression [10]. However, neither LDT mutant was on average shorter than WT [10]. Together, these data suggest that

Table 1. Selected proteins identified as PBP1a-associated

Protein	Locus Tag	Description	Compartment*	Spectral Count
PBP1a	Atu1341	Penicillin-binding protein 1A	Periplasm, IM anchored	1552
MltG	Atu1099	Endolytic murein transglycosylase	Periplasm, IM anchored	69
-	Atu1328	Glycosyl hydrolase family 5	Periplasm	37
-	Atu1164	L,D-transpeptidase	Periplasm	17
AopB	Atu1131	Outer membrane protein	Periplasm, OM anchored	17
-	Atu1877	OmpA family protein	Periplasm	16
MurA	Atu0539	UDP-N-acetylglucosamine 1-carboxyvinyltransferase	Cytoplasm	15
RgsS	Atu1710	SPOR containing FtsN-like protein	Periplasm, Cytoplasm	11
-	Atu2336	L,D-transpeptidase	Periplasm	11
-	Atu1915	Periplasmic serine endoprotease DegP-like	Periplasm	11
ScsC	Atu1333	Outer membrane protein	Periplasm, OM anchored	10

*IM = inner membrane; OM = outer membrane

Atu2336 may fortify the growth pole during elongation and Atu1164 may be important in fortifying the cell under cell wall stress such as loss PBP1a activity.

The presence of MurA as a high abundance protein, as well as the presence of other components of the Mur pathway, suggest that the PBP1a-associated complex spans multiple compartments. Mur proteins constitute the cytoplasmic biosynthesis pathway for lipid II, the precursor to peptidoglycan [11]. That lipid II synthesis potentially tracks sites of active peptidoglycan synthesis and PBP1a is a compelling observation worthy of additional characterization.

PBP1a-associated proteins include putative outer membrane proteins

Since the activator of PBP1a in *E. coli* is an outer-membrane-anchored lipoprotein (LpoA) [4-6], we hypothesized that regulators of *A. tumefaciens* PBP1a might also be anchored in the outer membrane. Thus, we identified the subset of proteins identified in our PBP1a-associated proteins that are annotated as outer membrane proteins (Table 2). One intriguing candidate was the uncharacterized protein Atu1877. While Atu1877 is annotated with an outer-membrane protein A (OmpA)-like domain and many proteins that contain this domain are outer-membrane proteins, Atu1877 does not have the characteristic β-barrel structure of outer-membrane proteins. Further, a SignalP 6.0 analysis found no evidence of a lipoprotein signal peptide, suggesting that Atu1877 is not anchored into the outer membrane (Table 2). Instead, it contained a general

Table 2. Predicted subcellular targeting of select PBP1a-associated proteins

Protein	Locus Tag	Other	SP (Sec)	LSP (Sec)	SP (Tat)	LSP (Tat)	PSP (Sec)
AopB	Atu1131	0.0006	0.9983	0.0003	0.0004	0.0003	0.0002
-	Atu1877	0.0007	0.9984	0.0003	0.0002	0.0002	0.0002
ScsC	Atu1333	0.0007	0.5082	0.4904	0.0003	0.0003	0.0002
-	Atu1328	0.0173	0.9814	0.0004	0.0003	0.0002	0.0002

secretion signal peptide, indicating it is likely periplasmic. The OmpA-like domain likely noncovalently binds peptidoglycan as it shares structural and sequence similarity with Pal, another OmpA-like domain protein (Figure 5). Additionally, it has a long, poorly conserved, and unstructured low complexity region. It is unclear what function this protein, if any, plays in complex with PBP1a.

AopB is an outer-membrane β-barrel protein that is covalently linked to peptidoglycan by the activity of LD-transpeptidases (Figure 5) [12]. AopB expression is controlled by the ChvG-ChvI two-component system and activated by PBP1a depletion [3]. Although, the biological function of AopB is not currently known, we speculate that it functions in fortifying the cell envelope during stressful conditions.

Orthologs of Atu1328 and Atu1333 are putative components of the Rhizobiales PBP1a elongasome complex

Atu1328 and Atu1333 are uncharacterized proteins of interest that were identified as PBP1a-associated proteins (Table 1). Atu1328 is a predicted periplasmic

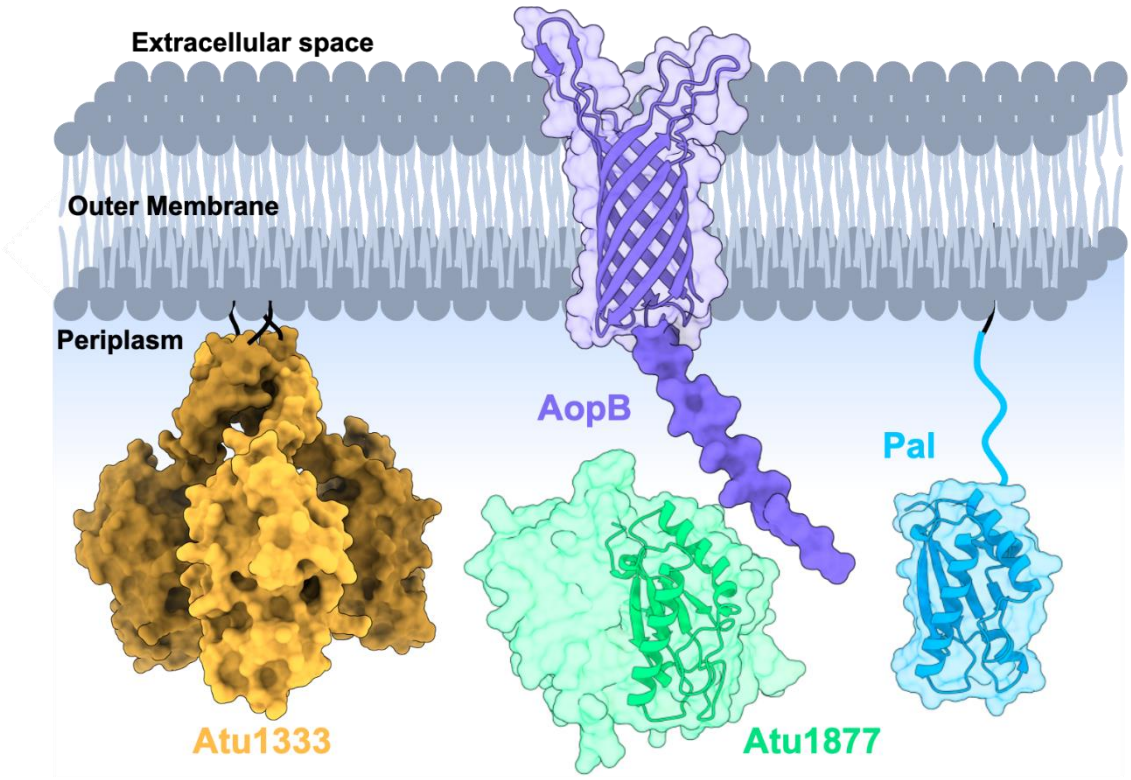

Figure 4.5. Schematic of AlphaFold predicted structures of select PBP1a-associated proteins. Although these proteins are annotated as outer membrane proteins, only AopB has canonical β-barrel structure. Atu1333 is a periplasmic protein anchored in the outer membrane and there is no evidence that Atu1877 is an outer membrane protein but rather it is likely to be periplasmic. Atu1877 shares notable structural similarity with Pal. AopB, Atu1333, and Atu1877 are found in the periplasmic space and thus likely interact with PBP1a.

protein (Table 2) that contains a domain of unknown function (DUF2155). Atu1333 is an ortholog of the *Caulobacter crescentus* suppressor of copper sensitivity C protein (ScsC). ScsC is a disulfide isomerase that forms a trimeric structure and binds copper (I) ions (Figure 5) [13]. A SignalP 6.0 analysis predicts a possible lipoprotein (Table 2).

A synteny analysis of Atu1328 and Atu1333, showed that they share the same gene neighborhood with *mrcA*¸ encoding PBP1a. This neighborhood, which encodes orthologs of Atu1328 (blue arrows) and Atu1333 (gold arrows) and PBP1a (pink arrows), is largely conserved across the Rhizbiales and in other Alphaproteobacteria like *Caulobacter crescentus* (Figure 6A). Notably, another conserved member of this neighborhood is *amiC* (purple arrows), located consistently just upstream of just downstream of *mrcA*. Conserved synteny is a strong indicator of associated functionality and suggests that PBP1a, Atu1328, Atu1333, and AmiC function together.

To investigate the potential functions of Atu1328, we utilized a virtual fitness browser [14]. This browser utilizes a comprehensive database of transposon mutant libraries that have been evaluated under various conditions. The fitness browser provides co-fitness scores that identify genes with shared fitness profiles across multiple conditions. Essentially, if a transposon mutant exhibits decreased

A.

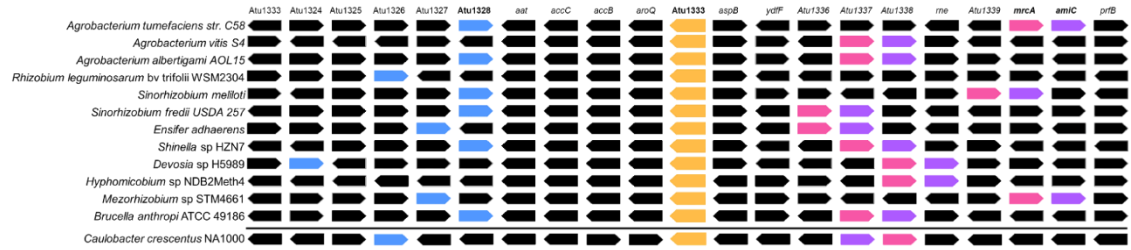

B.

Protein	Locus Tag (Sm)	Locus Tag (At)	Description	Cofitness	IP
PBP1a	SMc01334	Atu1341	penicillin-binding protein 1a	-	Yes
-	SMc02071	**Atu1328**	hypothetical protein	-	Yes
NlpC	SMc02827	Atu0211	hypothetical protein	0.65	No
-	SMa1641	NC	NreB protein	0.60	-
-	SMc03773	Atu2783	hypothetical protein	0.59	No
MltA	SMc02785	Atu0009	lytic murein transglycosylase A protein	0.59	Yes
ScsC	SMc01342	Atu1333	hypothetical protein	0.58	Yes
MepA	SMc02833	Atu0186	penicillin-insensitive murein endopeptidase	0.57	Yes

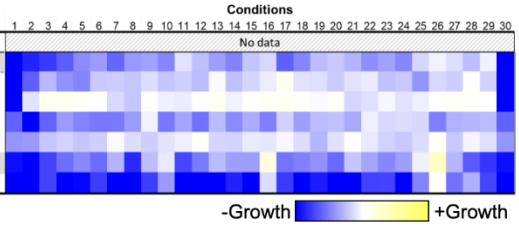

Figure 4.6. Several PBP1a associated protein are encoded near PBP1a or share similar fitness profiles. **A.** Genome neighborhoods for selected Alphaproteobacteria are shown. The locus tag labels for the Agrobacterium tumefaciens str C58 are shown along the top. Orthologs genes are colored-coded. The genomic regions are centered on *atu1333* (gold arrows). *mrcA* (pink arrows) encodes PBP1a and is found in genome neighborhoods with *amiC* (purple arrows), and atu1333 and atu1328 (blue arrows) which encode PBP1a-associated proteins. **B.** Co-fitness analysis of the *Sinorhizobium meliloti* ortholog of Atu1328 (SMc02071) reveals that additional PBP1a-associated proteins including Atu0009, Atu1333, and Atu0186 share co-fitness profiles. This data provides further support for a link among PBP1a-associated proteins.

growth in five specific conditions, the co-fitness analysis will compare this mutant to all other transposon mutants and identify other mutants that display similar growth defects in those same conditions. The closest transposon hit of Atu1328 was in the ortholog from *S. meliloti* (SMc02071). The conditions that most greatly influenced the fitness of the transposon mutant of SMc02071 were cell envelope stressors, consistent with Atu1328 being involved in regulation of peptidoglycan degradation or biosynthesis. Remarkably, three of the top six genes with a high degree of cofitness to SMc02071 were also genes that encode orthologs of proteins that interact with PBP1a, including Atu1333, MltA and MepA (Figure 6B, Table S1). MltA is a murein lytic transglycosylase that cleaves the (1-4)-beta-glycosidic linkage between N-acetylmuramic acid (NAM) and N-acetylglucosamine (NAG) sugars of the peptidoglycan backbone. MepA is an endopeptidase that cleaves bonds between peptides of the peptide stem. These proteins are involved in peptidoglycan degradation and peptidoglycan recycling, suggesting that Atu1328 and Atu1333 may also play a role in these processes.

Remarkably, Atu1328 is conserved throughout much of the Alphaproteobacteria and co-occurs with the structural loop of PBP1a orthologs (Figure 7A). AlphaFold-multimer interaction predictions between Atu1328 and PBP1a predicted interaction between the DUF2155 domain of Atu1328 and the structural loop (Figure 7B). Orthologs in *C. crescentus* of Atu1328 (CCNA01963) and PBP1a (PBPY) were also predicted to interact in the same way. These predictions suggest that DUF2155 domains interact with PBP1as of the

Alphaproteobacteria. Additional work is necessary to confirm these interactions, but these observations hint that Atu1328 may function as a novel regulator PBP1a proteins of the Alphaproteobacteria.

RgsS resembles the SPOR domain protein FtsN

The final protein of interest identified in the PBP1a-associated proteins is RgsS. RgsS is a large protein of 1008 amino acids that is predicted to be mostly unstructured. It spans the cytoplasm and periplasm where it interacts with AmiC-dependent denuded peptidoglycan through its SPOR domain (Figure 8A-B; [15]). RgsS likely functions in an analogous way to FtsN, which is not encoded in the *A. tumefaciens* genome. FtsN binds and activates PBP1b in *E. coli* [16], making RgsS an intriguing candidate for PBP1a regulation.

FtsN contains a SPOR domain that binds denuded peptidoglycan, a characteristic structural motif generated by amidases [17]. The amidase-generated denuded peptidoglycan recruits FtsN to midcell. Members of the Rhizobiales of the Alphaproteobacteria lack an FtsN ortholog and instead have an FtsN-like protein called RgsS (Figure 8A). RgsS is similar to FtsN in that both have a well-conserved SPOR domain (Figure 8B) and both share some sequence homology in the periplasmic regions of each protein (Figure 8C). However, RgsS differs from FtsN in that it contains a disordered, poorly conserved cytoplasmic expansion.

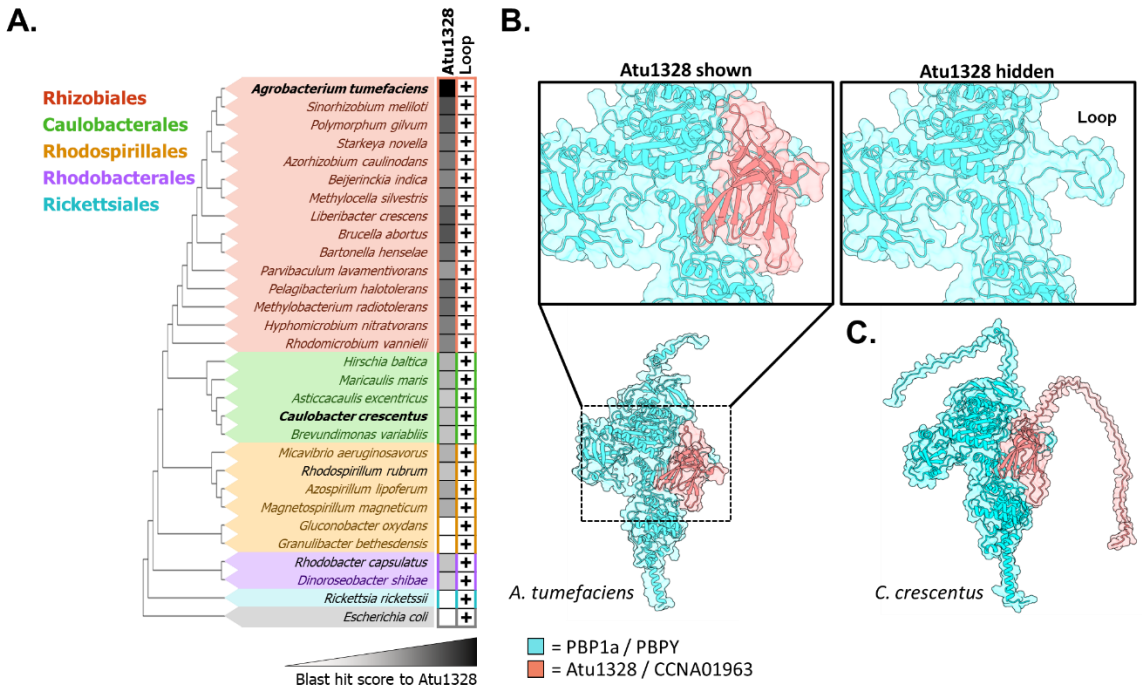

Figure 4.7. Phylogenetic and structural conservation of Atu1328 orthologs in Alphaproteobacteria. **A.** Phylogeny of the Alphaproteobacteria with each order color coded is shown. The conservation of Atu1328 is strongly conserved among the Rhizobiales, along with an extended loop in PBP1a. **B.** Schematic of AlphaFold predicted structures of select PBP1a in cyan and Atu1328 (pink) suggests that Atu1328 may bind the extended structural loop of PBP1a. The insets are zoomed in on the PBP1a structural loop with (left) and without (right) Atu1328. **C.** The structure of PBP1a from *C. crescentus* (known as PBPY) and predicted binding of CCNA01963, an Atu1328 ortholog, to the structural loop is conserved.

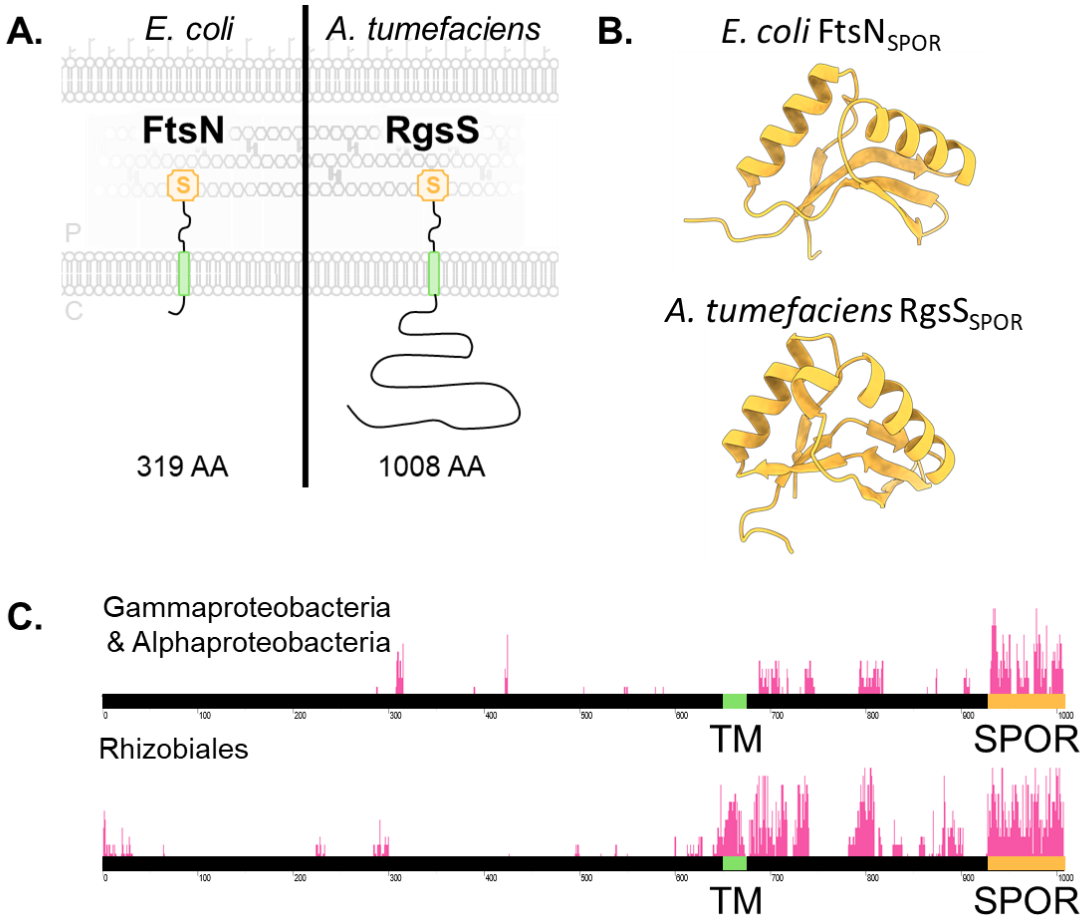

Figure 4.8. RgsS is an FtsN-like protein. **A.** Schematic comparing the structures of FtsN from *E. coli* and RgsS from A. tumefaciens. RgsS has an extension of nearly 700 amino acids comprised of an intrinsically disordered region. **B.** The AlphaFold predicted SPOR domains of FtsN and RgsS illustrate a high degree of structural similarity. **C.** The regions of high amino acid conservation are restricted to the SPOR domain in proteins from the Gammaproteobacteria and Alphaproteobacteria. Rhizobiales specific regions of conservation are identified and may be important for polar growth-related functions of RgsS.

Depletion of RgsS resulted in cells that failed to divide and branched from ectopic poles (Figure 9A). The division defect and branching phenotypes were reminiscent of the FtsZ depletion phenotype we reported previously [18]. FtsZ polymerizes into a discontinuous ring at midcell that served as scaffold for proteins required for cell division. It is conserved throughout nearly the entire bacterial domain and is strictly required for division. While branches from depletion with RgsS curved and eventually grew wider, branches of the FtsZ-depleted cells remain relatively straight and uniform in width. One possibility is that the branching observed during RgsS depletion is due to the mislocalization of FtsZ. To test this, we transformed the RgsS depletion strain with pRVMCS-2 FtsZ-sfGFP. After depletion of RgsS for 12 hours, clear localization of FtsZ-sfGFP was visible, with some cells having multiple foci (Figure 9B). This indicated that like FtsN in *E. coli* [19], RgsS is not required for midcell localization of FtsZ. Notably, FtsZ was localized at or near ectopic poles, suggesting that ectopic pole formation may originate at the site of the FtsZ-ring.

The extreme curvature of the RgsS depletion shared morphological similarities to the DipM and EnvC mutants in *A. tumefaciens* [20]. NlpD/DipM and EnvC are LytM-containing proteins that activate amidases required for the completion of cell division in *E. coli* [21,22] but seem to play a different role in the Alphaproteobacteria. In Alphaproteobacteria, deletion of *envC* phenocopies the deletion of *amiC* suggest that EnvC regulates the activity of AmiC [20]. AmiC is an amidase required to denude peptidoglycan at mid-cell enabling recruitment of RgsS to midcell [23]. This phenotype is a loss of straight rod shape and adoption

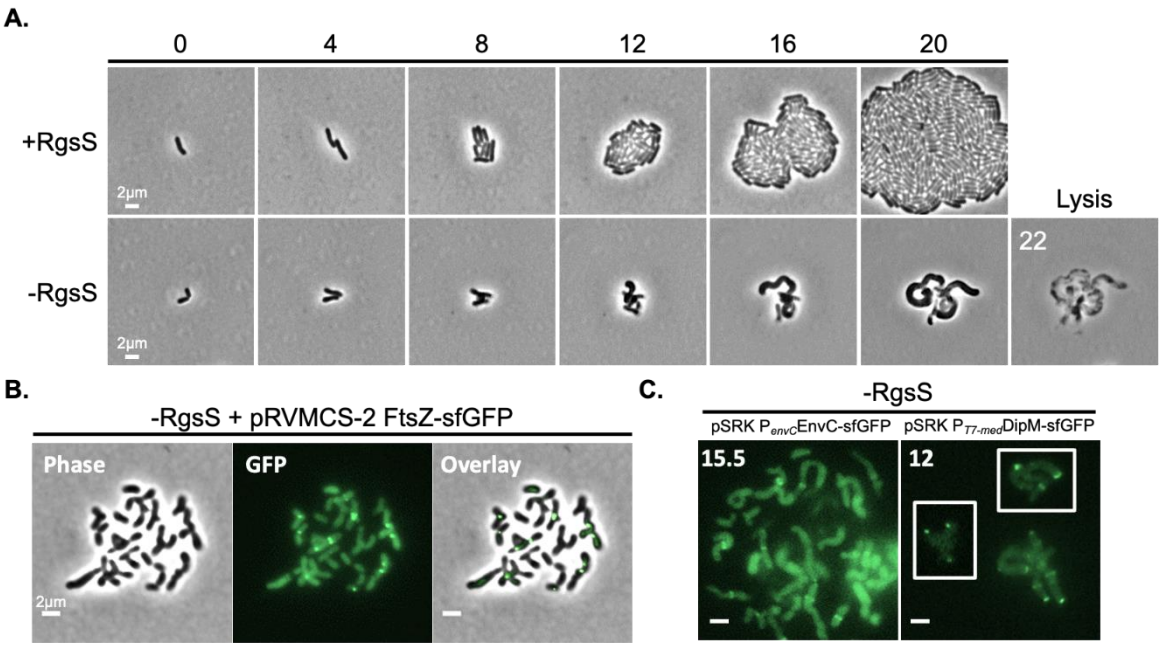

Figure 4.9. Characterization of an RgsS depletion strain. **A.** Timelapse microscopy of the RgsS depletion strain grown in the presence (top, +RgsS) or absence of the inducer IPTG (bottom, –RgsS). Timepoints in hours are indicated at the top of the panels. **B.** Localization of FtsZ-sfGFP indicates that FtsZ rings can form in the absence of RgsS suggesting that RgsS has a later role in bacterial cell division. **C.** Localization of EnvC-sfGSP to mid-cell in the absence of RgsS suggests that EnvC localization not dependent on RgsS. In contrast, the polar trapping of DipM-sfGFP in the absence of RgsS suggests that DipM localization is dependent on RgsS.

of a hyper curved morphology. Depletion of the essential protein DipM results in failed division, mid-cell swelling, and ectopic pole formation [20]. Deletion of either the gene encoding EnvC or the amidase AmiC in this background restores midcell swelling upon depletion of DipM and introduces a curvature phenotype strikingly similar to the RgsS depletion. Loss of activity in these proteins may be responsible for the failed division and curvatures of the RgsS depletion.

To test this possibility, we introduced plasmid-driven copies of EnvC and DipM tagged with GFP into the RgsS depletion strain. DipM localizes to both the growth pole and midcell of predivisional cells, while EnvC localizes at midcell of predivisional cells [20]. During depletion of RgsS, EnvC-sfGFP localization was similar to FtsZ localization. There was no polar localization in any of the cells. However, DipM-sfGFP showed only polar localization (Figure 9C). These data suggest that RgsS is required to recruit DipM to midcell but is not required for the recruitment of EnvC. Without recruitment of DipM to the midcell, the RgsS-depleted cells cannot divide.

RgsS regulates the rate of polar growth

To test if the interaction with RgsS is regulating PBP1a activity, we measured the rate of growth in RgsS with and without IPTG, as well as in the FtsZ depletion. To do this, we predepleted RgsS for 12 hours and FtsZ for 5 hours, representing the point in which each strain is no longer able to divide. We then incubated each

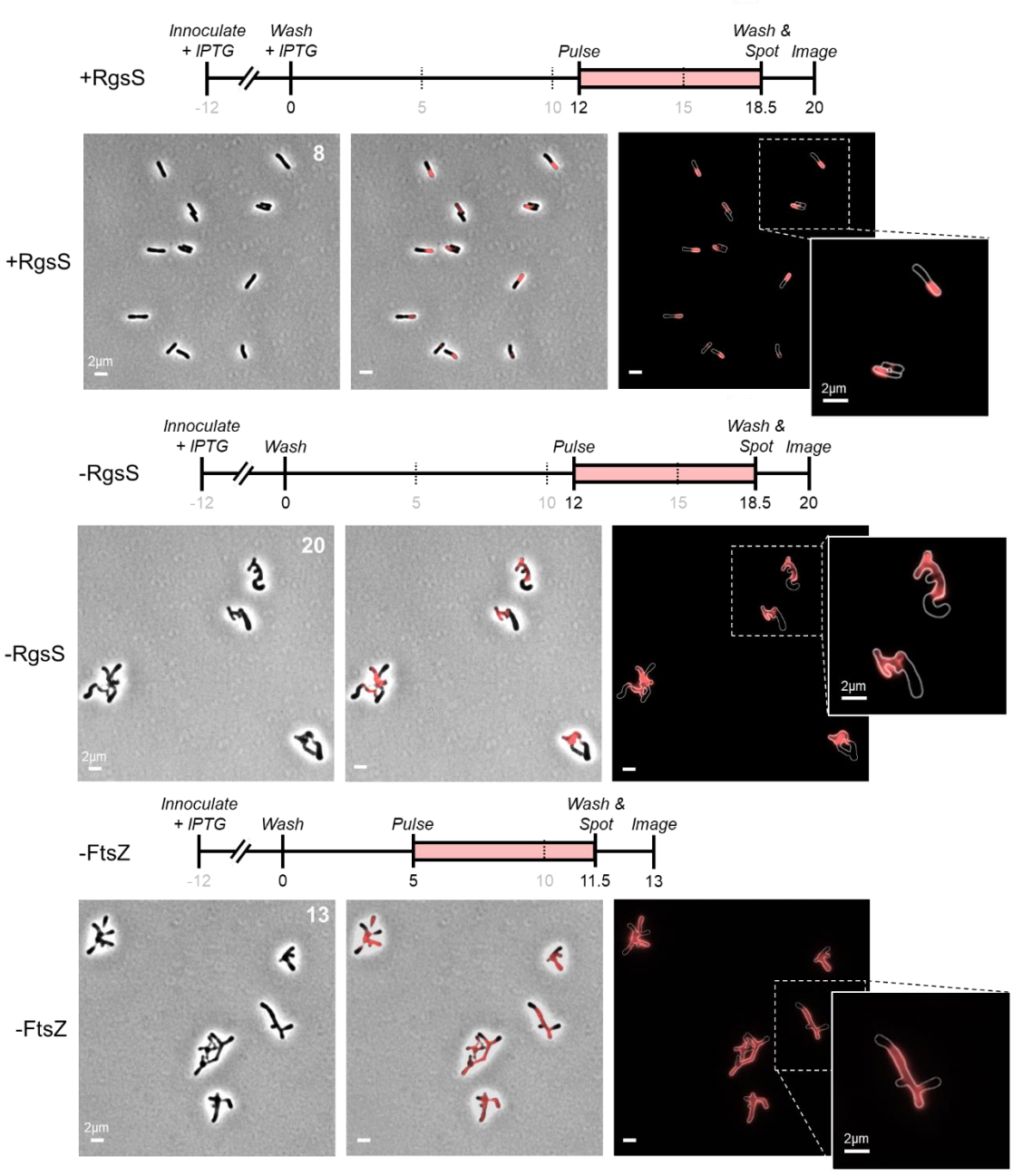

Figure 4.10. Monitoring new growth of RgsS and FtsZ depletion strains. Cells expressing RgsS (top) or depleted of RgsS (middle) were growth for 12 hours in the presence of absence of inducer prior to labeling with the fluorescent d-amino acid, TADA for 6.5 hours. Cell depleted of FtsZ (bottom) were growth for 5 hours in the presence of absence of inducer prior to labeling with the fluorescent d-

amino acid, TADA for 6.5 hours. The TADA fully labeled all of the cells allowing new growth to be visualized as areas lacking fluorescence. Depletion of RgsS and FtsZ results in accumulation of growth poles as evidenced by multiple cellular regions lacking TADA labeling. Insets provide a magnified view of the observed labeling patterns.

strain with the growth marker TADA [24,25] for 6.5 hours. We washed the cells of excess TADA and spotted on an ATGN agarose pad and incubated for 1.5 hours (Figure 10). Unlabeled zones represent nascent peptidoglycan synthesis from the point of washing the cells. While only a single growth pole displays nascent peptidoglycan synthesis in the induced RgsS cells, RgsS- and FtsZ-depleted cells show multiple growth poles.

Total growth per cell in these strains was measured by taking the total length of unlabeled regions per cell and dividing it by 1.5 hours. RgsS-depleted cells showed a much higher total growth rate when compared to induced RgsS cells and the FtsZ-depleted cells (Figure 11A). To test if this increase growth rate was due to increased expression of aPBPs or activity, we incubated lysate from RgsS-induced and depleted cells with Bocillin-FL, a fluorescent penicillin antibiotic that specially binds PBPs. We ran the treated lysates in a protein gel and imaged (Figure 11B). Very little, if any difference between the strains was noticeable, indicating that the increased growth rate was not due to increased protein abundance.

Next, we hypothesized that RgsS may taper PBP1a activity through direct protein-protein interaction. We ran AlphaFold-multimer interaction predictions [26] between PBP1a and conserved fragments of the periplasmic region of RgsS and an interaction was detected. We expected to find an interaction analogous to

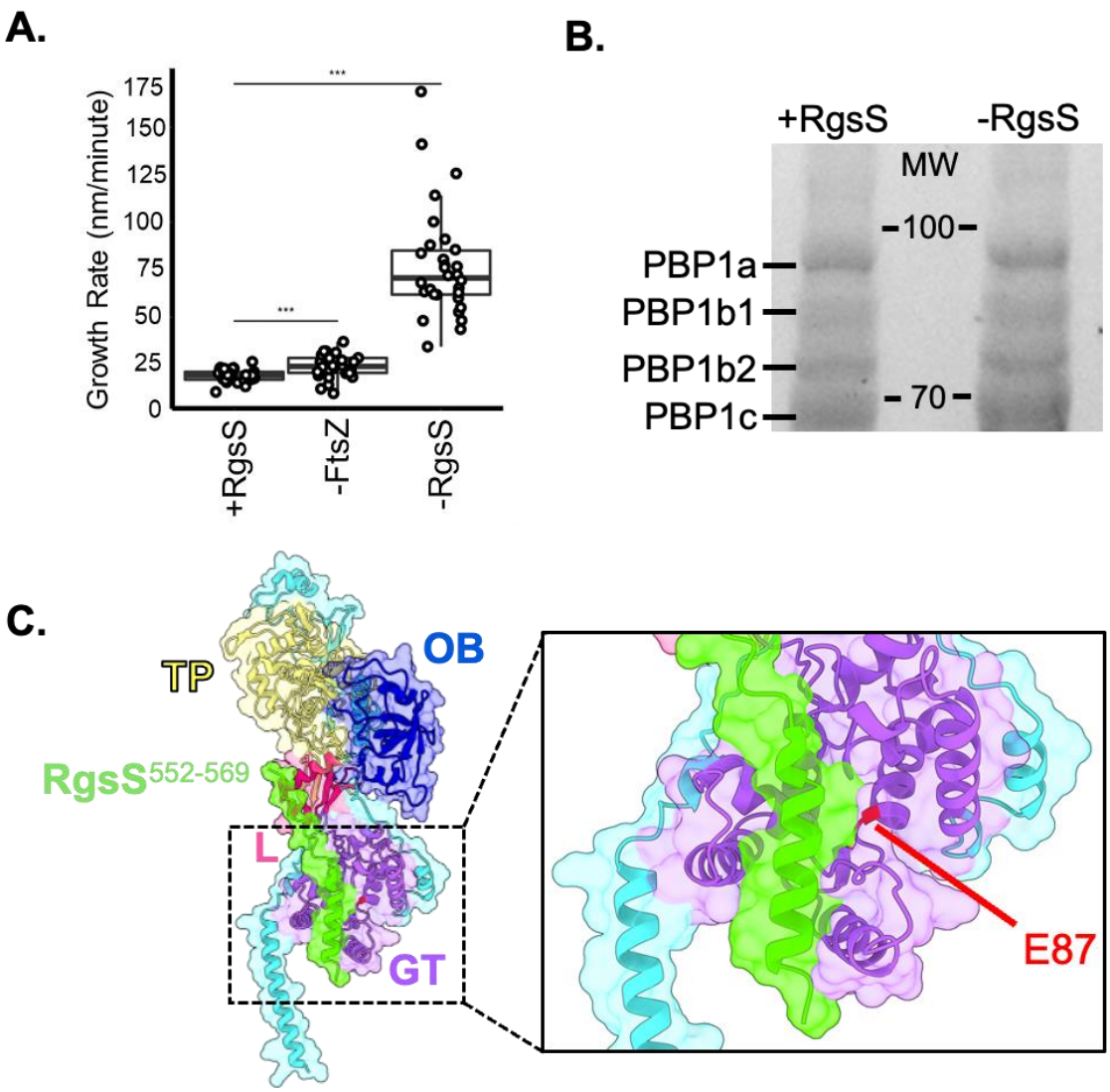

Figure 4.11. Depletion of RgsS increases growth rate per cell. **A.** Total growth per cell per minute. RgsS depletion was compared to induced RgsS cells and FtsZ-depleted cells. **B.** Bocillin gel showing similar patterning and fluorescence of Bocillin-FL labeled protein. **C.** Predicted interaction between RgsS$^{552-569}$ and the glycosyltransferase domain of PBP1a using AlphaFold-Multimer. E87 is the catalytic residue of the glycosyltrasferease domain.

FtsN binding a noncatalytic region of the glycosyltransferase of PBP1b in *E. coli* [16], but instead had the surprising result of an interaction predicted between a conserved alpha helix ($RgsS^{552-569}$) and the catalytic pocket of the glycosyltransferase domain of PBP1a (Figure 11C). Together our observations fit a model that RgsS functions as a negative regulator of PBP1a by blocking glycosyltransferase activity. Upon depletion, PBP1a is unregulated and the growth rate increases. Further work is necessary to confirm the interaction between PBP1a glycosyltransferase domain and $RgsS^{552-569}$ and the mechanism of RgsS regulation of PBP1a activity.

DISCUSSION

We genetically dissected PBP1a of *A. tumefaciens* and analyzed its interacting partners to uncover how PBP1a is regulated during polar growth. Our study shows that both the transpeptidase and glycosyltransferase activities of PBP1a are essential and that expression of PBP1a containing an OB-fold deletion is dominantly lethal. Taken together, these findings support previous evidence that PBP1a is the primary driver of elongation in *A. tumefaciens* [2]. PBP1a forms homodimeric structures in *E. coli* [27], perhaps PBP1aΔOB forms nonfunctional dimers with full-length PBP1a, effectively resulting in a PBP1a depletion. While this is a compelling hypothesis, it does not fully explain the cell width analysis results. How do the cells get short, without also getting wider as we have reported previously in our PBP1a depletion [2]. One possibility is that expression of PBP1aΔOB is so potent that active PBP1a depletes more quickly than our

PBP1a depletion strain, resulting in shorter cells before they have time grow wider. This hypothesis agrees with the observation that *A. tumefaciens* not only elongates at its growth pole, but also grows in width [28]. These data suggest that the OB-fold was a site of regulation for PBP1a as it is in Gammaproteobacteria [4–6]

Immunoprecipitation of PBP1a complexes identified proteins with a diversity array of functions spanning multiple cellular compartments. Focusing on the highest abundance proteins, we found interactions that seem to point at an elongasome complex centered around PBP1a. Two of the proteins were LDTs, suggesting that LD-transpeptidation may be important for polar growth. Sites of active peptidoglycan synthesis are likely the most susceptible to stress. LD-crosslinks are resistant to various stresses, such as treatment with the cell wall degradation enzyme lysozyme [29].

MurA, and in lower abundance MurG and MurE, were also interactors of PBP1a, suggesting that lipid II biosynthesis is localized to active peptidoglycan synthesis in *A. tumefaciens*. Notably, cytoplasmic synthesis of lipid II necessitates a protein to flip this molecule across the inner membrane. SEDS proteins like RodA and FtsW function in this capacity, but FtsW is confined to the midcell where it functions in cell division, and *A. tumefaciens* does not retain a gene encoding RodA. *A. tumefaciens* does have an ortholog of MurJ, which has conflicting *in*

vivo and *in vitro* evidence for its ability to “flip” lipid II into the periplasm [30,31]; however, MurJ was not identified as a PBP1a binding partner.

The DUF2155-containing protein Atu1328 is well conserved in the Alphaproteobacteria. AlphaFold-multimer interaction analysis between PBP1a and Atu1328 as well as PBPY and CCNA01963 suggests that the DUF2155 domain may be a PBP1a-binding domain. The DUF2155 domain is predicted to dock between the linker and the conserved structural loop of PBP1as in the Alphaproteobacteria. While not much is known about this protein, its predicted binding of the linker leaves us with a hypothesis for function. While the PBP1a linker is a flexible domain [32] and binding of Atu1328 may be able “lock” PBP1a into an active state. This would suggest that this interaction is spatially and temporally coordinated to facilitate elongation. However, this would seem to suggest that Atu1328 would have an essential role in PBP1a activation. While genetic analysis is currently underway, transposon mutagenesis in LB suggests the protein is nonessential [33]. Cofitness analysis of a transposon mutant of an ortholog of Atu1328 in *S. meliloti* found high cofitness with enzymes involved in peptidoglycan metabolism, namely NlpC, MepA, and MltA [34]. Therefore, an alternative hypothesis is that Atu1328 helps coordinate peptidoglycan metabolism and peptidoglycan synthesis.

The ScsC ortholog Atu1333 came out of both the PBP1a immunoprecipitation and the cofitness analysis with Atu1328, in addition to being part of a conserved

gene neighborhood with PBP1a. ScsC and Atu1333 are both upregulated by ChvG-ChvI in *C. crescentus* and *A. tumefaciens*, making them part of a conserved regulon that responds to cell wall stress [9,35]. ScsC binds copper (I) ions with high affinity [13]. In *Salmonella enterica* ScsC contributes to copper resistance. ScsC also has isomerase activity. It remains unclear how the function of this protein pertains to PBP1a, however it seems possible that isomerase activity may be important in disulfide bond formation between proteins of the PBP1a complex. For example, in *E. coli* DsbA's isomerase activity is required for disulfide bond formation and proper assembly of the cell division regulator FtsN, while DsbC is required for proper assembly of the lipopolysaccharide insertion protein LptD [36]. Atu1333 may function in an analogous way in *A. tumefaciens*. Like FtsN, RgsS may also require disulfide bond formation, or perhaps dimerization of PBP1a may depend on disulfide bonds [37].

The discovery of an interaction between PBP1a and RgsS was surprising, as a previously published pull-down experiment with RgsS in S. meliloti did not report any such interaction [23]. It is possible that this interaction is unique to *A. tumefaciens*, or more likely, the low copy numbers of PBP1a prevented detection of the interaction in the previous experiment. For instance, in *E. coli*, the number of PBP1a molecules maintained is only 100-600 per cell [38]. By using PBP1a as the bait instead of RgsS, we were able to overcome this issue in detection. Depletion of RgsS resulted in cell division defects, likely due to DipM being trapped at the poles. RgsA, a putative polar hub in members of the Rhizobiales

interacts with both DipM and RgsS, possibly serving as a proxy in shuttling DipM to midcell. Another explanation for the cell division defects is that RgsS itself may also be necessary to trigger cell division. For instance, in *E. coli*, FtsN binds PBP1b to activate it in an LpoB-independent manner to initiate cell division [16].

The increased total rate of growth in the RgsS depletion along with the observation that overexpression of RgsS results in shorter cells in *S. meliloti* [39], strongly implicates RgsS as a negative regulator of PBP1a activity. RgsS may directly bind the catalytic pocket of the PBP1a glycosyltransferase domain through a conserved alpha helix. Together, these data provide us with a working model for regulation of polar growth and cell division in *A. tumefaciens* (Figure 12). In this working model, prior to cell division, EnvC activates AmiC at midcell, generating denuded PG motifs that recruit the SPOR domain of RgsS molecules. RgsS then shuttles the elongasome complex, including inactive PBP1a, RgsA, other Rgs proteins (not depicted), and DipM to midcell to initiate cell division and eventually establishment of the new growth pole. Notably, this model is agreement with previous data that deletion of *amiC* results in unreliable establishment of the proper growth pole in the daughter cell [15,20]. support a model by which RgsS regulates growth and division by recruiting proteins essential for cell division and regulating activity of PBP1a.

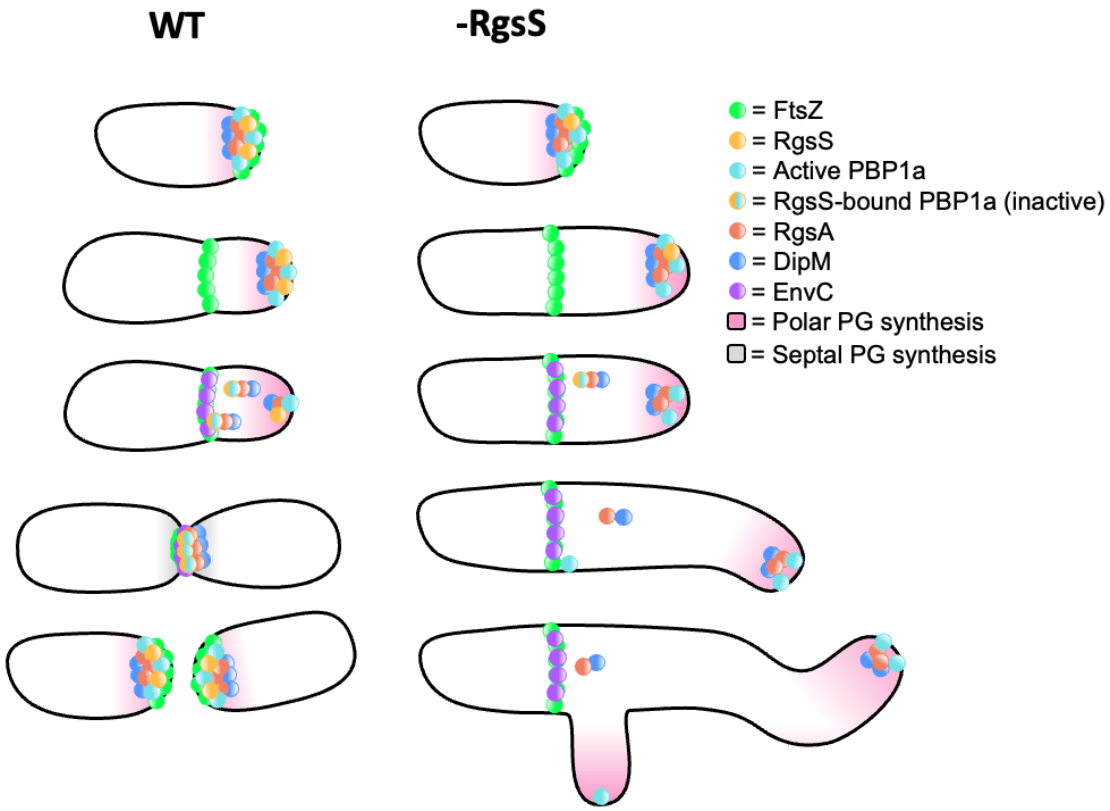

Figure 4.12. Working model of the regulation of growth and division by RgsS. Under WT conditions, FtsZ localizes to midcell, polymerizes, and recruits proteins required for cell division including RgsA, DipM, and EnvC. During depletion of RgsS, DipM-GFP foci were only polarly localized, suggesting that RgsS is required for mid-cell localization of DipM. This may be the causative mechanism for failed division in the RgsS depletion. In *Sinorhizobium meliloti* RgsA was shown to interact with DipM and and RgsS, suggesting that RgsA may shuttle DipM to midcell by with RgsS. EnvC-GFP still localized to midcell during depletion of RgsS, suggesting its localization is independent of RgsS. The continued polar elongation in the RgsS depletion also suggests that PBP1a is not being relocated to midcell and remains active at the pole. Together, these data

MATERIALS AND METHODS

Bacterial strains, plasmids, and growth conditions. A list of all bacterial strains and plasmids used in this study is provided in the Strains and Plasmids Table. *Agrobacterium tumefaciens* C58 and derived strains were grown in ATGN minimal media [40] without exogenous iron at 28°C with shaking. When appropriate, kanamycin (KAN) was used at the working concentration of 300 µg/ml. When indicated, isopropyl β-D-1-thio-galactopyranoside (IPTG) was used as an inducer at a concentration of 1 mM and cumate was used as an inducer at a concentration of 100 µM. *E. coli* DH5α and S17-1 λ pir were grown in Lysogeny Broth medium at 37°C and when appropriate 50 µg/ml or 30 µg/ml of KAN were added, respectively.

Construction of plasmids and strains. 3xFLAG-tagged PBP1a was generated using synthesized gene fragments from Twist Bioscience and cloned to generate both pSRKKm P_{cym}-PBP1a-3xFLAG (expression plasmid) and pNPTS139-PBP1a-3xFLAG (allelic exchange plasmid). Vectors for gene replacement by allelic exchange were constructed using recommended methods for *A. tumefaciens* [41]. PBP1a transpeptidase and glycosyltransferase point mutants (TP* and GT*) were generated using pSRKKm P_{cym}-PBP1a with the Q5 site-directed mutagenesis kit (E0552S) and the primers listed in the primer list.
The allelic exchange plasmids were introduced into *A. tumefaciens* by mating using an *E. coli* S17 conjugation strain to create kanamycin resistant, sucrose sensitive primary integrants. Primary integrants were grown overnight in media

with no selection. Secondary recombinants were screened by patching for sucrose resistance and kanamycin sensitivity. Colony PCR with primers P5/P6 for the respective gene target and sequencing of the PCR product was used to confirm addition of the C-terminal FLAG tag.

Growth curve. One colony of each strain was inoculated in 1 mL of ATGN containing 300 µg/mL kanamycin and 1 mM IPTG. Overnight culture of each strain was diluted to an OD_{600} of 0.1 and allowed to grow for 4 hours with IPTG and kanamycin. Each culture was then diluted to an OD_{600} of 0.01 and separated into three wells each of a 96 well plate with 1 mM IPTG when appropriate and with 100 uM cumate when inducing expression from the pSRKKm P_{cym}-PBP1aΔOB plasmid. OD_{600} was monitored for 24 hours using a BioTek Synergy H1 plate reader and growth was graphed with ggplot2 in R.

Phase and fluorescence microscopy. A small volume (~1 µl) of cells in exponential phase (OD600 = 0.2 - 0.4) was applied to a 1% ATGN agarose pad as described previously [46]. Phase contrast and epifluorescence microscopy were performed with an inverted Nikon Eclipse TiE and a QImaging Rolera em-c2 123 1K EMCCD camera with Nikon Elements Imaging Software. For time-lapse microscopy, images were collected every ten minutes, unless otherwise stated. For quantitative image analysis, live cells were imaged using phase-contrast microscopy, and cell length and width distributions of the indicated

number of cells per strain were determined as measured using MicrobeJ software [47].

For calcofluor agar pad assays, calcofluor was added to agarose pads at a concentration of 25 µg/mL and exposed to DAPI filter for 40 ms. When appropriate agar pads were supplemented with 1mM IPTG.
For growth rate experiments, cells were depleted or repleted with 1 mM IPTG for the time indicated. Cells were washed and 1 mM IPTG was readded when appropriate. 4 µL of a 100 mM stock solution of TADA was added to 400 µL of culture and cells were incubated in a 28^{o}C shaking incubator for 1.5 hours. Cells were washed twice and immediately imaged with an emission wave length of 580 nm.

Growth and isolation of PBP1a-3xFLAG crosslinked proteins. *Agrobacterium tumefaciens* strains containing wild-type PBP1a or 3xFLAG-tagged PBP1a were grown in 2mL ATGN media overnight at 28^{o}C 220rpm. Strains were subcultured into 200mL of ATGN in 500mL flasks to a starting inoculum of 0.04-0.1 and incubated in dry shaking incubator at 28^{o}C 220rpm for 12-14 hours until exponential phase was reached at OD_{600} 0.4-0.7. 37% w/w Formaldehyde (Fisherbrand) was added to each flask (final concentration in growth media: 0.2%) and samples crosslinked at 28^{o}C 220 rpm for 15 minutes. 1.875 M Glycine (final concentration in growth media: 0.375 M) was added to each flask and samples quenched at 28^{o}C 220rpm for 10 minutes. Cells were centrifuged at

4000 x g for 10 minutes and supernatant discarded. Cell pellets were washed once with 25mL TE buffer (pH8.0) + 0.1% N-Lauroylsarcosine (Sigma), centrifuged at 4000 x g for 10 minutes and supernatant discarded. Cells were washed twice more with 50 mL ice-cold 1xDPBS -Mg++-Ca++ (Gibco), centrifuged at 4000 x g for 10 minutes and supernatant discarded. Cell pellets were stored at -80^{o}C overnight. Samples were resuspended on ice in 715 ul 7x Millipore cOmplete inhibitor (Millipore) in water and 50 ul of 10 mg/ml lysozyme (GoldBio) stock in 1xTEpH8.0. 5 ml of 1x Bugbuster (Millipore) was added for a final concentration of 1x protease inhibitor and 10 ug/mL Lysozyme. Samples were secured to a rocker at room temperature and cells allowed to lyse at room temperature for 20 minutes. Samples were centrifuged at 25000 x g 4^{o}C for 1 hour and supernatants moved to 15ml Tubes and stored at -80^{o}C. Sigma-Aldrich FLAG Immunoprecipitation Kit (FLAGIPT1-1KT, Sigma-Aldrich) protocols were used to eluate FLAG-tagged and wild-type background control samples.

Eluate Digestion. Six micrograms of protein were denatured with 3Murea/1Mthiourea/5 mM DTT at 56^{o}C for 30 minutes, the samples were cooled down and alkylated with 15 mM IAA for 30 minutes at RT, in the dark. Protein were digested with LyC (NEB) for 3hrs then with Trypsin (Thermo Scientific) overnight at the ratio of 1:50 trypsine:protein. Digestion was stopped with 0.5% TFA.

Mass Spectrometry. Peptides were desalted using Evosep C18 tips (Pierce) and loaded directly to the Pepsep 15c m x150 um x 1.5 um column. LC gradient for 44 minutes using 30SPD program on an Evosep One LC system connected to a Bruker timsTOF-PRO mass spectrometer via a Bruker CaptiveSpray source. MS data were collected in positive-ion data-dependent PASEF mode over an m/z range of 100 to 1700. PASEF and TIMS were set to “on”. One MS and ten PASEF frames were acquired per cycle of 1.17 sec. Target MS intensity for MS was set at 10,000 with a minimum threshold of 2500. A charge-state-based rolling collision energy table was used from 20-59 eV. An active exclusion/reconsider precursor method with release after 0.4min was used. If the precursor (within mass width error of 0.015 m/z) was >4X signal intensity in subsequent scans, a second MSMS spectrum was collected. Isolation width was set to 2 m/z (<700m/z) or 3 (800-1500 m/z).

Mass spectrometry analysis. Results are the consensus of three independent sample runs for C58 background and PBP1a-3xFLAG crosslinked eluates. The DDA-PASEF individual runs were analyzed with Fragpipe version 19.0 which included database search against the Uniprot (TrEMBL) database of *Agrobacterium fabrum* (strain C58 / ATCC 33970) OX=176299 (163,920 protein counts) with provided protein sequences of PBP1a-FLAG with MSFragger version 3.6, and Philosopher version 4.6.0 for PSM validation and protein inference. Data were searched with stricttrypsin as enzyme (allow to cut K/R after P), 2 missed cleavages allowed; carbamidomethyl cysteine as a fixed

modification; oxidized methionine and N-terminal acetylation as variable mods; 20 ppm mass tolerance for precursor ions and 0.1 Da for-fragment ions. Data were exported and further analyzed in Excel. Only proteins with at least 4 spectral count and FDR≤0.01 were used for identification.

COG functional annotation. Amino acid sequences for all proteins in *A. tumefaciens* were downloaded in a single FASTA file from GenBank and uploaded to EGGNOG-MAPPER [48,49].

Fitness Browser Cofitness analysis. The Fitness Browser webapp was accessed using https://fit.genomics.lbl.gov/cgi-bin/geneSearch.cgi. Atu1328 amino acid sequence was collected from UniProt and pasted under the Fitness Browser BLAST tab. Cofit was selected and top hits along with their cofitness scores were recorded.

Western blot analysis. One colony of the PBP1a-3xFLAG strain and one colony of the PBP1aΔOB-3xFLAG strain were inoculated and grown overnight in 1 mL ATGN each. Overnight cultures were diluted to an OD600 of 0.1 and allowed to grow in fresh media for four hours. Each culture was used to seed a 25 mL bottle of ATGN and allowed to grow to an OD of ~0.6. All cultures were pelleted at 5000 x g for 15 minutes and resuspended in 1 mL of BugBuster and 100 µg/mL of lysozyme was added to each sample. The samples were vortexed at max speed and incubated for 30 minutes at 37^{o}C.

Protein concentrations were measured using a Pierce BCA Protein Assay Kit. Each sample was normalized to 1 µg/mL of protein. 10 µL of 4X loading buffer was added to 30 µL of each sample. All nine protein samples with 4X loading buffer were boiled for five minutes and added to a 4-20% Bis-Tris GenScript *SurePAGE* gel. BlueStain Protein ladder (P007-500) was loaded into the first well. Proteins were transferred to a PVDF membrane cut to the size of the gel using a BioRad Thermo-Blot-Turbo-Transfer device. The membrane was blocked for 1 hour in 20 mL of 5% milk in TBS + 0.05% Tween 20. 1:1000 dilution of Anti-DYKDDDDK mouse monoclonal antibody (Invitrogen) was added, and the membrane was gently shaken overnight at 4ºC. The membrane was washed 3 times with fresh TBS + 0.05% Tween 20 for 5 minutes each. Immediately after wash steps, membranes were transferred to TBS + 0.05% Tween 20 with 1:10000 dilution of goat anti-mouse IgG secondary antibody (Invitrogen) and gently shaken for 1 hour. The membrane was washed 3 times with fresh TBS + 0.05% Tween 20 and then developed for 5 minutes using SuperSignal West Femto Maximum Sensitivity Substrate (34095). The membrane was imaged using a BioRad ChemiDoc Imager.

Bocillin-FL Gel. 3 mg of lysate from RgsS depleted or RgsS induced was incubated with 20ug/ml of Bocillin-FL at 28ºC for 10 minutes. 10uL of 4xProtein loading dye was added to 30uL Bocillin-treated lysate. The samples were boiled for 5 minutes and 35uL of each were loaded into a SurePAGE™, Bis-Tris, 10x8,

4-12%, 15-well protein gel (M00654) alongside Thermo Scientific™ PageRuler™ Plus Prestained Protein Ladder, 10 to 250 kDa. For best resolution, the gel was run at 150V until the everything below 55 kDa was run off the gel. Gel was imaged using a BioRad ChemiDoc imager set to the Alexa488 setting.

Bioinformatic analysis. All structural modeling was done using AlphaFold2 and AlphaFold-multimer. The computation was performed on the high-performance computing infrastructure provided by Research Support Solutions and in part by the National Science Foundation under grant number CNS-1429294 at the University of Missouri, Columbia MO and The Foundry Cluster at Missouri S&T.

Synteny analysis was performed using GeCoViz [50] centered around the gene locus Atu1333 with representative genomes of other Alphaproteobacteria. The Subcellular localization targets were predicted using SignalP 6.0 [51].

The phylogenetic tree was generated from sequences collected previously [3]. The amino acid sequence of *A. tumefaciens* Atu1328 was blasted against each organism's proteome and max score values of top hits were recorded. Max score values under 50 were deemed too different and were therefore not considered an Atu1328 ortholog. Additionally, sequences of each top hit were blasted against the proteome of *A. tumefaciens.* If the top hit was not Atu1328, it was also not considered an Atu1328 ortholog in this analysis.

STRAINS AND PLASMIDS

Strain or Plasmid	Relevant Genotype, Features or Characteristics	Source or Reference
Source Plasmids		
pNTPS139	Km^r; Suicide vector containing *oriT* and *sacB*	D. Alley
pSRKKm-P_{cym}	Km^r, CymR expression, P_{lac} expression vector with cymR operators replacing lacI operators. Contains *oriV* and MCS with c-terminal GFP.	Brown Lab
pRVMCS-2		[42]
Exchange Plasmids		
pNTPS139*mrcA*-3xflag	Km^r Suc^s; allelic exchange plasmid for tagging native copy of *mrcA* with 3xflag	This Study
Expression Plasmids		
pSRKKm-P_{cym}*mrcA*	Km^r, Cumate-inducible copy of the PBP1a	This Study
pSRKKm-P_{cym}*mrcA* S477A	Km^r, Cumate-inducible copy of the PBP1a transpeptidase point mutant	This Study
pSRKKm-P_{cym}*mrcA* E87Q	Km^r, Cumate-inducible copy of the PBP1a glycosyltransferase point mutant	This Study
pSRKKm-P_{cym}*mrcA*-3xflag	Km^r, Cumate-inducible copy of the PBP1a-3xFLAG	This Study
pSRKKm-P_{cym}*mrcA*ΔOB-3xflag	Km^r, Cumate-inducible copy of the PBP1aΔOB-3xFLAG	This Study
pRVMCS-2-P_{van}ftsZ2-sfGFP	Km^r, Vanilate-inducible copy of the FtsZ-sfGFP. Constitutive expression in *A. tumefaciens*	[18]
pSRKKm-P_{envC}envC-sfGFP	Km^r, EnvC-sfGFP expression from native promoter	[20]
pSRKKm-$P_{T7\text{-}med}$DipM-sfGFP	Km^r, DipM-sfGFP expression from the T7 medium expression promoter	[20]
***E. coli* strains**		
DH5α	Cloning strain	Life Technologies
S17-1	Smr;RP4-2 TC::MU Km-Tn7; for plasmid mobilization	[43]
***A. tumefaciens* strains**		
C58ΔtetRA::a-attTn7 (WT)	Replacement of the tetRA locus with an artificial attTn7 site	[44]
C58	Parent strain	[45]
C58ΔtetRA::mini-Tn7-GM-Plac -pbp1a, Δpbp1a	Gm^r, Chromosome-based complementation of Δpbp1a with C58ΔtetRA::mini-Tn7-GM-Plac-pbp1a allowing depletion of PBP1a under control of the lac promoter	[2]
C58ΔtetRA::a-attTn7 + pSRKKm-P_{cym}	Km^r, WT strain carrying pSRKKm- P_{cym}Empty	This Study
C58ΔtetRA::mini-Tn7-GM-P_{lac}-*mrcA*, Δ*mrcA* + pSRKKm-P_{cym}	Km^r, PBP1a depletion strain carrying pSRKKm- P_{cym}Empty	This Study
C58ΔtetRA::mini-Tn7-GM- P_{lac}-*mrcA*, Δ*mrcA* + pSRKKm-P_{cym}*mrcA*	Km^r, PBP1a depletion strain carrying pSRKKm with cumate-inducible expression of PBP1a	This Study
C58ΔtetRA::mini-Tn7-GM- P_{lac}-*mrcA*, Δ*mrcA* +	Km^r, PBP1a depletion strain carrying pSRKKm with cumate-inducible expression of PBP1a transpeptidase point mutant	This Study

pSRKKm-P_{cym}*mrcA* S477A		
C58ΔtetRA::mini-Tn7-GM- P_{lac}-*mrcA*, Δ*mrcA* + pSRKKm-P_{cym}*mrcA* E87Q	Km^r, PBP1a depletion strain carrying pSRKKm with cumate-inducible expression of PBP1a glycosyltransferase point mutant	This Study
C58ΔtetRA::mini-Tn7-GM- P_{lac}-*mrcA*, Δ*mrcA* + pSRKKm-P_{cym}*mrcA*-3xFLG	Km^r, PBP1a depletion strain carrying pSRKKm with cumate-inducible expression of PBP1a-3xFLG	This Study
C58ΔtetRA::mini-Tn7-GM- P_{lac}-*mrcA*, Δ*mrcA* + pSRKKm-P_{cym}*mrcA*ΔOB-3xFLG	Km^r, PBP1a depletion strain carrying pSRKKm with cumate-inducible expression of PBP1aΔOB-3xFLG	This Study
C58ΔtetRA::a-attTn7 *mrcA*-3xFLG	Allelic exchange of *mrcA* with *mrcA-3xFLG*. Expression is controlled by native mrcA promoter	This Study
C58ΔtetRA::mini-Tn7-GM-P_{lac}-*rgsS*, Δ*rgsS*	Gm^r, Chromosome-based complementation of Δ*rgsS* with C58ΔtetRA::mini-Tn7-GM-P_{lac}-*rgsS* allowing depletion of RgsS under control of the lac promoter	Brown Lab
C58ΔtetRA::mini-Tn7-GM-Plac-rgsS, ΔrgsS + pRVMCS-2-P_{van}ftsZ2-sfGFP	Gm^r, Km^r, RgsS depletion with constitutive expression of FtsZ-sfGFP	Brown Lab
C58ΔtetRA::mini-Tn7-GM-P_{lac}-*rgsS*, Δ*rgsS* + pSRKKm-P_{envC}envC-sfGFP	Gm^r, Km^r, RgsS depletion with plasmid-driven expression of EnvC-sfGFP behind its native promoter.	Brown Lab
C58ΔtetRA::mini-Tn7-GM-P_{lac}-*rgsS*, Δ*rgsS* + pSRKKm-$P_{T7\text{-}med}$DipM-sfGFP	Gm^r, Km^r, RgsS depletion with plasmid-driven expression of DipM-sfGFP behind a constitutively active promoter.	Brown Lab

REFERENCES

1. Egan AJF, Errington J, Vollmer W. Regulation of peptidoglycan synthesis and remodelling. Nature Reviews Microbiology. 2020. doi:10.1038/s41579-020-0366-3
2. Williams MA, Aliashkevich A, Krol E, Kuru E, Bouchier JM, Rittichier J, et al. Unipolar peptidoglycan synthesis in the Rhizobiales requires an essential class A penicillin-binding protein. mBio. 2021;12. doi:10.1128/mBio.02346-21
3. Williams MA, Bouchier JM, Mason AK, Brown PJB. Activation of ChvG-ChvI regulon by cell wall stress confers resistance to β-lactam antibiotics and initiates

surface spreading in Agrobacterium tumefaciens. PLoS Genet. 2022;18: e1010274. doi:10.1371/journal.pgen.1010274

4. Typas A, Banzhaf M, Van Den Berg Van Saparoea B, Verheul J, Biboy J, Nichols RJ, et al. Regulation of peptidoglycan synthesis by outer-membrane proteins. Cell. 2010;143: 1097–1109. doi:10.1016/j.cell.2010.11.038
5. Markovski M, Bohrhunter JL, Lupoli TJ, Uehara T, Walker S, Kahne DE, et al. Cofactor bypass variants reveal a conformational control mechanism governing cell wall polymerase activity. Proc Natl Acad Sci U S A. 2016;113: 4788–4793. doi:10.1073/PNAS.1524538113/SUPPL_FILE/PNAS.1524538113.SAPP.PDF
6. Jean NL, Bougault CM, Lodge A, Derouaux A, Callens G, Egan AJF, et al. Elongated Structure of the Outer-Membrane Activator of Peptidoglycan Synthesis LpoA: Implications for PBP1A Stimulation. Structure. 2014;22: 1047–1054. doi:10.1016/J.STR.2014.04.017
7. Yunck R, Cho H, Bernhardt TG. Identification of MltG as a potential terminase for peptidoglycan polymerization in bacteria. Mol Microbiol. 2016;99: 700–718. doi:10.1111/MMI.13258/SUPPINFO
8. Bohrhunter JL, Rohs PDA, Torres G, Yunck R, Bernhardt TG. MltG activity antagonizes cell wall synthesis by both types of peptidoglycan polymerases in Escherichia coli. Mol Microbiol. 2021;115: 1170–1180. doi:10.1111/MMI.14660
9. Williams MA, Bouchier JM, Mason AK, Brown PJB. Activation of ChvG-ChvI regulon by cell wall stress confers resistance to β-lactam antibiotics and initiates surface spreading in Agrobacterium tumefaciens. PLoS Genet. 2022;18: e1010274. doi:10.1371/JOURNAL.PGEN.1010274

10. Williams MA. MECHANISMS OF POLAR GROWTH IN THE ALPHAPROTEOBACTERIAL ORDER RHIZOBIALES. University of Missouri-Columbia. 2019.
11. Bouhss A, Trunkfield AE, Bugg TDH, Mengin-Lecreulx D. The biosynthesis of peptidoglycan lipid-linked intermediates. FEMS Microbiol Rev. 2008;32: 208–233. doi:10.1111/J.1574-6976.2007.00089.X
12. Godessart P, Lannoy A, Dieu M, Van der Verren SE, Soumillion P, Collet JF, et al. β-Barrels covalently link peptidoglycan and the outer membrane in the α-proteobacterium Brucella abortus. Nat Microbiol. 2021;6: 27–33. doi:10.1038/S41564-020-00799-3
13. Petit GA, Hong Y, Djoko KY, Whitten AE, Furlong EJ, McCoy AJ, et al. The suppressor of copper sensitivity protein C from *Caulobacter crescentus* is a trimeric disulfide isomerase that binds copper(I) with subpicomolar affinity. Acta Crystallogr D Struct Biol. 2022;78: 337. doi:10.1107/S2059798322000729
14. Price MN, Wetmore KM, Waters RJ, Callaghan M, Ray J, Liu H, et al. Mutant phenotypes for thousands of bacterial genes of unknown function. Nature. 2018;557: 503–509. doi:10.1038/s41586-018-0124-0
15. Krol E, Stuckenschneider L, Kästle Silva JM, Graumann PL, Becker A. Stable inheritance of *Sinorhizobium meliloti* cell growth polarity requires an FtsN-like protein and an amidase. Nature Communications 2021 12:1. 2021;12: 1–13. doi:10.1038/s41467-020-20739-3
16. Boes A, Kerff F, Herman R, Touze T, Breukink E, Terrak M. The bacterial cell division protein fragment EFtsN binds to and activates the major peptidoglycan

synthase PBP1b. J Biol Chem. 2020;295: 18256. doi:10.1074/JBC.RA120.015951

17. Yahashiri A, Jorgenson MA, Weiss DS. The SPOR Domain, a Widely Conserved Peptidoglycan Binding Domain That Targets Proteins to the Site of Cell Division. J Bacteriol. 2017;199. doi:10.1128/JB.00118-17
18. Howell M, Aliashkevich A, Sundararajan K, Daniel JJ, Lariviere PJ, Goley ED, et al. *Agrobacterium tumefaciens* divisome proteins regulate the transition from polar growth to cell division. Mol Microbiol. 2019;111. doi:10.1111/mmi.14212
19. Attaibi M, den Blaauwen T. An Updated Model of the Divisome: Regulation of the Septal Peptidoglycan Synthesis Machinery by the Divisome. Int J Mol Sci. 2022;23: 3537. doi:10.3390/ijms23073537
20. Figueroa-Cuilan WM, Randich AM, Dunn CM, Santiago-Collazo G, Yowell A, Brown PJB. Diversification of LytM protein functions in polar elongation and cell division of *Agrobacterium tumefaciens*. Front Microbiol. 2021;12. doi:10.3389/fmicb.2021.729307
21. Uehara T, Parzych KR, Dinh T, Bernhardt TG. Daughter cell separation is controlled by cytokinetic ring-activated cell wall hydrolysis. EMBO J. 2010;29: 1412–1422. doi:10.1038/emboj.2010.36
22. Yang DC, Tan K, Joachimiak A, Bernhardt TG. A conformational switch controls cell wall-remodelling enzymes required for bacterial cell division. Mol Microbiol. 2012;85: 768–781. doi:10.1111/j.1365-2958.2012.08138.x

23. Krol E, Yau HCL, Lechner M, Schäper S, Bange G, Vollmer W, et al. Tol-pal system and Rgs proteins interact to promote unipolar growth and cell division in *Sinorhizobium meliloti*. mBio. 2020;11. doi:10.1128/MBIO.00306-20

24. Howell M, Daniel JJ, Brown PJB. Live Cell Fluorescence Microscopy to Observe Essential Processes During Microbial Cell Growth. J Vis Exp. 2017;2017: 56497. doi:10.3791/56497

25. Kuru E, Hughes HV, Brown PJ, Hall E, Tekkam S, Cava F, et al. In Situ probing of newly synthesized peptidoglycan in live bacteria with fluorescent D-amino acids. Angew Chem Int Ed Engl. 2012;51: 12519–12523. doi:10.1002/ANIE.201206749

26. Evans R, O'Neill M, Pritzel A, Antropova N, Senior A, Green T, et al. Protein complex prediction with AlphaFold-Multimer. bioRxiv. 2022; 2021.10.04.463034. doi:10.1101/2021.10.04.463034

27. Charpentier X, Chalut C, Rémy M-H, Masson J-M. Penicillin-Binding Proteins 1a and 1b Form Independent Dimers in *Escherichia coli*. J Bacteriol. 2002;184: 3749–3752. doi:10.1128/JB.184.13.3749-3752.2002

28. Cameron TA, Anderson-Furgeson J, Zupan JR, Zik JJ, Zambryski PC. Peptidoglycan synthesis machinery in Agrobacterium tumefaciens during unipolar growth and cell division. mBio. 2014;5. doi:10.1128/MBIO.01219-14/-/DCSUPPLEMENTAL

29. Aliashkevich A, Cava F. LD-transpeptidases: the great unknown among the peptidoglycan cross-linkers. FEBS J. 2022;289: 4718–4730. doi:10.1111/FEBS.16066

30. Sham LT, Butler EK, Lebar MD, Kahne D, Bernhardt TG, Ruiz N. MurJ is the flippase of lipid-linked precursors for peptidoglycan biogenesis. Science (1979). 2014;345: 220–222. doi:10.1126/SCIENCE.1254522/SUPPL_FILE/SHAM-SM.PDF

31. Kumar S, Mollo A, Kahne D, Ruiz N. The Bacterial Cell Wall: From Lipid II Flipping to Polymerization. Chem Rev. 2021. doi:10.1021/ACS.CHEMREV.1C00773/ASSET/IMAGES/LARGE/CR1C00773_0011.JPEG

32. Lovering AL, De Castro L, Strynadka NCJ. Identification of Dynamic Structural Motifs Involved in Peptidoglycan Glycosyltransfer. J Mol Biol. 2008;383: 167–177. doi:10.1016/J.JMB.2008.08.020

33. Curtis PD, Brun Y V. Identification of essential alphaproteobacterial genes reveals operational variability in conserved developmental and cell cycle systems. Mol Microbiol. 2014;93: 713–735. doi:10.1111/MMI.12686

34. Price MN, Wetmore KM, Waters RJ, Callaghan M, Ray J, Liu H, et al. Mutant phenotypes for thousands of bacterial genes of unknown function. Nature 2018 557:7706. 2018;557: 503–509. doi:10.1038/s41586-018-0124-0

35. Quintero-Yanes A, Mayard A, Hallez R. The two-component system ChvGI maintains cell envelope homeostasis in *Caulobacter crescentus*. PLoS Genet. 2022;18: e1010465. doi:10.1371/JOURNAL.PGEN.1010465

36. Collet J-F, Cho S-H, Iorga BI, Goemans C V. How the assembly and protection of the bacterial cell envelope depend on cysteine residues. Journal of Biological Chemistry. 2020;295: 11984–11994. doi:10.1074/jbc.REV120.011201

37. Zijderveld CAL;, Aarsman MEG;, Nanninga N. UvA-DARE (Digital Academic Repository) Differences between inner membrane and peptidoglycan associated BPB1B dimers of Escherichia coli. J Bacteriol. 1995;177: 1860–1863. doi:10.1128/jb.177.7.1860-1863.1995

38. Li GW, Burkhardt D, Gross C, Weissman JS. Quantifying absolute protein synthesis rates reveals principles underlying allocation of cellular resources. Cell. 2014;157: 624–635. doi:10.1016/J.CELL.2014.02.033

39. Krol E, Yau HCL, Lechner M, Schäper S, Bange G, Vollmer W, et al. Tol-pal system and rgs proteins interact to promote unipolar growth and cell division in *Sinorhizobium meliloti*. mBio. 2020;11: 1–21. doi:10.1128/MBIO.00306-20/FORMAT/EPUB

40. Morton ER, Fuqua C. Laboratory Maintenance of *Agrobacterium*. Current Protocols in Microbiology. 2012. doi:10.1002/9780471729259.mc03d01s24

41. Morton ER, Fuqua C. Genetic manipulation of *Agrobacterium*. Curr Protoc Microbiol. 2012. doi:10.1002/9780471729259.mc03d02s25

42. Thanbichler M, Iniesta AA, Shapiro L. A comprehensive set of plasmids for vanillate- and xylose-inducible gene expression in *Caulobacter crescentus*. Nucleic Acids Res. 2007;35: e137–e137. doi:10.1093/nar/gkm818

43. Simon R, Priefer U, Pühler A. A broad host range mobilization system for in vivo genetic engineering: transposon mutagenesis in gram negative bacteria. Bio/Technology. 1983;1: 784–791. doi:10.1038/nbt1183-784

44. Figueroa-Cuilan W, Daniel JJ, Howell M, Sulaiman A, Brown PJB. Mini-Tn7 insertion in an artificial *att*Tn7 site enables depletion of the essential master

regulator *ctrA* in the phytopathogen *Agrobacterium tumefaciens*. Appl Environ Microbiol. 2016;82. doi:10.1128/AEM.01392-16

45. Watson B, Currier TC, Gordon MP, Chilton MD, Nester EW. Plasmid required for virulence of *Agrobacterium tumefaciens*. J Bacteriol. 1975;123: 255–64. doi:10.1128/jb.123.1.255-264.1975

46. Howell M, Daniel JJ, Brown PJB. Live cell fluorescence microscopy to observe essential processes during microbial cell growth. Journal of Visualized Experiments. 2017;2017. doi:10.3791/56497

47. Ducret A, Quardokus EM, Brun Y v. MicrobeJ, a tool for high throughput bacterial cell detection and quantitative analysis. Nat Microbiol. 2016;1: 16077. doi:10.1038/nmicrobiol.2016.77

48. Sayers EW, Bolton EE, Brister JR, Canese K, Chan J, Comeau DC, et al. Database resources of the national center for biotechnology information. Nucleic Acids Res. 2022;50: D20–D26. doi:10.1093/nar/gkab1112

49. Huerta-Cepas J, Szklarczyk D, Heller D, Hernández-Plaza A, Forslund SK, Cook H, et al. eggNOG 5.0: a hierarchical, functionally and phylogenetically annotated orthology resource based on 5090 organisms and 2502 viruses. Nucleic Acids Res. 2019;47: D309–D314. doi:10.1093/nar/gky1085

50. Botas J, Rodríguez del Río A, Giner-Lamia J, Huerta-Cepas J. GeCoViz: genomic context visualisation of prokaryotic genes from a functional and evolutionary perspective. Nucleic Acids Res. 2022;50:W352-W357. doi:10.1093/nar/gkac367

51. Teufel F, Almagro Armenteros JJ, Johansen AR, Gíslason MH, Pihl SI, Tsirigos KD, Winther O, Brunak S, von Heijne G, Nielsen H. SignalP 6.0 predicts all five types of signal peptides using protein language models. Nat Biotechnol. 2022 Jul;40(7):1023-1025. doi: 10.1038/s41587-021-01156-3

PRIMER LIST

Synthesized DNA	Sequence (5' – 3')
Primers for deletion vectors in *A. tumefaciens*	
PBP1a S477A (TP*) Forward	CCAGCCGGGTGCGTCCTTCAAGC
PBP1a S477A (TP*) Reverse	CGCATGGCCTGCGTGGAG
PBP1a S477A (TP*) Sequencing	ATGGTGGTGATGGACCCG
PBP1a E87Q (GT*) Forward	CCTGTCCGCCCAGGACAAGAATTTCTACAATCACC
PBP1a E87Q (GT*) Reverse	AAGGCGGCCTTCACGCGG
PBP1a Forward NdeI	GCACCATATGATCAGACTGATTGGATATTTTTTCGG
PBP1a C-term Forward	GCCTACCAGACGACGTCCATG
PBP1a N-term Reverse	CATGGACGTCGTCTGGTAGG
3xFLAG Reverse BamHI	GCACGGATCCTCACTTGTCGTCGTCGTCC
PBP1a OB Deletion GA Reverse	atcaccaccatgccaccctgACCGCGGCGTTCGTCATATT
PBP1a OB Deletion GA Forward	aatatgacgaacgccgcggtCAGGGTGGCATGGTGGTGATG

CHAPTER 5

Conclusions and Future Directions

Author Contributions

Jacob Bouchier wrote the original draft and completed the visualization and

Jacob Bouchier and Pamela Brown reviewed and edited this dissertation chapter

On the interplay between host-invasion and polar growth

Chapter 2 described how the classical host-invasion switch ChvG-ChvI could have an ancestral role in detecting and responding to cell envelope stress and was later coopted for host invasion. Indeed, many Alphaproteobacteria that retain orthologs of ChvG-ChvI are free-living organisms throughout their lifecycle. For instance, *Caulobacter crescentus* is a free-living fresh water oligotroph that is never naturally associated with a host. What reason would *C. crescentus* retain ChvG-ChvI if it didn't have additional functions? As work on ChvG-ChvI in *C. crescentus* accumulates [1–3], we can't help but wonder what an extensive comparative analysis on ChvG-ChvI regulon in these bacteria would reveal about its conserved and divergent functions.

One way this pathway may have evolved to function in host-invasion is the apparent overlap in cell wall stress and the stresses the bacteria experience during invasion. For example, plants produce antimicrobial peptides that target bacterial growth machinery [4]. Therefore, activation of cell envelope stress response in these environments would have given plant-associated ancestors of *A. tumefaciens* a survival advantage. We also reason that tapering growth during invasion would help evade deleterious effects from the plant defenses. In other words, an antimicrobial peptide that targets PBP1a would only kill the bacteria if they were actively growing. Interestingly, transcription of *mrcA*, encoding PBP1a, is down regulated in *A. tumefaciens* cells isolated from crown gall tissue [5]. Given that we showed that decreased PBP1a activity activates ChvG-ChvI

(Chapters 2 and 3), this may be a biologically relevant trigger for ChvG-ChvI activation. Perhaps *A. tumefaciens* tapers expression of PBP1a to increase activation of the ChvG-ChvI pathway during host invasion.

Future work to test this idea will require a knock-down strategy instead of knock-out strategy as it pertains to the PBP1a depletion. Cells depleted of PBP1a eventually die, therefore our PBP1a depletion strain is not a viable option for host invasion. An alternative strategy is to use CRISPRi, which can be optimized to knock-down without completely knocking out expression of PBP1a. A sublethal decrease in PBP1a expression would allow us to better explore some of these ideas regarding plant infection.

Regulation of the ChvG-ChvI TCS during cell envelope stress

We reported the lack of conservation of the ChvG-ChvI regulator ExoR across many of the bacteria that have orthologs of ChvG and ChvI and we demonstrated that cell wall stress activates ChvG-ChvI independent of ExoR in *A. tumefaciens* (Chapter 2, [6]). Yet our understanding of this system suggests that it must be regulated in some way to not always be active. How is ChvG regulated under cell envelope stress? One possibility is that depletion of PBP1a or treatment with cell-wall targeting antibiotics does not simply derepress ChvG, but instead induces a protein that directly activates ChvG. Without deeper understanding of proteins that interact with ChvG, identifying this protein would be challenging. However, after the recent success of the PBP1a immunoprecipitation (Chapter 4), ChvG seems like the next logical protein to investigate using this method.

Another possibility is that another protein like ExoR functions in a similar way. One obvious candidate is RgsF [7]. RgsF is structurally very similar to ExoR (Figure 1A), and notably, preliminary bacterial 2-hybrid results suggest that RgsF and ExoR may interact (data not included). AlphaFold-multimer [8] predicted an interaction between the two proteins (Figure 1B). Additional experimentation will have to be performed to confirm these findings and identify their biological relevance. Notably, RgsF is essential, and its depletion in *Sinorhizobium meliloti* results in short, round cells not unlike those during depletion with PBP1a [6]. Indeed, for these reasons RgsF remains a compelling target for ChvG regulation studies.

Novel insights into the polar elongasome

Our findings, in combination with recent work in *S. meliloti* and the identification of a novel suite of polar rhizobial growth and septation (Rgs) proteins [7] has helped us build a putative polar elongasome complex for members of the polar-growing clade Rhizobiales (Figure 2C). While the life cycles of *A. tumefaciens* and *Escherica coli* are vastly different (Figures 2A and 2B), we expected much of the underlying proteins to be the same. Afterall, peptidoglycan synthesis is a conserved process, and the molecular make up of peptidoglycan between the two species isn't all that different. One exception is that *A. tumefaciens* doesn't have the genes that encode orthologs for RodA, PBP2, or MreB, all proteins that

are central to the function of lateral growing bacteria like *E. coli.* Instead, *A. tumefaciens* relies primarily on the function of PBP1a to synthesize nascent peptidoglycan at the pole. Our findings confirmed that at the core of the polar elongasome complex is PBP1a (Figure 2C).

Many of the proteins found in the elongasome such as the peptidoglycan metabolism protein MltG, MltB, and MepA, as well as the LD-transpeptidase Atu1164 and the Tol-Pal complex, all have direct counterparts in *E. coli*, suggesting that many of the underlying elongasome elements are indeed conserved. However, other proteins that we identified as interactors of PBP1a such as the outer-membrane protein AopB, the LD-transpeptidase Atu2336, and the FtsN-like protein RgsS, are unique proteins to the Rhizobiales and are distinct from any protein found in the lateral elongasome of bacteria like *E. coli*. In these proteins we are likely to find novel functions that gave rise to polar growth.

In chapter 2, we demonstrate that depletion of PBP1a and in chapter 3 treatment with cell-wall targeting antibiotics activates ChvG-ChvI. However, how and under which conditions does ChvG localize? And if it is localizing to areas of stress, as we propose, does that mean it is targeted to the polar elongasome where *A. tumefaciens* likely experiences the most envelope stresses? In *Caulobacter crescentus* localization of ChvG is dependent on a short 72 amino acid segment that surprisingly does not include the sensor domain. Instead, localization appears dependent on the HAMP domain. ChvG localizes “patchy-spotty” in *C.*

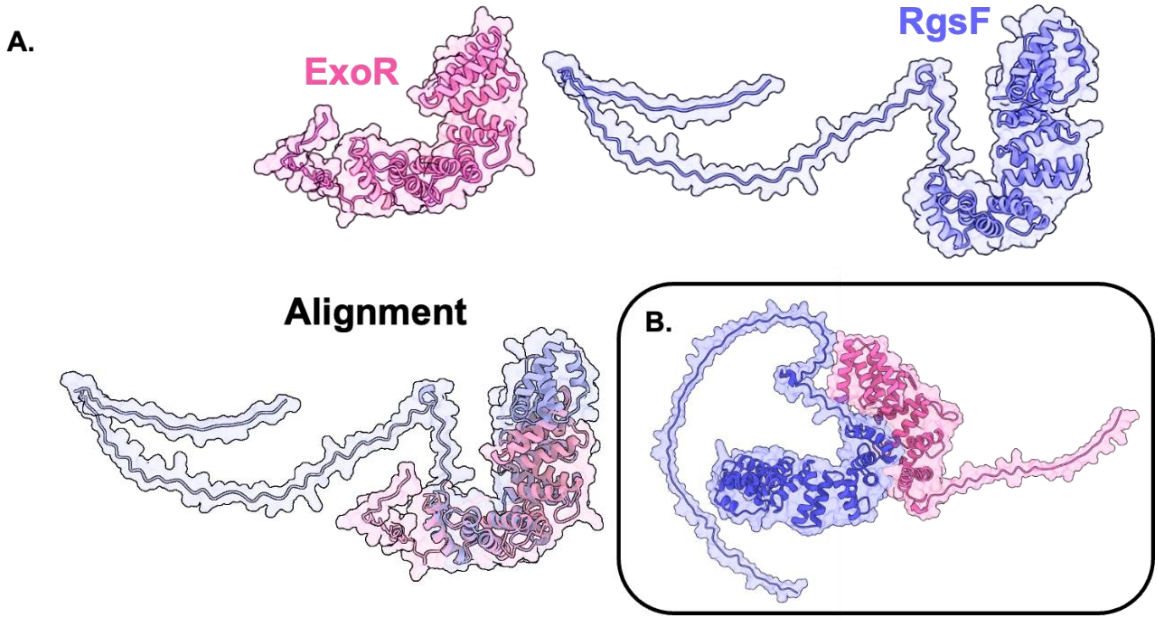

Figure 5.1. ExoR and RgsF have structural similarity. **A**. AlphaFold2 predicted models for ExoR and RgsF and an alignment of the two. **B**. AlphaFold-multimer interaction prediction between ExoR (pink) and RgsF (purple).

crescentus [3], similar to the localization pattern we see in *A. tumefaciens* ChvG-GFP when grown in ATGN (Chapter 3). Localization is instead dependent on a change in osmolality of the growth media. ChvG localizes to midcell in *C. crescentus* in response to rapid changes in media osmolality, such as growing in PYE, washing with M2G (a defined medium), and then imaging immediately afterwards. Perhaps a similar change in osmolality is occurring between liquid ATGN and ATGN agarose pads, or between ATGN and LB media (Chapter 3). One compelling idea is that these conditions may disrupt the elongasome in some way that avtivates Chv-ChvI signaling. To better flesh out these idea, additional work is needed.

Concluding remarks

Taken together, these chapters highlight the uniqueness in growth regulation and stress tolerance in *A. tumefaciens* and other polar-growing bacteria. This group contains many clinically important pathogens including *Bartonella henselae* and *Brucella abortus*, as well as bacteria important for mutualistic relationships with their host like *S. meliloti.* Further, *A. tumefaciens* is a plant pathogen that devastates famers globally. Research into bacteria like *E. coli* can only take us so far in our understanding of divergent traits. Therefore, the breadth of strategies bacteria use to withstand cell envelope stresses like those endured during treatment with cell-wall targeting antibiotics has yet to be explored. Luckily, many researchers and funding agencies are more actively pursuing studies in diverse bacteria such as *A. tumefaciens* as it is becoming increasingly

clear that the *E. coli* paradigm is not a “one size fits all” and should therefore not be treated as such.

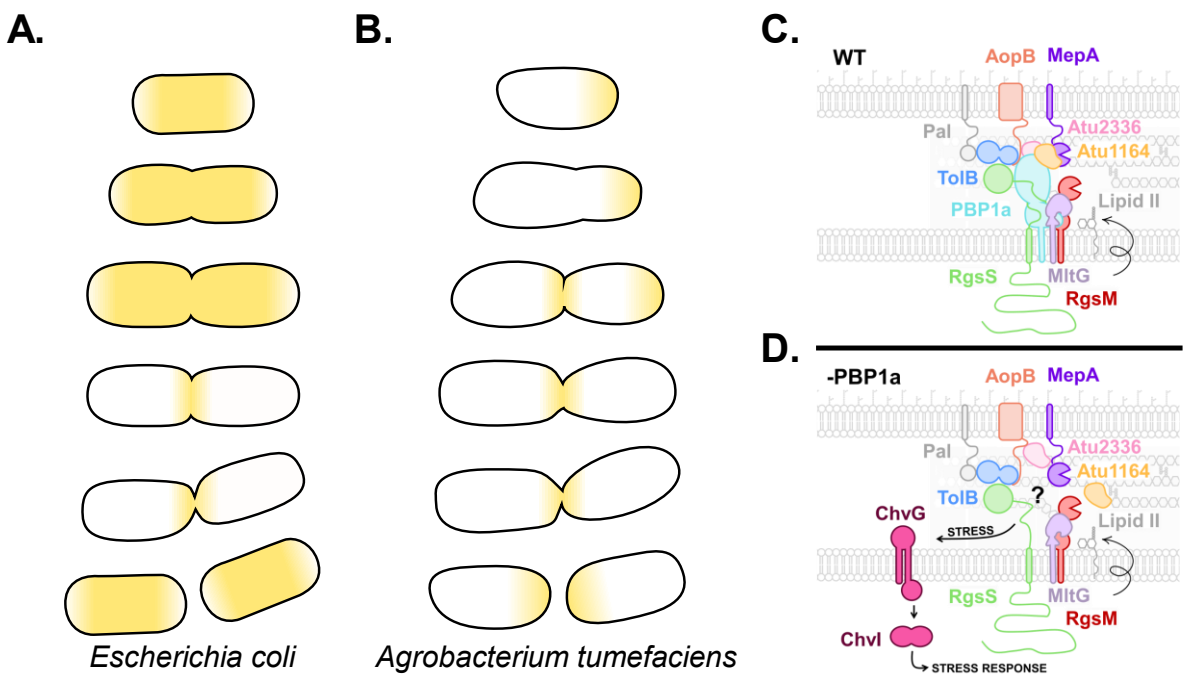

Figure 5.2. Working model for the putative elongasome of *Agrobacterium tumefaciens*. **A.** Peptidoglycan synthesis patterning across the life cycle of Escherichia coli. Yellow represents active peptidoglycan synthesis. **B.** Peptidoglycan synthesis patterning across the life cycle of *A. tumefaciens*. **C.** The elongasome with al functioning PBP1a. **D.** The elongasome without a functioning PBP1a is a placeholder for a yet to be identified signal that activates ChvG under envelope stress.

REFERENCES

1. Stein BJ, Fiebig A, Crosson S. The chvg-chvi and ntry-ntrx two-component systems coordinately regulate growth of *Caulobacter crescentus*. J Bacteriol. 2021;203. doi:10.1128/JB.00199-21/SUPPL_FILE/JB.00199-21-S0001.PDF
2. Vallet SU, Hansen LH, Bistrup FC, Laursen SA, Chapalay JB, Chambon M, et al. Loss of bacterial cell pole stabilization in *Caulobacter crescentus* sensitizes to outer membrane stress and peptidoglycan-directed antibiotics. MBio. 2020;11. doi:10.1128/MBIO.00538-20/SUPPL_FILE/MBIO.00538-20-S0001.DOCX
3. Quintero-Yanes A, Mayard A, Hallez R. The two-component system ChvGI maintains cell envelope homeostasis in *Caulobacter crescentus*. PLOS Genet. 2022;18: e1010465. doi:10.1371/JOURNAL.PGEN.1010465
4. Arnold MFF, Penterman J, Shabab M, Chen EJ, Walker GC. Important Late-Stage Symbiotic Role of the *Sinorhizobium meliloti* Exopolysaccharide Succinoglycan. J Bacteriol. 2018;200. doi:10.1128/JB.00665-17
5. González-Mula A, Lang J, Grandclément C, Naquin D, Ahmar M, Soulère L, et al. Lifestyle of the biotroph *Agrobacterium tumefaciens* in the ecological niche constructed on its host plant. New Phytol. 2018;219: 350–362. doi:10.1111/nph.15164
6. Williams MA, Bouchier JM, Mason AK, Brown PJB. Activation of ChvG-ChvI regulon by cell wall stress confers resistance to β-lactam antibiotics and initiates surface spreading in Agrobacterium tumefaciens. PLOS

Genet. 2022;18: e1010274. doi:10.1371/JOURNAL.PGEN.1010274

7. Krol E, Yau HCL, Lechner M, Schäper S, Bange G, Vollmer W, et al. Tol-pal system and rgs proteins interact to promote unipolar growth and cell division in *Sinorhizobium meliloti*. MBio. 2020;11: 1–21. doi:10.1128/MBIO.00306-20/FORMAT/EPUB

8. Evans R, O'Neill M, Pritzel A, Antropova N, Senior A, Green T, et al. Protein complex prediction with AlphaFold-Multimer. bioRxiv. 2022; 2021.10.04.463034. doi:10.1101/2021.10.04.463034

VITA

I was born in Bloomington, Minnesota to parents Jane and DJ Bouchier and grew up with my sister Katy. I attended Thomas Jefferson High School and after I graduated, attended college at Truman State University from 2014-2018. During college, I wasn't really sure what I wanted to do for a future career. At first I thought I would try for medical school so I did a clinical research internship at A.T. Still University in the summer of 2016. While I enjoyed the research, I wasn't convinced that being a clinician is what I wanted to do. The following summer in 2017, I did a summer research experience in the lab of Dr. Pam Brown at the University of Missouri. I fell in love with microbiology and the research environment and decided to pursue graduate school at the University of Missouri (MU) after that summer. I was accepted into the PhD graduate program at MU in the Division of Biological Sciences (DBS) with a Life Sciences Fellowship fully funded my stipend for four years while earning my degree. After just two rotations, I decided to join Dr. Pam Brown's lab in December of 2018. At Mizzou I was active in many different organizations including being a member of Alternative Career Exploration in the Sciences (ACES) for four years, serving as secretary of the Biology Graduate Student Association (BGSA), being a member of the DBS Seminar Organization Committee, briefly being a member of microbiology club, and also serving as graduate student representative on the non-tenure-track teaching faculty search committee. Additionally, I was a teaching assistant for general microbiology lab and cell biology. I also taught General Microbiology as instructor of record. Following completion of my

dissertation, I have accepted a position as a post-doctoral researcher in the lab of Dr. Aimee Shen at Tufts Medical Center in Boston, MA where I will study the mechanisms of sporulation and germination in *Clostridoides difficile.* After completion of my post-doc, I plan on pursuing a career in Academia.